Entanglement, coherence and correlation in atomic and molecular systems.

Juan Felipe Pulgarín Mosquera

Bachelor's thesis in
Physics

Tutor

Jose Luis Sanz Vicario, PhD.

Atomic and Molecular Physics Group, Institute of Physics,
University of Antioquia

Institute of Physics

Faculty of Exact and Natural Sciences

University of Antioquia

Medellín, Colombia

Abstract

In the present work, we have computed the entanglement between the electronic and nuclear motions in two molecular model systems: the one-dimensional hydrogen molecular ion (H_2^+) and the Shin-Metiu model, considering the molecules as a bipartite systems: electron and nuclear motion. For that purpose, we have computed the Born-Oppenheimer and non-Born-Oppenheimer (Born-Huang) wave function in terms of the Fourier Grid Hamiltonian basis that expands both the electronic and nuclear wave functions. Also, according to the Schmidt decomposition theorem for bipartite systems, widely used in quantum-information theory, there is a much shorter but equivalent expansion in terms of the Schmidt bases for the electronic and nuclear sub-spaces. In these models of distinguishable coupled particles we have shown that the entanglements contents do not increase monotonically with the excitation energy. In the hydrogen molecular ion and in the Shin-Metiu model, the entanglements contents for each Born-Oppenheimer electro-nuclear state is quantified through the von-Neumann and linear entropies and we have shown that entanglement serves as a witness of distinguishability of nuclear states related to different Born-Oppenheimer molecular energy curves or electronic excitation modes.

Acknowledgements

I would like to thank all the little people who made this thesis possible.

Table of Contents

List of Tables

Chapter 1

Introduction

Electrons and nuclei are the fundamental particles that determine the nature of the matter of our every world: atoms, molecules, condensed matter. This is because a piece of matter can be imagined as a collection of interacting atoms, sometimes under the influence of an external field. The description of the physical and chemistry properties of matter is a central issue, that has been studied along many years and it is because the multi-electronic and nuclear many-body problem does not have exact solution [14, 19]. Most quantum chemistry calculations are done by following nuclear motions on potential energy surfaces obtained a priori based on the Born-Oppenheimer (BO) approximation for a molecule, which can be thought of as a bipartite coupled system composed of electrons and nuclei according to quantum information theory. The BO wave function can be expressed as a direct product of an electronic wave function (which depends parametrically on the nuclear geometry) and a nuclear wave function. However, such a molecular BO wave function is not a true eigen-function of the molecular Hamiltonian, since the so-called non-adiabatic coupling terms are missing and with them, some of the intricate features of the correlation between electrons and nuclei [1, 12].
The screening of the long-range Coulomb forces in those systems may produce effects on their structure and dynamics, still unexplored or unexpected. The lack of exactly solvable problems, including screening effects, has been perhaps the reason for the little attention paid in the literature to solve, from first principles, complex molecular systems under the effect of screening interactions [1].

Another tool to analyze states in quantum systems is through entanglement measures, such as von-Neumann and linear entropies of entanglement. Needless to say that entanglement is one of the most crucial properties of multipartite systems in quantum theory that brings essential inseparability and non-classical correlations among their constituents, it is

subject to a continuous debate on its nature and potential applications. Previous studies have focused their attention on analyzing entanglement entropies of bound levels in artificial model atoms. More recently, these studies have been extended to realistic two-electron atoms considered as bipartite entangled systems, although restricted to the analysis of the ground state and low-lying singly excited states [21].

In the present work, the objective is to compute the entanglement between the electronic and nuclear motions in two molecular model systems: the one-dimensional hydrogen molecular ion (H_2^+) and the Shin-Metiu model, where we have considered the molecules as a bipartite systems, composed by the electron and nuclear motion. For that purpose, we will compute the Born-Oppenheimer and non-Born-Oppenheimer (Born-Huang) wave functions in terms of the Fourier Grid Hamiltonian basis that expand the electronic and nuclear wave functions. Also, according to the Schmidt decomposition theorem for bipartite systems, we will compute a much shorter but equivalent expansion in terms of the Schmidt bases for the electronic and nuclear sub-spaces separately and analyze how the values of the entropy can affect this expansion.

The thesis is organized as follows. In chapter 2 we have described the theoretical tools required to understand both calculations and results. This chapter is dedicated to explain how the wave functions are built and under what conditions the Born-Oppenheimer and Born-Huang wave functions are valid. Also, we have explained the relation between the density operator, the entropy and the Schmidt decomposition for a quantum system. In chapter 3 we have described the two molecular model systems; the one-dimensional hydrogen molecular ion (H_2^+) and the Shin-Metiu model. In chapter 4 we have introduced the methods and different parameters which we have used to solve the two molecular model systems and in the chapters 5, 6 and 7 we have introduced our results. We end up with some conclusions in chapter 8.
Atomic units (a.u.) are used throughout unless otherwise explicitly stated.

Chapter 2

Theoretical Tools

2.1 Atomic and Molecular Problem

We can unambiguously describe all atomic and molecular systems as a set of atomic nuclei and electrons interacting through Coulombian forces. We begin by considering a system of K non-relativistic spinless electrons N and nuclei, which can be described by the Hamiltonian (2.1)

$$\hat{H} = \underbrace{\sum_{I=1}^{N} \frac{\hat{\mathbf{P}}_I^2}{2M_I}}_{\hat{T}_N} + \underbrace{\frac{1}{2m_e} \sum_{j=1}^{K} \hat{\mathbf{p}}_j^2}_{\hat{T}_e} + \underbrace{\hat{V}(\hat{\mathbf{R}}_\mathbf{1}, ..., \hat{\mathbf{R}}_\mathbf{N}, \hat{\mathbf{x}}_\mathbf{1}, ..., \hat{\mathbf{x}}_\mathbf{K})}_{\hat{U}_{NN}+\hat{U}_{Ne}+\hat{U}_{ee}}, \tag{2.1}$$

which has been splitted into three parts: nuclear and electronic kinetic energies plus the interactions between the nuclei and the electrons, i.e:

- $\hat{T}_N$ is the nuclear kinetic energy operator. M_I and $\hat{P}_I$ are the mass and the momentum operator of the I-th nucleus respectively.
- $\hat{T}_e$ is the electronic kinetic energy operator. m_e is the electron mass and $\hat{p}_j$ is the momentum operator of the j-th electron.
- $\hat{V}$ is total interaction potential. It is composed by the Coulomb interactions nucleus-nucleus ($\hat{U}_{NN}$), nucleus-electron ($\hat{U}_{Ne}$) and electron-electron ($\hat{U}_{ee}$) operators.

So, to find the energy and stationary states of the full molecular system, one would solve the time independent Schrödinger equation (equation 2.2)

$$\hat{H}\,|\Psi\rangle = W\,|\Psi\rangle\,, \tag{2.2}$$

where $\hat{H}$ is the Hamiltonian operator and W is the energy of the stationary eigenstate $|\Psi\rangle$. Solving the equation (2.2) may be very difficult for systems composed by several particles, nuclei plus electrons. Only in a few cases, such as hydrogen-like atoms or the 3D hydrogen molecular ion H_2^+, a full analytic solution is available. Very accurate numerical solutions are also possible. There are several features that contribute to this difficulty, but the most important is that this is a multi-component many-body system, which makes the above Schrodinger equation not separable.
The usual choice is to resort to a few reasonable and well controlled approximations which can encompass a wide variety of problems. But, there are systems where the hypotheses leading to these approximations are violated. They require a much larger theoretical and computational effort [14, 6, 26].
It is why on this work we will make emphasis in two different methods: The Born-Oppenheimer (BO) approximation and the, in principle, exact Born-Huang (BH) expansion.

2.1.1 Born-Oppenheimer (BO) approximation

The main idea of the Born-Oppenheimer approximation, commonly being confused with the adiabatic approximation, is to replace the coupled problem by a pair of uncoupled single particle problems. Sometimes it can be used if the time scale associated to the nuclear motion is usually much slower than the associated with electrons.
The most unfavorable case of a single proton corresponds to a mass ratio of 1:1836, i.e. less than 1%. Within a classical picture we could say that, under typical conditions, the velocity of the electron is much larger than that of the heavy particle (the proton). In other words, since the nuclei are much heavier than electrons, they move more slowly. Thus, one can consider the electrons in a molecule to be moving in the field of fixed nuclei. As the nuclei follow their dynamics, the electron instantaneously adjust their wave function according to the nuclear (vibrational and rotational) wave function. This approximation ignores the possibility of having non-radiative (through non-adiabatic couplings) transitions between different electronic eigenstates. Transitions can only arise through the radiative coupling with an external electromagnetic field, if the selection rule allows for them.
Within this approximation, the first term of the equation (2.1), the nuclear kinetic energy, can be neglected and the nucleus-nucleus interaction among nuclei can be considered as

a constant; any constant added to an operator only adds to the operator eigenvalues and does not have effect on the operator eigenstates. Thus, the remaining terms in the equation (2.1) are called the electronic Hamiltonian

$$\hat{H}_e = \frac{1}{2m_e}\sum_{j=1}^{K}\hat{\mathbf{p}}_j^2 + +\hat{U}_{Ne}(\hat{\mathbf{R}},\hat{\mathbf{x}}) + \hat{U}_{ee}(\hat{\mathbf{x}}), \tag{2.3}$$

where $\hat{\mathbf{R}} = \left\{\hat{\mathbf{R}}_I,\ I = 1, ..., N\right\}$ is a set of N nuclear coordinates, and $\hat{\mathbf{x}} = \{\hat{\mathbf{x}}_j,\ j = 1, ..., K\}$. Also, the Hamiltonian (2.3) follows a corresponding Schröodinger equation (2.4)

$$\hat{H}_e\phi_n(\mathbf{x};\mathbf{R}) = \epsilon_{\text{elec}}^{(n)}(\mathbf{R})\phi_n(\mathbf{x};\mathbf{R}), \tag{2.4}$$

where $\phi_n(\mathbf{x};\mathbf{R})$ is the n-th electronic wave function, which describes the motion of electrons for a fixed nuclear geometry $\mathbf{R}$, and explicitly depends on the electronic coordinate, but depends parametrically of the nuclear coordinates, as the electronic energy $\epsilon_{\text{elec}}^{(n)}(\mathbf{R})$. Also, $\phi_n(\mathbf{x};\mathbf{R})$ is a different function of the electronic coordinates for each nuclear configuration $\mathbf{R}$.

The total electronic energy $E_n(\mathbf{R})$ for fixed nuclei must also include the constant nuclear Coulombic interaction, it is

$$E_n(\mathbf{R}) = \epsilon_{\text{elec}}^{(n)}(\mathbf{R}) + \hat{U}_{NN}(\hat{\mathbf{R}}). \tag{2.5}$$

Thus, the energy $E_n(\mathbf{R})$ provides a potential surface in the remaining nuclear motion in the nuclear Hamiltonian

$$\hat{H}_{nucl}^{(n)} = \sum_{I=1}^{N}\frac{\hat{\mathbf{P}}_I^2}{2M_I} + E_n(\mathbf{R}), \tag{2.6}$$

and the solutions to this nuclear Hamiltonian is provided by the nuclear Schrödinger equation

$$\hat{H}_{nucl}^{(n)}\chi_{n,m}(\mathbf{R}) = W_m\chi_{n,m}(\mathbf{R}), \tag{2.7}$$

where $\chi_{n,m}(\mathbf{R})$ is the m-th nuclear wave function associated to the n-th electronic state, it describes the vibration and rotation of a molecule. W_m is the Born-Oppenheimer approximation to the total energy of the Schrödinger equation (2.2), which includes electronic, vibrational, rotational and translational energies. The corresponding BO-approximation to the total wave function of the Schrödinger equation (2.2) is thus the product

$$\Psi(\mathbf{x},\mathbf{R}) = \phi_n(\mathbf{x};\mathbf{R})\chi_{n,m}(\mathbf{R}). \tag{2.8}$$

In the BO-approximation, additional coupled terms are neglected, i.e. we are not considering couplings between different electronic states, so that electrons remain described by the same n-th adiabatic electronic state and the dynamics is said to be adiabatic [14, 7, 26].

2.1.2 Born-Huang (BH) expansion

This method modify the potential energy of the nuclei, which is not the energy eigenvalue of the electronic state considered plus the nucleus-nucleus interaction, equation (2.5). The Born-Huang method has the additional advantage that it leads to a system of coupled equations for all electronic states, which implies the inherent inner coupling between the electronic and nuclear motions.
We will start trying to solve the Schrödinger equation (2.2), proposing a total wave function with the form

$$\Psi(\mathbf{x},\mathbf{R}) = \sum_n \phi_n(\mathbf{x};\mathbf{R}) f_n(\mathbf{R}), \tag{2.9}$$

where $\phi_n(\mathbf{x};\mathbf{R})f_n(\mathbf{R})$ are the electronic and the vibrational wave functions (in this work we will not consider the rotational motion) respectively. Multiplying the result by $\phi^*_{n'}(\mathbf{x};\mathbf{R})$ and integrating over $\mathbf{x}$, we obtain the set of coupled equations for the vibrational wave functions

$$\left(\hat{T}_N + E_n(\mathbf{R}) - W_n\right) f_n(\mathbf{R}) + \sum_{n'} \hat{C}_{n,n'}(\hat{\mathbf{R}},\hat{\mathbf{P}}) f_{n'}(\mathbf{R}) = 0, \tag{2.10}$$

where $E_n(\mathbf{R})$ is the electronic potential energy surface in the BO-approximation, equation (2.5). W_n is the total energy in the Schrödinger equation (2.2) and $C_{n,n'}$ correspond to the so-called non-adiabatic couplings.
These non-adiabtic couplings are defined as follows

$$\hat{C}_{n,n'} = \sum_{I=1}^{N} \frac{1}{M_I} \left(\hat{A}^{(I)}_{n,n'}(\hat{\mathbf{R}})\hat{\mathbf{P}}_I + \hat{B}^{(I)}_{n,n'}(\hat{\mathbf{R}})\right). \tag{2.11}$$

- $\hat{A}^{(I)}_{n,n'}(\mathbf{R})$ is defined by

$$\hat{A}^{(I)}_{n,n'}(\mathbf{R}) = \int d\mathbf{x} \phi^*_n(\mathbf{x};\mathbf{R}) \hat{\mathbf{P}}_I \phi_{n'}(\mathbf{x};\mathbf{R}), \tag{2.12}$$

and its diagonal elements ($n = n'$) are equal to zero when $\phi_n(\mathbf{x};\mathbf{R})$ are chosen to be real functions. Also it is an anti-symmetric operator, since

$$\hat{A}^{(I)}_{n,n'}(\mathbf{R}) \doteq \frac{-i\hbar}{2}\partial_{\mathbf{R}_I}\int d\mathbf{x}\,|\phi_n(\mathbf{x};\mathbf{R})|^2 = 0 \qquad n = n', \tag{2.13}$$

$$\hat{A}^{(I)}_{n,n'}(\mathbf{R}) = -\hat{A}^{(I)}_{n',n}(\mathbf{R}) \qquad n \neq n'. \tag{2.14}$$

Also, using the off-diagonal Hellmann-Feynman theorem (Appendix A), we can evaluate the matrix elements (equation (2.12) as

$$\hat{A}^{(I)}_{n,n'}(\mathbf{R}) = -\frac{i\hbar}{E_{n'}(\mathbf{R}) - E_n(\mathbf{R})}\left\langle \phi_n \left| \frac{\partial \hat{H}_e}{\partial \mathbf{R}_I} \right| \phi_{n'} \right\rangle = -i\hbar F^{(I)}_{n,n'}(\mathbf{R}). \tag{2.15}$$

- $\hat{B}^{(I)}_{n,n'}(\mathbf{R})$ is defined by

$$\hat{B}^{(I)}_{n,n'}(\mathbf{R}) = \frac{1}{2}\int d\mathbf{x}\phi^*_n(\mathbf{x};\mathbf{R})\hat{\mathbf{P}}^2_I\phi_{n'}(\mathbf{x};\mathbf{R}). \tag{2.16}$$

Writing the momentum operator in the position representation $\left(\hat{\mathbf{P}}_I \doteq -i\hbar\partial_{\mathbf{R}_I}\right)$, $\hat{B}^{(I)}_{n,n'}$ can be written as

$$\begin{aligned}
\hat{B}^{(I)}_{n,n'}(\mathbf{R}) &= -\frac{\hbar^2}{2}\int d\mathbf{x}\phi^*_n(\mathbf{x};\mathbf{R})\partial_{\mathbf{R}_I}\left(\partial_{\mathbf{R}_I}\phi_{n'}(\mathbf{x};\mathbf{R})\right), \qquad (2.17)\\
&= -\frac{\hbar^2}{2}\left(\partial_{\mathbf{R}_I}\underbrace{\int d\mathbf{x}\phi^*_n(\mathbf{x};\mathbf{R})\partial_{\mathbf{R}_I}\phi_{n'}(\mathbf{x};\mathbf{R})}_{\hat{A}^{(I)}_{n,n'}(\mathbf{R})} + \underbrace{\int d\mathbf{x}\left(\partial_{\mathbf{R}_I}\phi_n(\mathbf{x};\mathbf{R})\right)^\dagger\left(\partial_{\mathbf{R}_I}\phi_{n'}(\mathbf{x};\mathbf{R})\right)}_{\xi^{(I)}_{n,n'}(\mathbf{R})}\right).
\end{aligned}$$

where is clear that the first term is the partial derivative with respect to the nuclear coordinate $\mathbf{R_I}$ of $A^{(I)}_{n,n'}(\mathbf{R})$. For the second term we use the completeness relation of the electronic states functions to obtain

$$\begin{aligned}
\xi^{(I)}_{n,n'}(\mathbf{R}) &= \sum_j\left(\int d\mathbf{x}\left\langle\phi_j\right|\left(\partial_{\mathbf{R}_I}\phi_n(\mathbf{x};\mathbf{R})\right)^\dagger\left\langle\phi_j\right|\left(\partial_{\mathbf{R}_I}\phi_{n'}(\mathbf{x};\mathbf{R})\right)\right)\\
&= \sum_j\left(\int d\mathbf{x}A^{(I)}_{n,j}(\mathbf{x};\mathbf{R})A^{(I)}_{j,n'}(\mathbf{x};\mathbf{R})\right) = (\mathbf{A}^{(I)}\cdot\mathbf{A}^{(I)})_{n,n'}(\mathbf{R}) \qquad (2.18)
\end{aligned}$$

that compared with the property showed in the Appendix B, the term $\xi^{(I)}_{n,n'}(\mathbf{R})$ is the matrix element n, n' of the square of the matrix $\mathbb{A}$, i.e, $\mathbb{A} \cdot \mathbb{A}$.
In general $B_{n,n'}(R)$ written in matrix form is

$$\mathbb{B}^{(I)} = -\frac{\hbar^2}{2}\left(\frac{\partial}{\partial \mathbf{R_I}}\mathbb{F} + \mathbb{F}^{\mathbf{2}}\right) = -\frac{\hbar^2}{2}\mathbb{H}^{(\mathbf{I})}. \tag{2.19}$$

$\hat{B}^{(I)}_{n,n'}(\mathbf{R})$ is not symmetric or anti-symmetric, its first term is anti-symmetric and the second is symmetric.

Thus, we can rewrite the non-adiabatic coupling $\mathbf{C}$ in matrix form as

$$\mathbb{C} = -\sum_{I=1}^{N}\frac{\hbar^2}{2M_I}\left[2\mathbb{F}^{(I)}\partial_{\mathbf{R}_I} + \mathbb{H}^{(I)}\right], \tag{2.20}$$

the terms $\mathbf{H}^{(\mathbf{I})}$ and $2\mathbf{F}^{(I)}\partial_{\mathbf{R}_I}$ compensate to each other, so that C is a symmetric (Hermitian) matrix, as it should be since adds to the Hamiltonian [10].

After that, we can rewrite the equation (2.10) in the form

$$\left(\hat{T}_N + U_n(\mathbf{R}) - W_n\right) f_n(\mathbf{R}) + \sum_{n' \neq n}\hat{C}_{n,n'}(\hat{\mathbf{R}}, \hat{\mathbf{P}}) f_{n'}(\mathbf{R}) = 0, \tag{2.21}$$

where the diagonal terms in C are omitted on the summation and included in the potential, i.e.

$$U_n(\mathbf{R}) = E_n(\mathbf{R}) + \sum_I \frac{1}{M_I}\hat{B}^{(I)}_{n,n}(\hat{\mathbf{R}}). \tag{2.22}$$

The total wave function within the BH expansion can be written in the BO wave functions as an expansion of nuclear functions multiplied by a set coefficients, then a general expansion for a BH-like wave function may have the form

$$\Psi(\mathbf{x}, \mathbf{R}) = \sum_n \phi_n(\mathbf{x}; \mathbf{R})\left(\sum_m c_{n,m}\chi_{n,m}(\mathbf{R})\right). \tag{2.23}$$

Finally, an important assumption must be mentioned. If electronic wave functions vary sufficiently slowly with the nuclear coordinates, $C_{n,n'} \approx 0$; the last term of the equation (2.21) may usually be neglected. In this case, the vibrational wave functions are decoupled from each other [5, 3].

2.1.3 Diabatic Coupling

We need to pass from an adiabatic to a diabatic representation of the total wave function by an unitary matrix transformation, diabatic molecular eigenfunctions are readily constructed from the adiabatic eigenfunctions by using the identities

$$\begin{aligned} \mathbf{f}^d = \mathbb{U}^\dagger \mathbf{f} \quad &\Rightarrow \quad f_m^d = \sum_k (U_{m,k})^\dagger f_k = \sum_k U_{k,m}^* f_k, \\ \boldsymbol{\phi}^d = \mathbb{U}\boldsymbol{\phi} \quad &\Rightarrow \quad \phi_m^d = \sum_k (U_{m,k})^\dagger \phi_k = \sum_k U_{k,m}^* \phi_k, \end{aligned} \tag{2.24}$$

thus, the total wave function is invariant under unitary transformations and can be written in a new basis defined by the orthogonal transformation used in the relations (2.24)

$$\begin{aligned} \Psi(\mathbf{x},\mathbf{R}) &= \sum_n \phi_n(\mathbf{x};\mathbf{R}) f_n(\mathbf{R}) = \boldsymbol{\phi}_n^T(\mathbf{x};\mathbf{R})\mathbf{f_n}(\mathbf{R}) = (\mathbb{U}\boldsymbol{\phi}^d)^T(\mathbb{U}\mathbf{f}^d) \\ &= \sum_n \phi_n^d(\mathbf{x};\mathbf{R}) f_n^d(\mathbf{R}). \end{aligned} \tag{2.25}$$

The relationship between the adiabatic and diabatic states is illustrated by

$$\begin{gathered} \left(-\frac{\hbar^2}{2M}\nabla^2 + \mathbb{E}(\mathbf{R}) - W + \mathbb{C}\right)\mathbf{f_n}(\mathbf{R}) = 0, \\ \Updownarrow \\ \left(-\frac{\hbar^2}{2M}\nabla^2 + \mathbb{V}_d(\mathbf{R}) - W_d\right)\mathbf{f_n^d}(\mathbf{R}) = 0, \end{gathered} \tag{2.26}$$

where $\mathbb{V}_d(\mathbf{R}) = \mathbb{U}^{-\mathbf{1}}(\mathbf{R})\mathbb{E}(\mathbf{R})\mathbb{U}(\mathbf{R})$ will have diagonal elements which may cross and non-zero diagonal elements which drive transitions between the molecular states.
We have used that there is not adiabatic couplings between the diabatic electronic wave functions, i.e.

$$
\begin{aligned}
F^d_{n,m} &= \left\langle \phi^d_n \left| \frac{\partial}{\partial \mathbf{R}} \right| \phi^d_m \right\rangle = 0 \qquad (2.27)\\
&= \sum_{k,l} \left\langle U_{m,k}\phi_k \left| \frac{\partial}{\partial \mathbf{R}} \right| U^*_{l,m}\phi_m \right\rangle \\
&= \sum_{k,l} \langle U_{m,k}\phi_k | \cdot \left(\left| \frac{\partial}{\partial \mathbf{R}} U^*_{l,m}\phi_m \right\rangle + \left| U^*_{l,m} \frac{\partial}{\partial \mathbf{R}} \phi_m \right\rangle \right) \\
&= \sum_k U_{m,k} \left\langle \phi_k \left| \cdot \sum_l U^*_{l,m} \right| \frac{\partial}{\partial \mathbf{R}} \phi_m \right\rangle + \sum_{k,l} U_{m,k} \frac{\partial}{\partial \mathbf{R}} U^*_{l,m} \delta_{k,l} \\
&= \mathbb{U}^\dagger \mathbb{A} \mathbb{U} + \mathbb{U}^\dagger \frac{\partial}{\partial \mathbf{R}} \mathbb{U} = \mathbb{U}^\dagger \underbrace{\left(\mathbb{A}\mathbb{U} + \frac{\partial}{\partial \mathbf{R}} \mathbb{U} \right)}_{=0}, \qquad (2.28)
\end{aligned}
$$

with this last relation one might find the relation between the non-adiabatic couplings and the unitary transformation matrix [17, 8, 20].

- Two Electronic Surfaces Case: If the adiabatic coupling is strong over a limited region, as it is typical of avoided crossings (Figure 2.1), in many such cases, the diabatic coupling are weak and the equations for $f^d(R)$ may be solved using the distorted-wave approximation

  If n=2, the transformation matrix $\mathbb{U}$ takes a particularly simple form, where it can be expressed in terms of a single parameter $\lambda(\mathbf{R})$

$$
\mathbb{U} = \begin{pmatrix} Cos\ \lambda(\mathbf{R}) & Sin\ \lambda(\mathbf{R}) \\ -\ Sin\ \lambda(\mathbf{R}) & Cos\ \lambda(\mathbf{R}) \end{pmatrix}, \qquad (2.29)
$$

  where

$$
\lambda(\mathbf{R}) = \int_{\mathbf{R}}^{\infty} \mathbf{dR'} \mathbf{A_{0,1}}(\mathbf{R'}). \qquad (2.30)
$$

  The potential matrix takes the form

$$
\mathbb{V}_\mathbf{d} = \begin{pmatrix} E_1 Cos^2\lambda + E_2 Sin^2\lambda & \frac{1}{2}(E_1 - E_2) Sin^2\lambda \\ \frac{1}{2}(E_1 - E_2) Sin^2\lambda & E_1 Sin^2\lambda + E_2 Cos^2\lambda \end{pmatrix}. \qquad (2.31)
$$

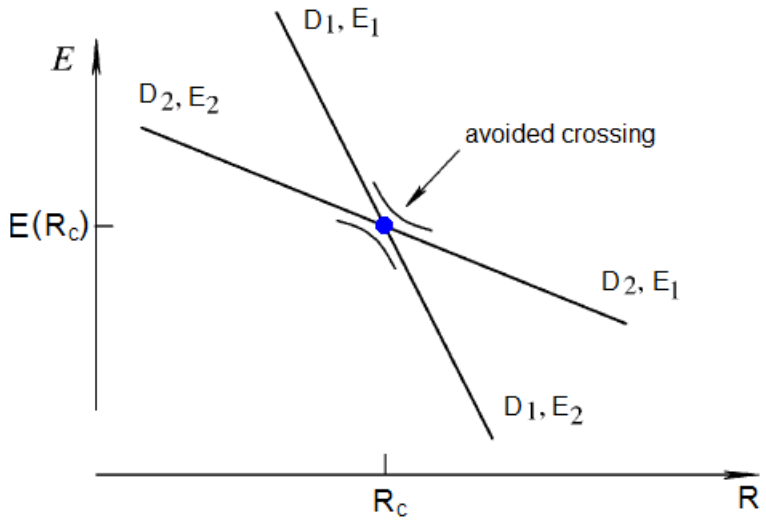

Figure 2.1:
Diabats $D_{1,2}$ are coupled by $H_{1,2}$. Where interaction is negligible, adiabats $E_{1,2}$ are identified with the $D_{1,2}$, namely, for $x << 0$, $E_1 = D_1$ and $E_2 = D_2$, while for $x >> 0$, $E_1 = D_2$ and $E_2 = D_1$ [28].

The diabatic potential energy surfaces cross where $V_{0,0}(R) = V_{1,1}(R)$. The function $\lambda(R)$ is the area under the curve of $A_{0,1}$ in the interval $[R, \infty]$. In the weak-coupling limit the diabatic and adiabatic surfaces coincide. In the strong-coupling limit, many crossings occur of the diabatic curves which oscillate between $E_1(R)$ and $E_2(R)$ [17, 8, 20].

2.2 Schmidt decomposition and Von-Neumann Entropy

First we need to assume that a state of a system arises by a quantum process, so that the state $|\Psi_\alpha\rangle$ is prepared with probability p_α. We call this situation a mixture of the states $|\Psi_\alpha\rangle$.

Thus, we will define the density operator of an ensamble of α systems as

$$\hat{\rho} = \sum_\alpha p_\alpha \left|\Psi_\alpha\right\rangle \left\langle\Psi_\alpha\right|. \tag{2.32}$$

We will focus in a special case of the equation (2.32). For a single element within the ensamble, described by a pure state, the density operator can be written as

$$\hat{\rho} = |\Psi\rangle \langle\Psi| . \tag{2.33}$$

It is important to remark that a mixture of states is a very different thing from a superposition. A superposition yields a definite state vector, whereas a mixture does not and so must be described by a density operator [23].

Assuming that $|\Psi\rangle$ represents a molecular state (electrons + nuclei). If one partially trace over the degrees of freedom $\mathbf{x}$ or $\mathbf{R}$, we find the reduced density operators $\hat{\rho}^{(\mathbf{R})}$ and $\hat{\rho}^{(\mathbf{x})}$ respectively, which can be written as

- Reduced density operator $\hat{\rho}^{(\mathbf{R})}$

$$\hat{\rho}^{(\mathbf{R})} = \hat{T}r_{\mathbf{x}} [\hat{\rho}] = \int d\mathbf{x} \langle\mathbf{x}|\Psi\rangle \langle\Psi|\mathbf{x}\rangle, \tag{2.34}$$

- Reduced density operator $\hat{\rho}^{(\mathbf{x})}$

$$\hat{\rho}^{(\mathbf{x})} = \hat{T}r_{\mathbf{R}} [\hat{\rho}] = \int d\mathbf{R} \langle\mathbf{R}|\Psi\rangle \langle\Psi|\mathbf{R}\rangle, \tag{2.35}$$

2.2.1 Schmidt decomposition

The Schmidt decomposition asserts that given a state $|\Psi\rangle$, whose wave function depends of $\mathbf{x}$ and $\mathbf{R}$, in this case, there exist orthogonal bases $\{|u_i\rangle_{i=1,..,l}\}$ and $\{|v_i\rangle_{i=1,..,k}\}$ for the Hilbert spaces $\mathcal{H}_A$ and $\mathcal{H}_B$ respectively such that the total state $|\Psi\rangle$ can be decomposed as

$$|\Psi\rangle = \sum_{i=1}^{n} \sqrt{\eta_i} |u_i\rangle \otimes |v_i\rangle, \tag{2.36}$$

where $n = \min(\dim(\mathcal{H}_A) = l, \dim(\mathcal{H}_B) = k)$. Equation (2.36) has n real expansion coefficients $\sqrt{\eta_i}$ related to the eigenvalues of the reduced density operators indicated above. The Schmidt bases $\{|u_i\rangle_{i=1,..,l}\}$ and $\{|v_i\rangle_{i=1,..,k}\}$ are the eigen-bases of the reduced density operators (2.34) and (2.35). These bases give us a much more compact and simple expression of $|\Psi\rangle$ [9, 23].

2.2.2 Von-Neumann Entropy

The Shannon entropy is the average information, in units of bits, which is given by the expected value of the information content over all possible events available under a given scheme, that is, the information gained, on average, by an agent witnessing its elements.
In the quantum case, information is quantified by the von-Neumann entropy, which provides the entanglement contained in a quantum state.
The standard measure of the quantum information associated with a quantum system can be found using its density operator, and the von-Neumann entropy is defined as

$$S = -Tr\left[\hat{\rho}\ln\hat{\rho}\right] = -\sum_{j}\eta_j \ln\eta_j, \tag{2.37}$$

it is a measure of the entanglement associated with a state and achieves its maximum value for the maximum entanglement.
Also, other way to measure the entanglement is the linear entropy, which gives information about the impurity of the system. The linear entropy is a linear approximation to the von-Neumann entropy and it is defined by

$$S = 1 - Tr\left[\hat{\rho}^2\right] = 1 - \sum_{j}\eta_j^2 = 1 - \gamma, \tag{2.38}$$

where γ is the purity of a state [9, 4, 23].

2.3 Electric dipole transitions

The electric dipole moment operator, between a initial electronic state of a molecule $\Psi_i(\mathbf{x},\mathbf{R})$ and a final electronic state $\Psi_f(\mathbf{x},\mathbf{R})$ is given by $\langle\Psi_f|\,\hat{\mathbf{d}}\,|\Psi_i\rangle$, where $\hat{\mathbf{d}}$ is the electric dipole moment operator. It is the sum of the electronic and nuclear contributions $\hat{\mathbf{d}} = \hat{\mathbf{d}}_{elec} + \hat{\mathbf{d}}_{nuc}$, where $\hat{\mathbf{d}}_{elec}$ and $\hat{\mathbf{d}}_{nuc}$ are given in terms of the coordinates of the electrons and the nuclei.

The electronic part of this matrix element can be evaluated by doing the integration

over electronic coordinates to obtain the **R**-dependent transition dipole moment

$$\begin{aligned}
\hat{\mathbf{d}}_{f,i}(\mathbf{R}) &= \langle \Psi_f | \, \hat{\mathbf{d}} \, | \Psi_i \rangle \, , \\
&= \langle \Psi_f | \, \hat{\mathbf{d}}_{elec} \, | \Psi_i \rangle + q \int d\mathbf{R} \, \langle \Psi_f | \mathbf{R} \rangle \, \mathbf{R} \, \langle \mathbf{R} | \Psi_i \rangle, \\
&= \langle \Psi_f | \, \hat{\mathbf{d}}_{elec} \, | \Psi_i \rangle + q \int d\mathbf{x} \int d\mathbf{R} \Psi_f(\mathbf{x}, \mathbf{R}) \mathbf{R} \Psi_i(\mathbf{x}, \mathbf{R}), \\
&= \langle \Psi_f | \, \hat{\mathbf{d}}_{elec} \, | \Psi_i \rangle + q \int d\mathbf{R} \mathbf{R} \left(\int d\mathbf{x} \, \langle \Psi_f | \mathbf{x} \rangle \, \langle \mathbf{x} | \Psi_i \rangle \right) | \mathbf{R} \, \rangle \langle \, \mathbf{R} |, \\
&= \langle \Psi_f | \, \hat{\mathbf{d}}_{elec} \, | \Psi_i \rangle + \delta_{i,f} \hat{\mathbf{d}}_{nuc}, \qquad (2.39)
\end{aligned}$$

which couple different initial and final electronic states of a molecule [2].

Chapter 3

Molecular model systems

3.1 One-dimensional hydrogen molecular ion (H_2^+)

This system is composed by two nuclei and an electron which moves along one axis, with degrees of freedom R_1, R_2 and x respectively, how is showed in the Figure (3.2). Thus, in principle the Hamiltonian of the system can be written as

$$\hat{H} = \frac{1}{2M_p}\sum_{I=1}^{2}\hat{P}_I^2 + \frac{\hat{p}_e^2}{2m_e} + \frac{Z_\alpha Z_\beta}{|\hat{R}_1 - \hat{R}_2|} - \frac{Z_\alpha e^2}{\sqrt{(\hat{x}-\hat{R}_1)^2 + a(|\hat{R}_1 - \hat{R}_2|)}} - \frac{Z_\beta e^2}{\sqrt{(\hat{x}-\hat{R}_2)^2 + a(|\hat{R}_1 - \hat{R}_2|)}}, \tag{3.1}$$

where M_p is the proton mass, m_e is the electron mass, Z_i is the charge for the i-th nucleus. Also, the function $a(|R_1 - R_2|)$ in the nucleus-electron interaction is the softening parameter (which depends on the inter-nuclear distance) for the Coulomb singularity, it is chosen to produce the exact three-dimensional $1\sigma_g$ BO potential energy curve solved in confocal elliptic coordinates [13, 29, 2].

In the Hamiltonians (3.3) amd (3.4) each term is labeled according to the the labels set in the equation (2.1).

Now, we will change the coordinates system to a center of mass system for the nuclei, where $R = |R_1 - R_2|$ and $R_{cm} = (R_1 + R_2)/2$ [11, 15]. Also, the total mass would be $M = 2M_p$ and the reduced mass $\mu' = M_p/2$ and the Hamiltonian (3.2) would be written as

$$\hat{H} = \frac{\hat{P}_{cm}^2}{2(2M_p)} + \frac{\hat{P}_R^2}{M_p} + \frac{\hat{p}_e^2}{2m_e} + \frac{Z_\alpha Z_\beta}{R} - \frac{Z_\alpha e^2}{\sqrt{(\hat{x} - \hat{R}_1)^2 + a(R)}} - \frac{Z_\beta e^2}{\sqrt{(\hat{x} - \hat{R}_2)^2 + a(R)}}, \quad (3.2)$$

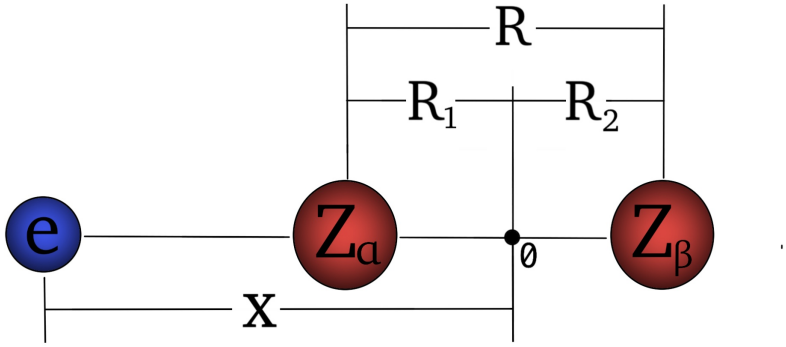

Figure 3.1:
Graphic scheme of the one-dimensional model of H_2^+, where Z_α and Z_β are the atomic charges of two nuclei, which are separated by a distance R in a center of mass reference system, and at distances R_1 and R_2 to an ordinary reference system with origin at the point 0. x is the degree of freedom associated to the electron which moves along the x-axis axis and R is the degree of freedom associated to the moving nuclei.

Finally we obtain Hamiltonian by changing the reference system for the electron, we obtain that its reduced mass is $\mu = 2M_p m_e/(2M_p + m_e)$ and discarting the movement of the center of mass, which is a cyclic variable, we obtain that the Hamiltonian with reduced dimensionality of the system is given by the equation (3.3).

$$\hat{H} = \underbrace{\frac{\hat{P}_R^2}{M_P}}_{\hat{T}_N} + \underbrace{\frac{\hat{p}_x^2}{2\mu}}_{\hat{T}_e} + \underbrace{\frac{Z_\alpha Z_\beta e^2}{\hat{R}}}_{\hat{U}_{NN}} \underbrace{- \frac{Z_\alpha e^2}{\sqrt{(\hat{x} + \hat{R}/2)^2 + a(\hat{R})}} - \frac{Z_\beta e^2}{\sqrt{(\hat{x} - \hat{R}/2)^2 + a(\hat{R})}}}_{\hat{U}_{Ne}}, \quad (3.3)$$

3.2 Shin-Metiu model

This one-dimensional model is composed by two fixed nuclei separated by a distance L and a third nucleus which is moving between the two fixed nuclei. Also an electron is moving through the whole space; along the x-axis. Thus, the system is composed by two degrees of freedom. A brief scheme is showed in the Figure (3.2) and the Hamiltonian of the Shin-Metiu model is given by

$$\hat{H} = \underbrace{\frac{\hat{P}_R^2}{2M_P}}_{\hat{T}_N} + \underbrace{\frac{\hat{p}_x^2}{2m_e}}_{\hat{T}_e} + \underbrace{\frac{Z_\alpha Z_\sigma e^2}{|\hat{R}+L/2|} + \frac{Z_\beta Z_\sigma e^2}{|\hat{R}-L/2|}}_{\hat{U}_{NN}} \underbrace{- \frac{Z_\alpha e^2\ erf(x/R_{c\alpha})}{|\hat{x}+L/2|} - \frac{Z_\beta e^2\ erf(x/R_{c\beta})}{|\hat{x}-L/2|} - \frac{Z_\sigma e^2\ erf(x/R_{c\sigma})}{|\hat{x}-\hat{R}|}}_{\hat{U}_{Ne}}, \tag{3.4}$$

where where M_p is the proton mass, m_e is the electron mass, Z_i is the charge for the i-th nucleus, $erf(x/R_{ci})$ is the error function which screen the Coulomb potential and R_{ci} is a screening parameter in the pseudo-potential which is used as an adjustable parameter, to generate a variety of potential energy curves for the moving ion. By increasing R_{ci}, we diminish the ability of the moving ion to bind the electron, and this has a strong effect on the adiabatic energy curve [25, 24].

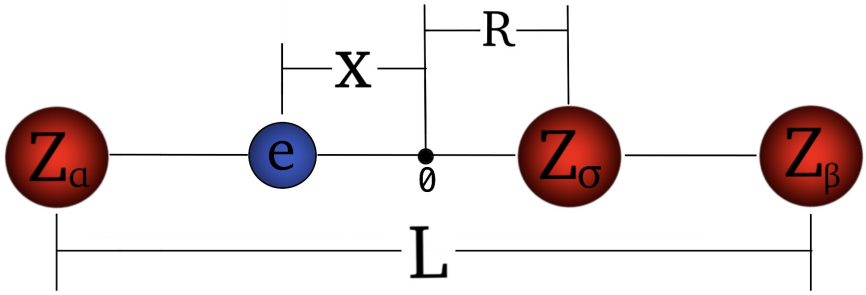

Figure 3.2:
Graphic scheme of the Shin-Metiu model, where Z_α and Z_β are the atomic numbers of the two nuclear charges located at a fixed distance L, and Z_σ is the atomic number of the moving nucleus. x is the degree of freedom associated to the electron which moves through the whole x-axis and R is the degree of freedom associated to the moving nucleus with charge Z_σ which moves between the two fixed nuclei.

Chapter 4

Methodology

For our computations, we have used the programming language python, version 3.7.0, using the Jupyter Notebook IDLE and the diagonalization routines of Scipy associated with the package Lapack.

4.1 Fourier Grid Hamiltonian (FGH) Method

The Fourier grid Hamiltonian method is an extremely simple numerical variational technique for calculating the bound state eigenvalues and eigenfunctions of the Schrödinger equation. The method can yield highly accurate eigenvalues and eigenvectors.
This is the simplest method within the family of discrete variable representation (DVR) methods which no explicit matrix transformations are required.
We start by considering the non-relativistic Hamiltonian of a particle with mass m under the presence of an external potential

$$\hat{H} = \frac{\hat{p}_x^2}{2m} + \hat{V}(\hat{x}), \tag{4.1}$$

and finding the Hamiltonian representation on the position representation, using the following properties

- $\hat{x}\,|x\rangle = x\,|x\rangle\,, \qquad \langle x'|x\rangle = \delta(x'-x) \qquad \text{and} \qquad \hat{I}_x = \int dx|x\,\rangle\langle\,x|.$
- $\hat{p}_x\,|k\rangle = k\hbar\,|k\rangle\,, \qquad \langle k'|k\rangle = \delta(k'-k) \qquad \text{and} \qquad \hat{I}_k = \int dk|k\,\rangle\langle\,k|.$

- $\langle k|x\rangle = \frac{1}{\sqrt{2\pi}} e^{-ikx}$.

We obtain that

$$\langle x|\,\hat{H}\,|x'\rangle = \frac{1}{2\pi}\int dk e^{-ik(x-x')} \underbrace{T_k}_{\frac{\hbar^2 k^2}{2m}} + V(x)\delta(x-x'). \tag{4.2}$$

Thus, the objective is to replace the continuous range of coordinate values x by a grid of discrete values x_i. We will use a uniform discrete grid of x_i values defined by

$$x_i = i\Delta x, \tag{4.3}$$

the grid size $L = N\Delta x$ and spacing Δx chosen in coordinate space determines the reciprocal grid size in momentum space. The total length of the coordinate space covered by the grid is $N\Delta x$. This length determines the longest wavelength and therefore the smallest frequency, which occurs in the reciprocal momentum space

$$\begin{aligned} \Delta k &= 2\pi/\lambda_{max}, \\ \Delta k &= 2\pi/N\Delta x. \end{aligned} \tag{4.4}$$

We now define an integer n by the relationship $2n = (N-1)$, where N is the (odd) number of grid points in the spatial grid. The basic bras and kets of the discretized coordinate space give the value of a wave function at the grid points

$$\langle x_i|\psi\rangle = \psi(x_i) = \psi_i, \tag{4.5}$$

and the normalization condition would change following the property

$$\int dx\psi^*(x)\psi(x) = 1 \quad \Rightarrow \quad \Delta x \sum_{i=1}^{N} \psi^*(x_i)\psi(x_i) = 1, \tag{4.6}$$

thus, manipulating the equation (4.2) into a discrete representation, one can find that

$$H_{i,j} = \frac{1}{\Delta x}\left[\frac{2}{N}\sum_{l=1}^{N} cos\left(2\pi l(i-j)/N\right) T_l + V(x_i)\delta_{i,j}\right], \tag{4.7}$$

where $T_l = \hbar^2/(2m)(l\Delta k)^2$.
The expectation value of the energy corresponding to the state function $|\psi\rangle$ is

$$E = \frac{\langle\psi|\,\hat{H}\,|\psi\rangle}{\langle\psi|\psi\rangle} = \frac{\sum_{ij}\psi_i^*\Delta x H_{i,j}\Delta x\psi_j}{\Delta x\sum_i|\psi_i|^2}, \tag{4.8}$$

now, one can define a re-normalized Hamiltonian matrix by

$$H^0_{i,j} = \frac{2}{N}\sum_{l=1}^{N} cos\left(2\pi l(i-j)/N\right)T_l + V(x_i)\delta_{i,j}, \tag{4.9}$$

and in terms of this re-normalized Hamiltonian matrix, the expectation value of the energy now reads

$$E = \frac{\langle\psi|\,\hat{H}\,|\psi\rangle}{\langle\psi|\psi\rangle} = \frac{\sum_{ij}\psi_i^* H^0_{i,j}\psi_j}{\sum_i|\psi_i|^2}. \tag{4.10}$$

Minimizing this energy with respect to variation of the coefficients ψ_i yields the standard set of secular equations

$$\sum_j\left[H^0_{i,j} - E_\lambda\delta_{i,j}\right]\psi_j^\lambda = 0, \tag{4.11}$$

and the normalization condition for the Hamiltonian $H^0_{i,j}$ (equation (4.9)) is given by $\sum_i|\psi_i|^2 = 1$ [18].

In this work, the electronic and nuclear Hamiltonians (equations (2.3) and (2.6) respectively) are written according to the Hamiltonian matrix form (4.9), and diagonalized according to the eigenstate, eigenvalue equation (4.11).

4.2 One-dimensional hydrogen molecular ion (H_2^+)

This system has been solved using the FGH method for the values in Table 4.1[1].

[1]For this parameters, the energy of the equilibrium separation between the nuclei compared with the 3D H_2^+ molecule has a precision of 10^{-3} *a.u.*

[2]The proton box has a much larger number of points because we have represented more excited states for the nuclear problem, i.e. states with a larger number of oscillations. In the electronic problem we have represented just the first four states, which do not have a larger number of oscillations, thus we needed less points to represent it.

Parameters	Values
Atomic Numbers (Z)	-
Z_α	1
Z_β	1
Electron charge (e)	1
Masses	-
Protons Masses (M_p)	1836
Electron Mass (m_e)	1
FGH Parameters	-
Electron box size (x)	100
Electron box number of points (N)	601
Proton box size (R)	25
Proton box number of points [2](NN)	701

Table 4.1: Parameters for the one dimensional model of H_2^+, for the Hamiltonian and for the FGH numerical method used in this work.
All parameters are in atomic units (Bohr radius (a_0) = elementary charge (e) = Plank constant ($\hbar$) = Electron mass (m_e) = 1).

4.2.1 Calculations within the BO approximation

First we find the parametrized function $a(R)$ of the soft-Coulomb potential, by solving the one-dimensional electronic Schödinger equation and using a set of different values of $a(R)$ for a fixed inter-nuclear distance R, thus adjusting the value value of $a(R)$ that minimizes the difference between the 1D electronic energy $E^{(0)}_{elec}(R)$ and the 3D exact electronic energy for the state $1s\sigma_g$.

Next, we found the electronic curves $E_n(R)$ and their electronic wave functions for different inter-nuclear distances in the FGH electronic representation. It is clear that the function $a(R)$ is different for each electronic state n and it must be adjusted accordingly. For each separated electronic state n, we also may find the BO vibrational wave functions by solving the nuclear Schödinger equation in the FGH nuclear representation.

Once the electronic and nuclear wave functions are obtained for each inter-nuclear distance R, we can build the density operator for the molecular model system, within the FGH grid representation. For that, we find the reduced density operators (equations (2.34) and (2.35)) for each electro-nuclear BO pure state, whose wave functions follow the form of the equation (2.8).

- Reduced density operator $\hat{\rho}^{(R)}$ for the nuclear motion. According with the equation (2.34), we build the reduced density operator $\hat{\rho}^{(R)}$ for a electro-nuclear state as

$$\begin{aligned}\hat{\rho}^{(R)} &= \hat{T}r_x\left[\hat{\rho}\right] = \int dx \left\langle x|\Psi\right\rangle \left\langle \Psi|x\right\rangle, \\ &= \int dR'' \int dR' \left(\int dx \left\langle x, R''|\Psi\right\rangle \left\langle \Psi|x, R'\right\rangle \right) |R''\rangle \left\langle R'\right|, \\ &= \int dR'' \int dR' \int dx \phi_n(x;R'')\chi_{n,m}(R'')\phi_n^*(x;R')\chi_{n,m}^*(R') \left|R''\right\rangle \left\langle R'\right|. \end{aligned} \quad (4.12)$$

  Thus, the matrix element $\hat{\rho}_{i,j}^{(R)}$ corresponds to the projection of the density operator on the elements R_i and R_j respectively on the FGH nuclear base.

$$\left\langle R_i\right| \hat{\rho}^{(R)} \left|R_j\right\rangle = \hat{\rho}_{i,j}^{(R)} = \chi_{n,m}(R_i)\chi_{n,m}^*(R_j) \int dx \phi_n(x;R_i)\phi_n^*(x;R_j). \quad (4.13)$$

- Reduced density operator $\hat{\rho}^{(x)}$ for the electronic motion. According with the equation (2.35), we build the reduced density operator $\hat{\rho}^{(R)}$ for a electro-nuclear state as

$$\begin{aligned}\hat{\rho}^{(x)} &= \hat{T}r_R\left[\hat{\rho}\right] = \int dR \left\langle R|\Psi\right\rangle \left\langle \Psi|R\right\rangle, \\ &= \int dx'' \int dx' \left(\int dR \left\langle x'', R|\Psi\right\rangle \left\langle \Psi|x', R\right\rangle \right) |x''\rangle \left\langle x'\right|, \\ &= \int dx'' \int dx' \int dR \phi_n(x'';R)\chi_{n,m}(R)\phi_n^*(x';R)\chi_{n,m}^*(R) \left|x''\right\rangle \left\langle x'\right|. \end{aligned} \quad (4.14)$$

  The matrix element $\hat{\rho}_{i,j}^{(x)}$ corresponds to the projection of the density operator on the elements x_i and x_j respectively on the FGH electronic base.

$$\left\langle x_i\right| \hat{\rho}^{(x)} \left|x_j\right\rangle = \hat{\rho}_{i,j}^{(x)} = \int dR \phi_n(x_i;R)\phi_n^*(x_j;R)\chi_{n,m}(R)\chi_{n,m}^*(R). \quad (4.15)$$

Thus, diagonalizing the density matrix (4.13) and (4.15) with the FGH bases selected, we have a reduced density matrix for the nuclear motion with size 701x701 and for the electronic motion with size 601x601. These two matrices are isospectral, which means that 100 nuclear eigenvalues are zero. With the non-zero eigenvalues and eigenvectors, one may compose the total wave functions in the Schmidt form, according to the equation (2.36), where the electronic Schmidt bases now do not depend parametrically on the nuclear geometry. Also with the non-zero eigenvalues one may compose the von-Neumman and linear entropies, according to the equations (2.37) and (2.38).

4.2.2 Calculations using the Born-Huang expansion

For this system the non-adiabatic couplings among the lowest electronic states are very small, the BO states are a rather good approximation for the one-dimensional model of H_2^+, this is explained in detail in Chapter 5.

To find the non-adiabatic couplings according to the off-diagonal Hellmann-Feynman theorem, we found that the derivative of the electronic Hamiltonian with respect to the nuclear coordinate R is given by

$$\frac{\partial}{\partial R}\hat{H}_e = -\frac{Z^2e^2}{R^2} + \frac{Z^2e^2}{2}\left[\frac{(r+R/2)+a'(R)}{\left((r+R/2)^2+a(R)\right)^{3/2}} + \frac{(-r+R/2)+a'(R)}{\left((r-R/2)^2+a(R)\right)^{3/2}}\right]. \quad (4.16)$$

With the expression (4.16) and the equation (2.15) we have computed the $A_{n,n'(R)}$ matrix elements for the first three electronic states.
Next, we have computed the $B_{n,n'(R)}$ matrix elements according to the equation (2.19) and using a completeness relation with the first three electronic wave functions.

4.3 Shin-Metiu molecular model

This system has been solved using the FGH method and the values for the table 4.2 [3]

4.3.1 Calculations within the BO approximation

We compute the electronic potential energy curves $E_n(R)$ and the corresponding electronic wave functions for a set of nuclear configurations R using the FGH representation for the electronic coordinates. Also, for each potential energy curve $E_n(R)$ of the n-th electronic state, we compute the associated BO vibrational wave functions $\chi_{n,m}(R)$ in the FGH nuclear representation.

[3]For this parameters, the energy of the global minimum of the first energy potential curve $E_0(R)$ converges to an energy value with a precision of 10^{-3} $a.u.$

[4]The proton box has a much larger density of points because we have represented more excited states for the nuclear problem, i.e. states with a larger number of oscillations. In the electronic problem we have represented just the first five states, which do not have a larger number of oscillations, thus we needed a less density of points to represent it.

Parameters	Values
Atomic Numbers (Z)	-
Z_α	1
Z_β	1
Z_σ	1
Electron charge (e)	1
Masses	-
Protons Masses (M_p)	1836
Electron Mass (m_e)	1
Separation of the fixed protons (L)	18.9
Softening parameter R_{ci}	-
$R_{c\alpha}$	3.0
$R_{c\beta}$	2.2
$R_{c\sigma}$	4.0
FGH Parameters	-
Electron box size (x)	160
Electron box number of points[4](N)	605
Proton box size (R)	L-0.2
Proton box number of points (NN)	301

Table 4.2: Parameters foe the Shin-Metiu model, for the Hamiltonian and for the FGH numerical method used in this work.
All parameters are in atomic units (Bohr radius (a_0) = elementary charge (e) = Plank constant ($\hbar$) = Electron mass (m_e) = 1).

With these BO total wave functions, composed as a simple product, we compute the density operator and the reduced density operators (equations (4.13) and (4.15)), which are then diagonalized. Under the same arguments explained in the subsection 4.2.1 we compute the Schmidt bases and the von-Neumman and linear entropy.

4.3.2 Calculates on BH approximation

For this system, the derivative of the electronic Hamiltonian with respect to the nuclear coordinate R is

$$\begin{aligned}\frac{\partial}{\partial R}\hat{H}_e &= Z_\sigma^2 e^2\left[\frac{(L/2-R)}{|L/2-R|^3}-\frac{(L/2+R)}{|L/2+R|^3}\right] \\ &- Z_\sigma^2 e^2\frac{R-x}{|R-x|^2}\left[\frac{2}{\sqrt{\pi}R_{c\sigma}}\exp\left(-\frac{(R-x)^2}{R_{c\sigma}^2}\right)-\frac{1}{|R-x|}erf\left(\frac{|R-x|}{R_{c\sigma}}\right)\right] \qquad (4.17)\end{aligned}$$

With the expression (4.17) and the equation (2.15) we have calculated the $A_{n,n'(R)}$ matrix elements for the first three electronic states.
Next, we have computed the $B_{n,n'(R)}$ matrix elements according to the equation (2.19) and using a completeness relation with the first ten electronic wave functions[5], this is reason why the Born-Huang method computed in this work is an approximation.
With this, we have solved the equation (2.21) finding the form of the total wave function and finding its representation in the BO basis according to the equation (2.23), where we have used the first one hundred BO nuclear wave functions [6] for each electronic curve $\{\phi_n(x;R)\}_{n=0,1,2}$.

Once the electro-nuclear wave functions are obtained, we can build the density operator for the molecular model system, within the FGH grid representation. For that, we find the reduced density operators (equations (2.34) and (2.35)), using the same steps in the subsection 4.2.1, for each electro-nuclear pure state, whose wave functions follow the form of the equation (2.9).

[5]From this number of electronic wave functions using in the completeness relation the $B_{n,n'(R)}$ matrix elements do not vary for this molecular system.

[6]We use this number of BO wave functions because with this the calculation we may reach and represent correctly the BH wave functions.

1. Reduced density operator $\hat{\rho}^{(R)}$ for the nuclear motion.

$$\langle R_i | \hat{\rho}^{(R)} | R_j \rangle = \hat{\rho}^{(R)}_{i,j} = \sum_{n,m} f_n(R_i) f^*_m(R_j) \int dx \phi_n(x; R_i) \phi^*_m(x; R_j). \tag{4.18}$$

2. Reduced density operator $\hat{\rho}^{(x)}$ for the electronic motion.

$$\langle x_i | \hat{\rho}^{(x)} | x_j \rangle = \hat{\rho}^{(x)}_{i,j} = \sum_{n,m} \int dR \phi_n(x_i; R) \phi^*_m(x_j; R) f_n(R) f^*_m(R). \tag{4.19}$$

Chapter 5

Results on Electro-Nuclear Entanglement within the BO approximation.

5.1 One-dimensional hydrogen molecular ion (H_2^+)

5.1.1 Entanglement within the Born-Oppenheimer approximation

We solved the Schrödinger equation for the electronic problem at different nuclear configurations, to obtain the potential energy curves $E_0(R)$, $E_1(R)$, $E_2(R)$ and $E_3(R)$ for the nuclear problem. In the Figure (5.1), we may see the comparison between the ground state curve for the one-dimensional model of H_2^+ and the three dimensional H_2^+

For this system, the equilibrium separation of the nuclei occurs at $R_e = 2.000\ a.u.$ and the dissociation energy has a value of $E = 0.500\ a.u.$ for the ground state.
We also see in the Figure (5.1) that the green and the blue energy surfaces ($E_0(R)$ and $E_2(R)$) are bonding curves, i.e. attractive potentials, while the orange and red energy surfaces ($E_1(R)$ and $E_3(R)$) are anti-bonding curves, i.e. dissociative potentials.
For the three dimensional molecule of H_2^+, only the potential energy curves $1s\sigma_g$ and $3d\sigma_g$ has bonded states, the potential energy curves $E_2(R)$ is approximately good and it is because the softening parameter $a(R)$ only adjust the first potential energy curve, not the others. The calculations developed for the potential energy curve $E_2(R)$ and its BO nuclear states are just illustrative, this curve does not have a complete a physical meaning.

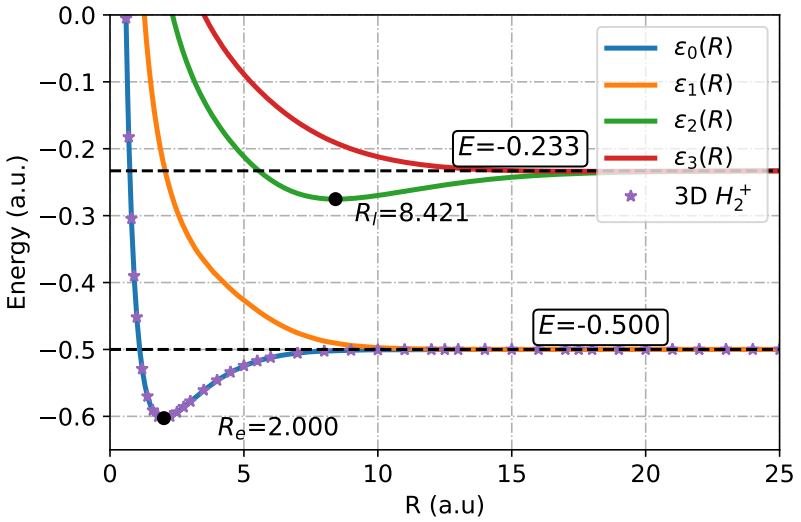

Figure 5.1:
Potential energy curves $E_n(R)$ of the 1D hydrogen molecular ion for the four lowest states. The soft parameter $a(R)$ has been adjusted only to fit the exact ground state $1s\sigma_g$ energy of the 3D H_2^+ molecule. The minimum is located at $R_e = 2.000$ $a.u.$, and the energy of the potential energy curves $E_0(R)$ and $E_1(R)$ converge asymptotically to $E = 0.500$ $a.u.$

We can see how the electronic wave functions and the potential energy changes to different nuclear configurations around the equilibrium position of the nuclear curve $E_0(R)$. In the Figures (5.2A) and (5.2B) we may see how the potential well changes around the the equilibrium separation of the nuclei ($R = 2.000$ $a.u.$), where before this value the energy well has one minimum and above it has two minima values.

We have also determined the R dependence in the transition dipole matrix elements between the three lowest electronic states $\phi_0(x, R)$, $\phi_1(x, R)$ and $\phi_2(x, R)$, how is showed in the Figure (5.3). In the dipole transition $d_{i,i}(R)_{\{i=0,1,2\}}$ are not equal to zero due to the last term in the equation (2.39). The transitions between the states $\phi_0(x, R)$ and $\phi_2(x, R)$ is equal to zero for any value of R and the dipole transitions between the states $\phi_1(x, R)$ and $\phi_1(x, R)$ converges to zero when the internuclear separation increases. Finally the dipole transitions between the states $\phi_0(x, R)$ and $\phi_1(x, R)$ diverges

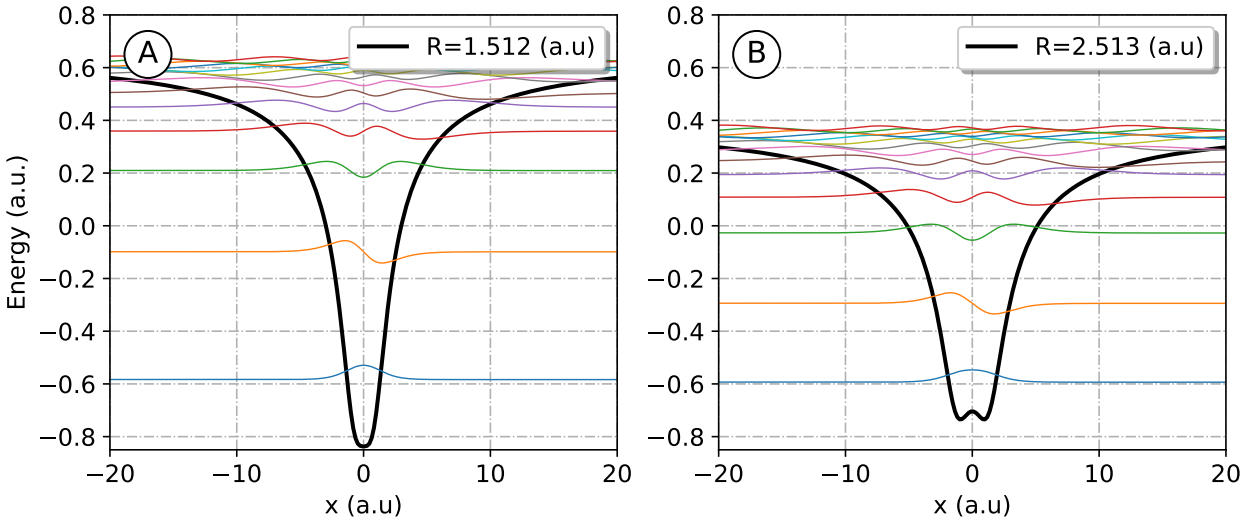

Figure 5.2:
Electronic wave functions for two different nuclear configurations around the equilibrium internuclear separation in the ground energy curve $E_0(R)$. The Figure A has the electronic wave functions for an internuclear separation of $R = 1.512$ $a.u.$ The Figure B has the electronic wave functions for an internuclear separation of $R = 2.513$ $a.u.$

Solving the nuclear Hamiltonian for the energy surfaces $E_0(R)$ and $E_2(R)$ because in this model they are attractive potentials, we find their vibrational wave functions $\chi_{0,m}$ and $\chi_{2,m}$ and their total energies W_m.
In the Figure (5.4A), we have showed the discrete spectrum for the energy surface $E_0(R)$. The discrete spectrum occurs to energies less than $E = -0.500$ $a.u.$, i.e. the first eighteen vibrational wave functions belong to the discrete spectrum.
In the Figure (5.4B), we have showed the first four vibrational wave functions[1] of the discrete spectrum for the energy surface $E_2(R)$. The discrete spectrum for this case occurs to energies less than $E = -0.233$ $a.u.$, i.e. the first twenty seven vibrational wave functions.

The entropy of the vibrational wave functions which belongs to the energy curves $E_0(R)$ and $E_2(R)$ are showed in the Figures (5.5A) and (5.5B) respectively.

[1]The energy difference between this vibrational states is very short, plot the whole discrete spectrum would made indistinguishable the vibrational wave functions.

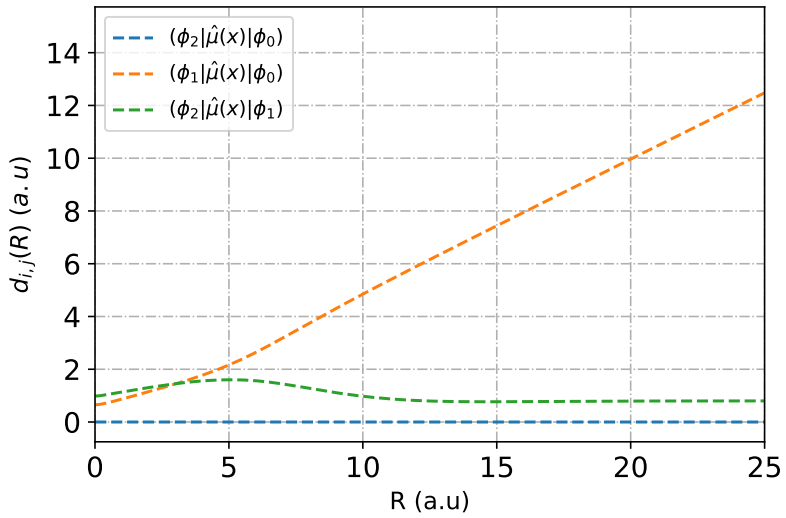

Figure 5.3:
Permanent dipole moment between the electronic states $\phi_0(x, R)$, $\phi_1(x, R)$ and $\phi_2(x, R)$ in a FGH nuclear box of 25 $a.u.$

In the Figure (5.5A), we may see how both linear and von-Neumann entropy increase smoothly between the first eighteen molecular wave functions (states with energies less than $E = -0.5$ $a.u.$). This increase of the entropy is because for the fixed electronic wave function $\phi_0(x; R)$, the increasing in the number of the vibrational wave function (higher energies) increases the number of oscillations on it, thus increasing entropy. For vibrational wave functions with energies larger than $E = -0.5$ $a.u.$ (continuous spectrum), the entropy increase abruptly, this states have a very large number of oscillations compared with the bound states. In Table 5.1 we have showed the first four eigenvalues of the reduced density matrices for the Schmidt decomposition and the corresponding values of entropy (von-Neumann and linear)

In the Figure (5.5B), we may see how both linear and von-Neumann entropy increase monotonically, between the first seventeen molecular wave functions, but faster than those corresponding to the ground state. This increase of the entropy is because for the fixed electronic wave function $\phi_2(x; R)$, the increasing in the number of the vibrational wave function (higher energies) increases the number of oscillations on it. Also the energy curve $E_2(R)$ is wider than the $E_0(R)$, making that the vibrational wave functions $\chi_{2,i}(R)$ be

State	Eigenvalues η_i				Entropies	
$\phi_0(x;R)\chi_{0,m}(R)$	$i=1$	$i=2$	$i=3$	$i=4$	S_{vN}	S_L
$m=0$	0.998	0.002	0.000	0.000	0.013	0.003
$m=1$	0.995	0.005	0.000	0.000	0.030	0.009
$m=2$	0.992	0.008	0.000	0.000	0.046	0.016
$m=3$	0.989	0.011	0.000	0.000	0.062	0.022
$m=4$	0.985	0.014	0.000	0.000	0.077	0.029
$m=5$	0.982	0.018	0.000	0.000	0.092	0.036
$m=6$	0.978	0.022	0.000	0.000	0.107	0.043
$m=7$	0.974	0.026	0.000	0.000	0.123	0.051
$m=8$	0.969	0.030	0.001	0.000	0.140	0.059
$m=9$	0.964	0.035	0.001	0.000	0.159	0.070
$m=10$	0.958	0.041	0.001	0.000	0.179	0.080
$m=11$	0.951	0.048	0.001	0.000	0.202	0.094
$m=12$	0.942	0.056	0.002	0.000	0.229	0.109
$m=13$	0.933	0.065	0.002	0.000	0.258	0.126
$m=14$	0.919	0.078	0.003	0.000	0.297	0.150
$m=15$	0.904	0.091	0.005	0.000	0.338	0.174
$m=16$	0.889	0.102	0.008	0.001	0.381	0.199
$m=17$	0.871	0.112	0.015	0.002	0.441	0.228

Table 5.1: Highest four eigenvalues of the reduced density matrices for the Schmidt decomposition of the total wave function $\phi_0(x;R)\chi_0, m(R)$ with $(m=0,...,17)$ i.e., the BO wave functions of the discrete spectrum. The von Neumann S_{vN} and linear S_L entropies for each state are included in the last two columns.

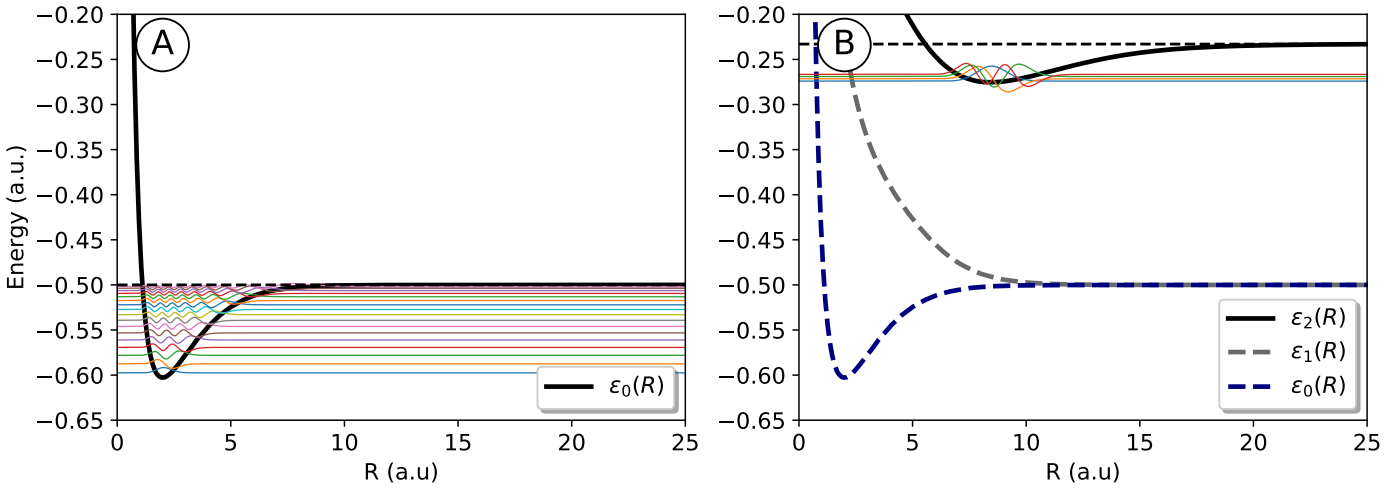

Figure 5.4:
Figure A: vibrational wave functions for the energy surface $E_0(R)$. The vibrational wave functions with energy less than $E = -0.500$ *a.u.*, the first eighteen, belong for the discrete spectrum. Figure B: First four vibrational wave functions for the energy surface $E_2(R)$. The vibrational wave functions with energy less than $E = -0.233$ *a.u.*, the first twenty seven, belong for the discrete spectrum.

wider than vibrational wave functions $\chi_{0,i}(R)$.

Now, in order to analyze the electo-nuclear entanglement within BO states, we also analyze the Schmidt decomposition for two specific cases, for illustrative purposes; the lowest and highest bound states for the potential energy curve $E_0(R)$ and the lowest and middle bound states for the potential energy curve $E_2(R)$.

1. Electronic ground state $\phi_0(x;R)$

   (a) BO state $\phi_0(x,R)\chi_{0,0}(R)$. We see in the Figure (5.6) how this wave functions may be separated approximately as $\Psi(x,R) \sim u_1(x)v_1(R) \sim \phi_0(x;R=2.000)\chi_{0,0}(R)$, i.e. the BO wave function (with a parametric dependence on R in the electronic wave function, evaluated only at the equilibrium distances $R = 2.000$ *a.u.*)

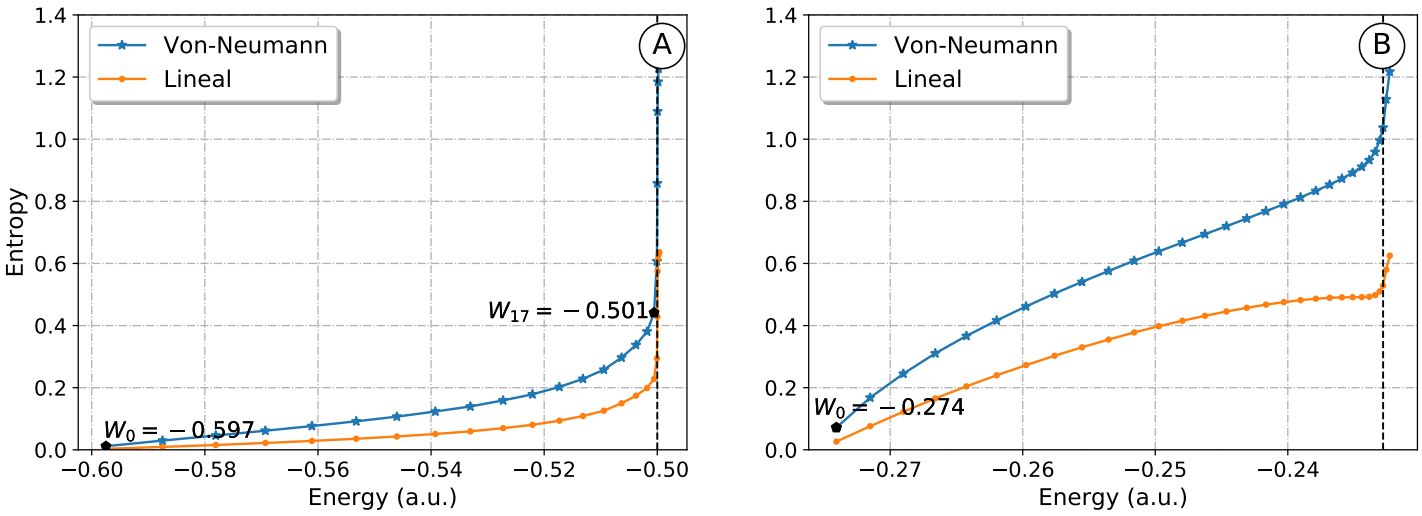

Figure 5.5:
Figure A: von-Neumann and linear entropy for the molecular wave functions $\phi_0(x;R)\chi_{0,n}(R)$ for the different lowest eigthteen bound vibrational eigenstates in the energy potential curve $E_0(R)$. Total BO energies $W_0 = -0.597$ $a.u.$ and $W_{17} = -0.501$ $a.u.$ are indicated for the lowest and highest bound states. Figure B: von-Neumann and linear entropy for the molecular wave functions $\phi_2(x;R)\chi_{2,n}(R)$ for the different lowest eigthteen bound vibrational eigenstates in the energy potential curve $E_2(R)$. Total BO energies $W_0 = -0.274$ $a.u.$ and $W_{13} = -0.246$ $a.u.$ are indicated for the lowest and middle bound states.

can be approximately expressed as the first term in the Schmidt decomposition ($\eta_1 \sim 1$), a direct product of a nuclear basis and an electronic basis (without parametric dependence).
In fact, in the Figure (5.6) we may see that the electronic Schmidt function $u(x)$ and the BO electronic wave function $\phi_0(x;R)$ evaluated at the equilibrium distance largely overlap. In fact, the nuclear wave function acts as a R-weigth factor for the electronic wave function and it enhances the contribution around the equilibrium distance for the ground state.

(b) BO state $\phi_0(x;R)\chi_{0,17}(R)$. We see in the Figure (5.7) how this wave functions can not be separated as a single Schmidt product of an electronic function $u(x)$

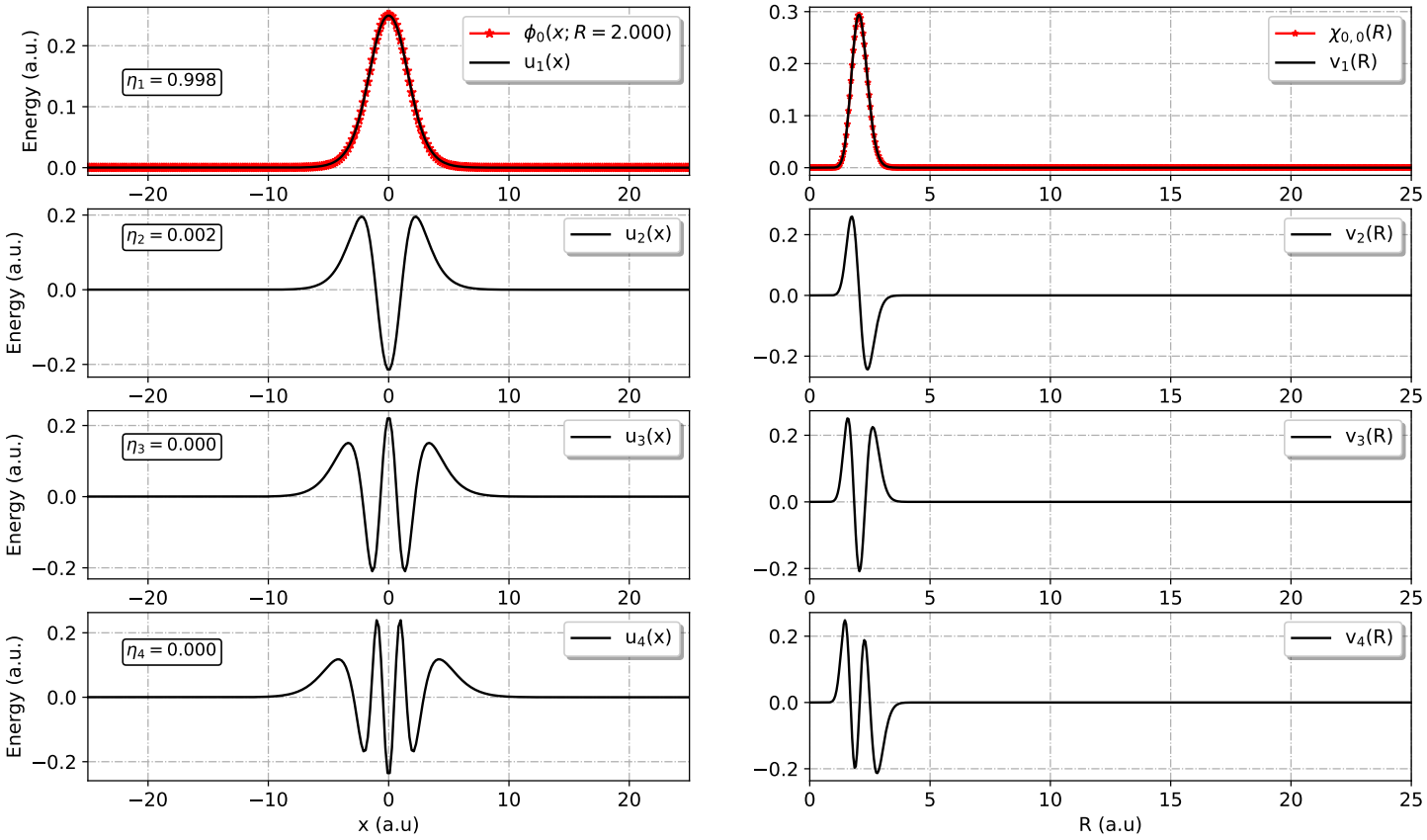

Figure 5.6:
First four lowest eigenfunctions and eigenvalues of the electronic and vibrational reduced density operators (Schmidt bases) for the BO wave function $\Psi(x, R) = \phi_0(x; R)\chi_{0,0}(R)$.

times a vibrational function $v(R)$. This because for this highly excited vibrational state, the highest eigenvalue is $\eta_1 = 0.871$. The von-Neumann entropy for this state has the highest value for the discrete spectrum, but this value is still rather small since most of these bound states are still poorly correlated (at least there are two important eigenvalues, and from them the first dominates).

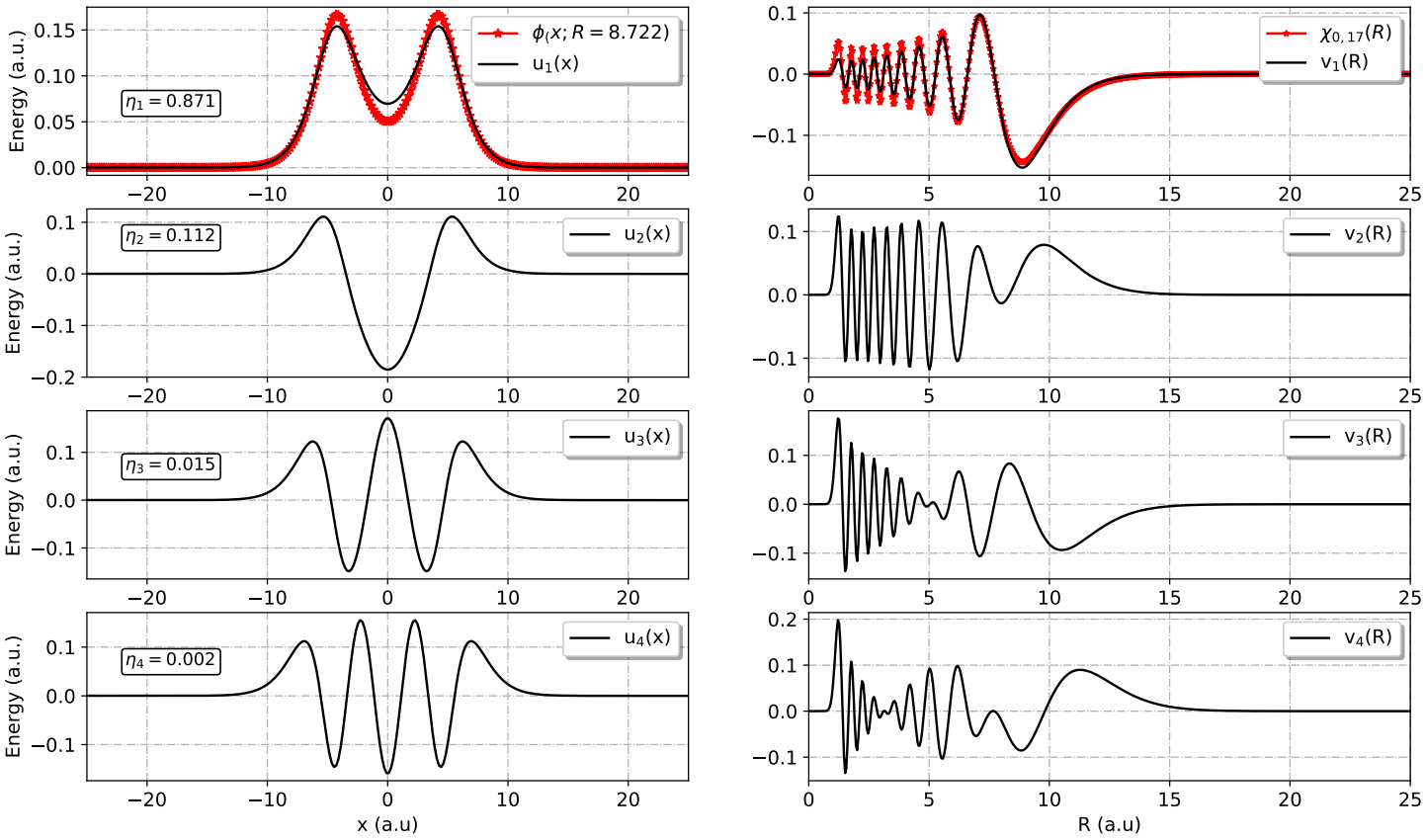

Figure 5.7:
First four lowest eigenfunctions and eigenvalues of the electronic and vibrational reduced density operators (Schmidt bases) for the BO wave function $\Psi(x, R) = \phi_0(x; R)\chi_{0,17}(R)$.

2. Electronic second excited state $\phi_2(x; R)$.

   (a) BO state $\phi_2(x, R)\chi_{2,0}(R)$. We see in the Figure (5.8) how this wave functions may be separated approximately as $\Psi(x, R) \sim u_1(x)v_1(R) \sim \phi_2(x; R = 8.421)\chi_{2,0}(R)$, i.e. the BO wave function (with a parametric dependence on R in the electronic wave function, evaluated only at the equilibrium distance $R = 8.421$ *a.u.* for the

potential energy curve$E_2(R)$) can be approximately expressed as the first term in the Schmidt decomposition ($\eta_1 \sim 1$), a direct product of a nuclear basis and an electronic basis (without parametric dependence).
In fact, in the Figure (5.8) we may see that the electronic Schmidt function $u(x)$ and the BO electronic wave function $\phi_2(x;R)$ evaluated at the equilibrium distance largely overlap. In fact, the nuclear wave function acts as a R-weigth factor for the electronic wave function and it enhances the contribution around the equilibrium distance for the ground state.

(b) BO state $\phi_2(x,R)\chi_{2,13}(R)$. We see in the Figure (5.9) how this wave functions cannot be separated as a direct product of an electronic and vibrational Schmidt functions. This state has two important eigenvalues of the Schmidt decomposition; $\eta_1 = 0.701$ and $\eta_2 = 0.278$. Thus, η_2 has a significant weight in the Schmidt decomposition.

The total BO wave functions for different electro-nuclear states are showed in the Figures (D.1) in the Appendix D.

5.1.2 Born-Huang calculations

To the calculates within the BH method, we start calculating the non-adiabatic couplings A and B.

In the Figures (5.10) and (5.11), we have showed the non-adiabatic couplings A and B respectively. Non-adiabatic couplings among the lowest electronic states in the one-dimensional model of H_2^+ are very small, since no avoided crossings between the curves are present. This is why BO is a rather good approximation for the one-dimensional model of H_2^+, and the BH expansions would add negligible corrections. We better move to another model in which corrections beyond the BO are relevant, the Shin-Metu molecular model.

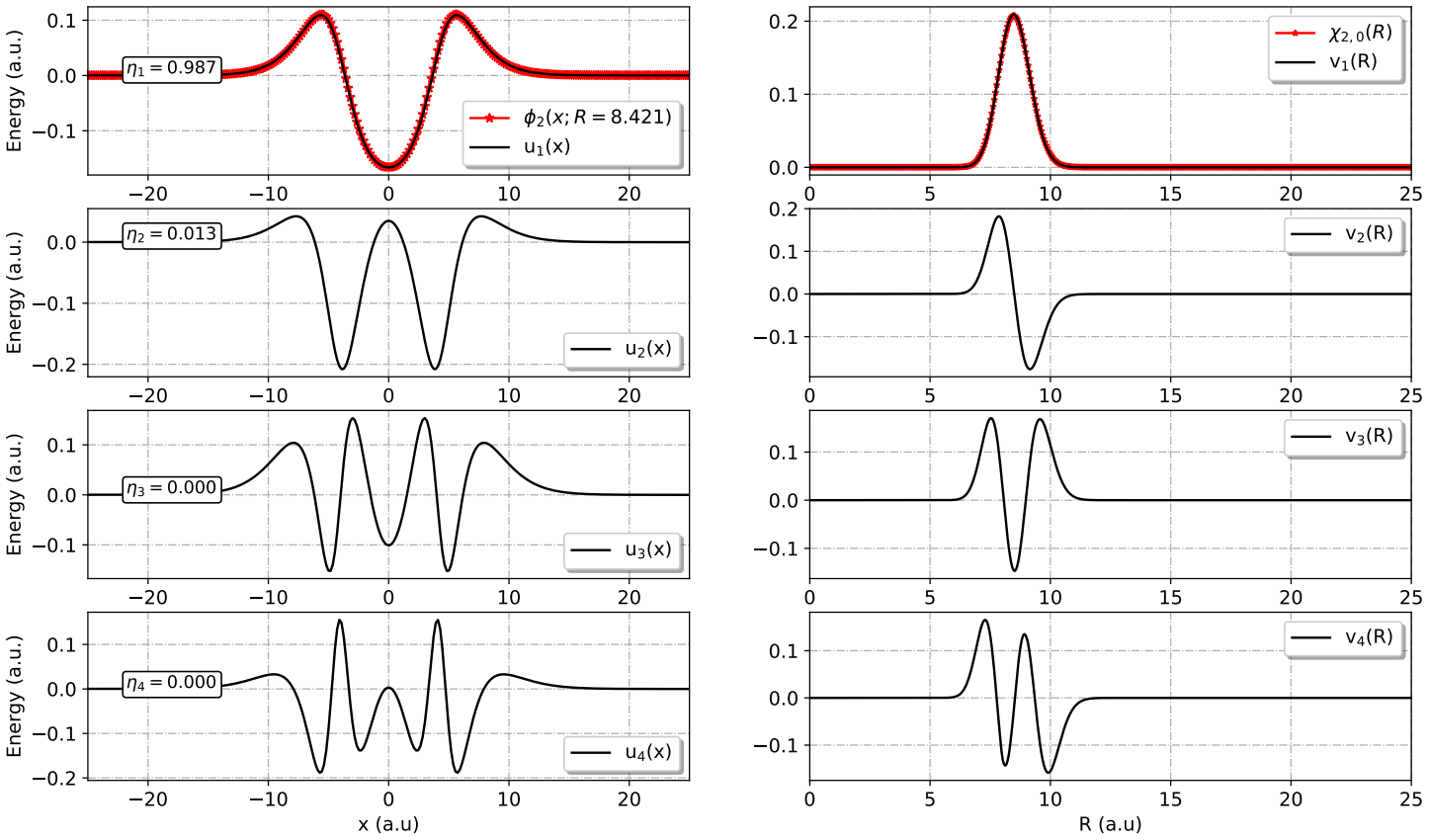

Figure 5.8:
First four lowest eigenfunctions and eigenvalues of the electronic and vibrational reduced density operators (Schmidt bases) for the BO wave function $\Psi(x, R) = \phi_2(x; R)\chi_{2,0}(R)$.

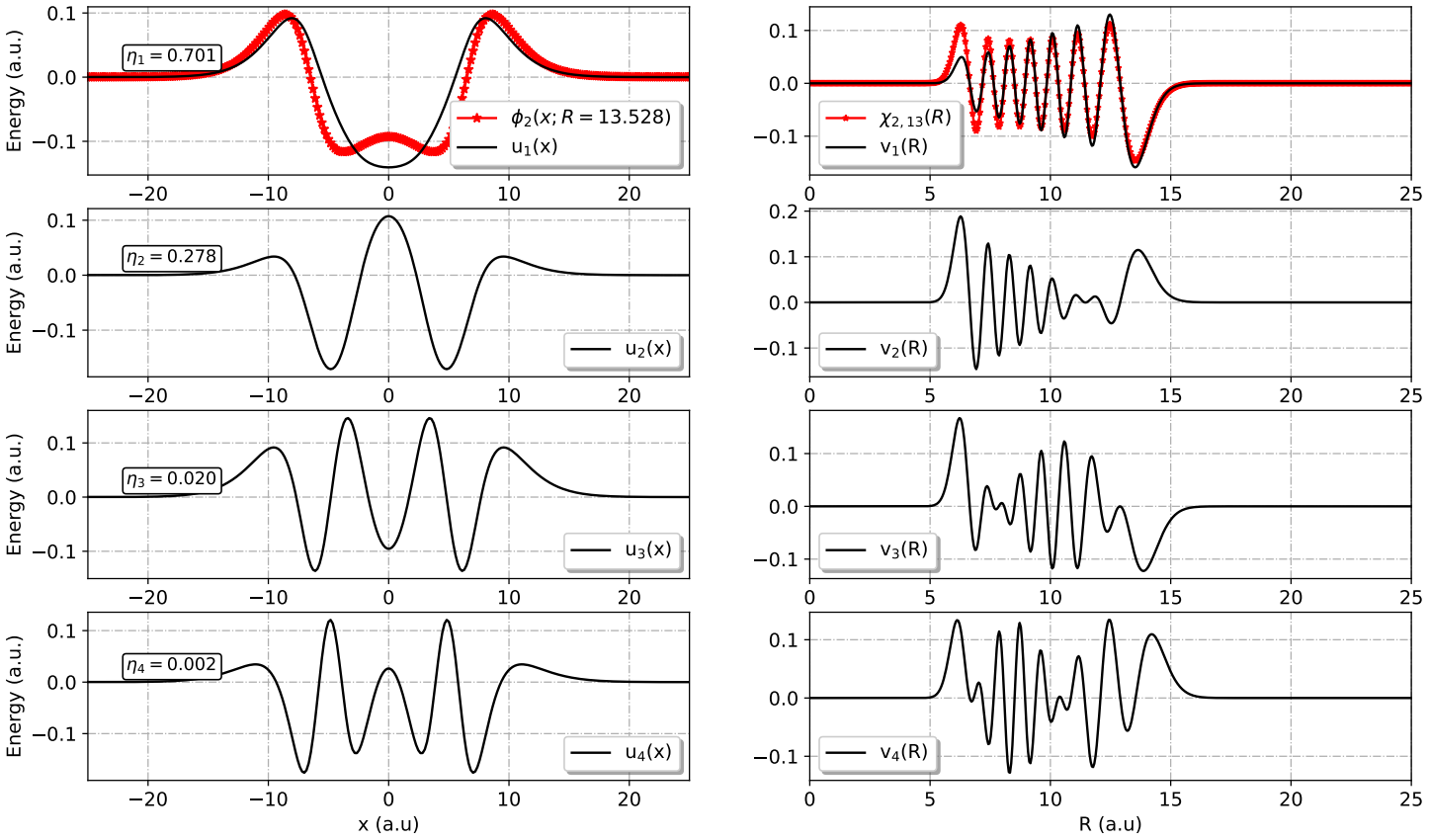

Figure 5.9:
First four lowest eigenfunctions and eigenvalues of the electronic and vibrational reduced density operators (Schmidt bases) for the BO wave function $\Psi(x, R) = \phi_2(x; R)\chi_{2,13}(R)$.

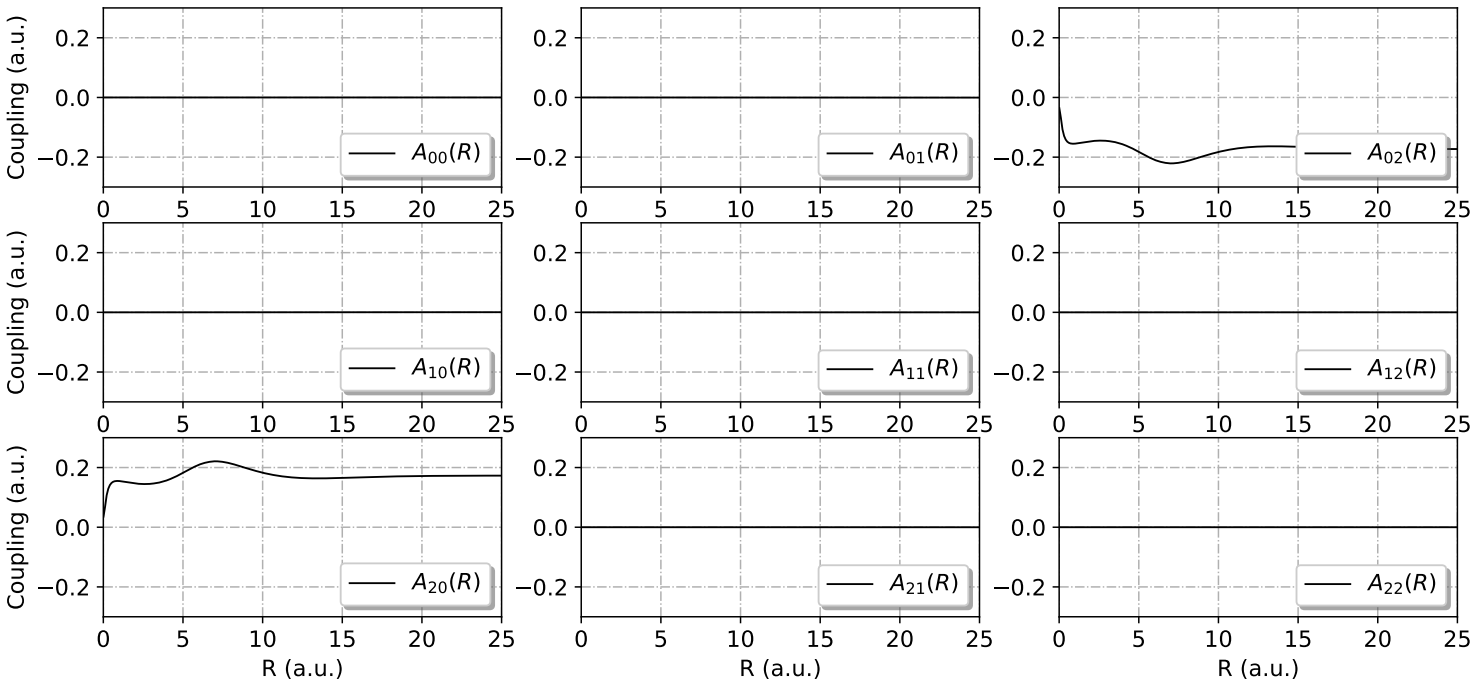

Figure 5.10:
Non-adiabatic couplings $A(R)$ between the electronic functions $\phi_0(x, R)$, $\phi_1(x, R)$ and $\phi_2(x, R)$.

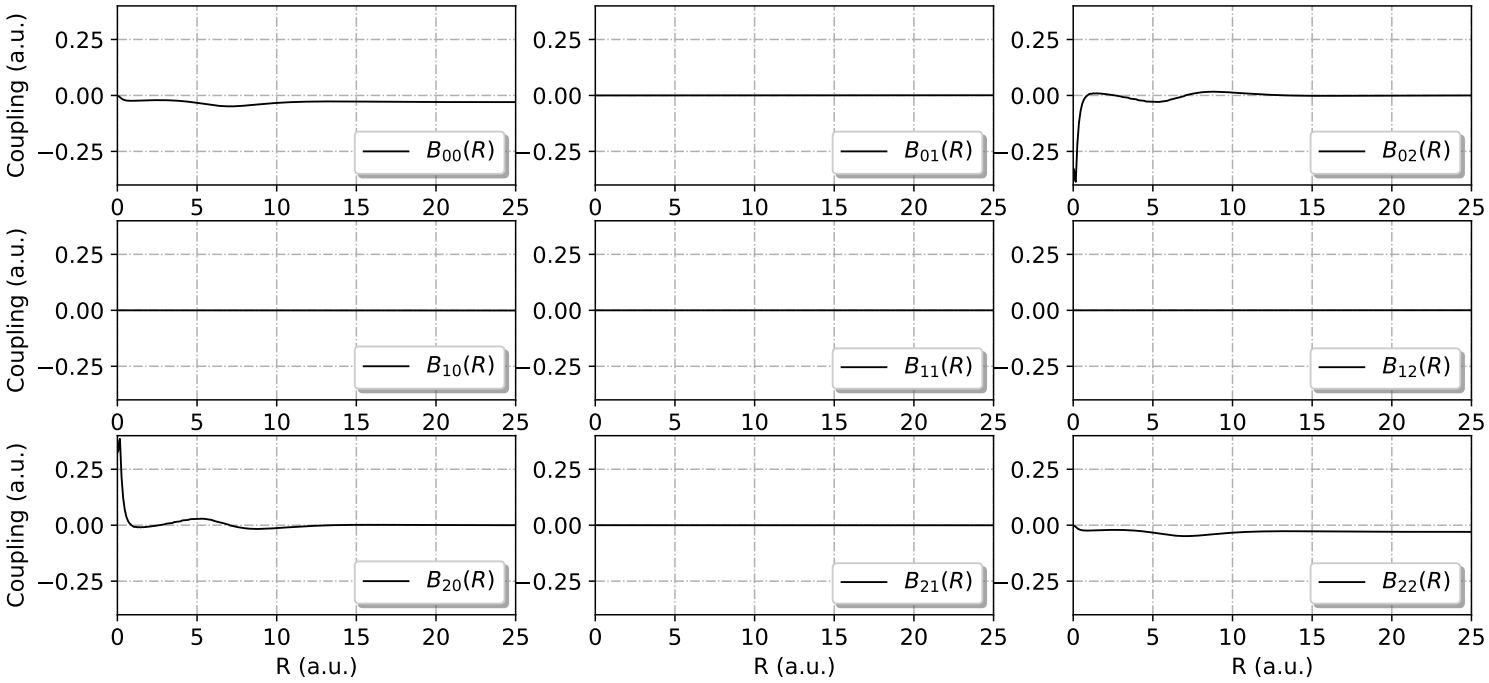

Figure 5.11:
Non-adiabatic couplings B between the electronic functions $\phi_0(x, R)$, $\phi_1(x, R)$ and $\phi_2(x, R)$.

Chapter 6

Results on Electro-Nuclear Entanglement beyond the BO approximation (Adiabatic).

6.1 Shin-Metiu molecular model

6.1.1 Entanglement within the Born-Oppenheimer approximation

By solving the Schrödinger equation for the electronic problem to different possible nuclear configurations, we obtain a set if electronic energies at a given nuclear configurations. We restrict ourselves to the lowest four states with potential energy curves $E_n(R)$ with $n = 0, ..., 3$ for the nuclear problem. In the Figure (6.1) we see on this system that there is a sharp avoided crossing at $R = -3.021$ $a.u.$, between the the energy curves $E_0(R)$ and $E_1(R)$ where the difference of energies on this point is less than 1^*10^{-3} $a.u.$
Also, at the point $R = 1.195$ $a.u.$, we see that between the energy curves $E_1(R)$ and $E_2(R)$ there is a small energy gap of $E = 1.29^*10^{-2}$ $a.u.$, so this point corresponds to the second noticeable avoided crossing, this time smoother than the former one located at $R = 1.194$ $a.u.$
Also, the electronic energy minimum for the ground state is located at the equilibrium distance $R = 3.489$ $a.u.$ so that nuclear wave functions start to accommodate on the region of positive values for R till reach energies close to $E = -0.303$ $a.u.$ where the potential

energy curve $E_0(R)$ reach a second local minimum.

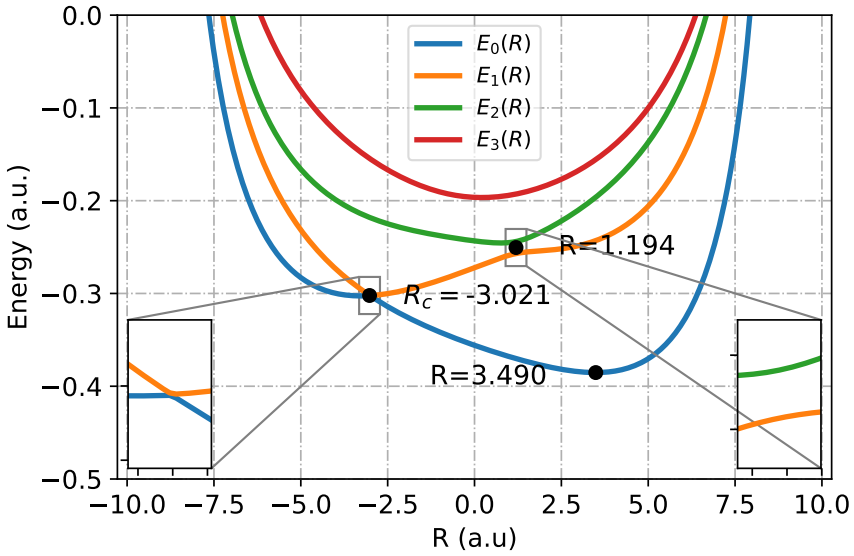

Figure 6.1:
Potential energy curves $\{E_n(R)\}_{n=1,2,3,4}$ for the Shin-Metiu molecular model, for the parameters included in the Table 4.2. The minimum is located at $R = 3.490$ $a.u.$, and two avoided crossings are presented at $R = -3.021$ $a.u.$ and $R = 1.194$ $a.u.$

Both, electronic energies and electronic wave functions change with the nuclear geometry according to the total interaction potential $V(x, R)$ in the equation (3.4) which depends upon the change in R. In Figure (6.2) we have showed the electronic wave functions (shifted to their energy eigenvalues) along with the corresponding electronic potential in the neighborhood of the avoided crossing locate at $R_c = -3.021$ $a.u.$, where Figures (6.2A), (6.2B) and (6.2C) are for distances such that $R < R_c$ and Figures (6.2D), (6.2E) and (6.2F) for distances such that $R > R_c$.
The total interaction potential $V(x, R)$ has two wells, for $x < 0$ and $x > 0$, the former wider than the latter. For $R < R_c$, the ground state accommodates in the left well and the first excited state is located on the right well. This situation changes for $R > R_c$, where the well at $x > 0$ becomes deeper and it starts to host the ground state and the excited state moves to the other well. Eventually, it indicated that there is a exchange in the character

between the two lowest states across the avoided crossing $R_c = -3.021\ a.u.$. An almost total exchange of character is a typical feature of sharp avoided crossing.

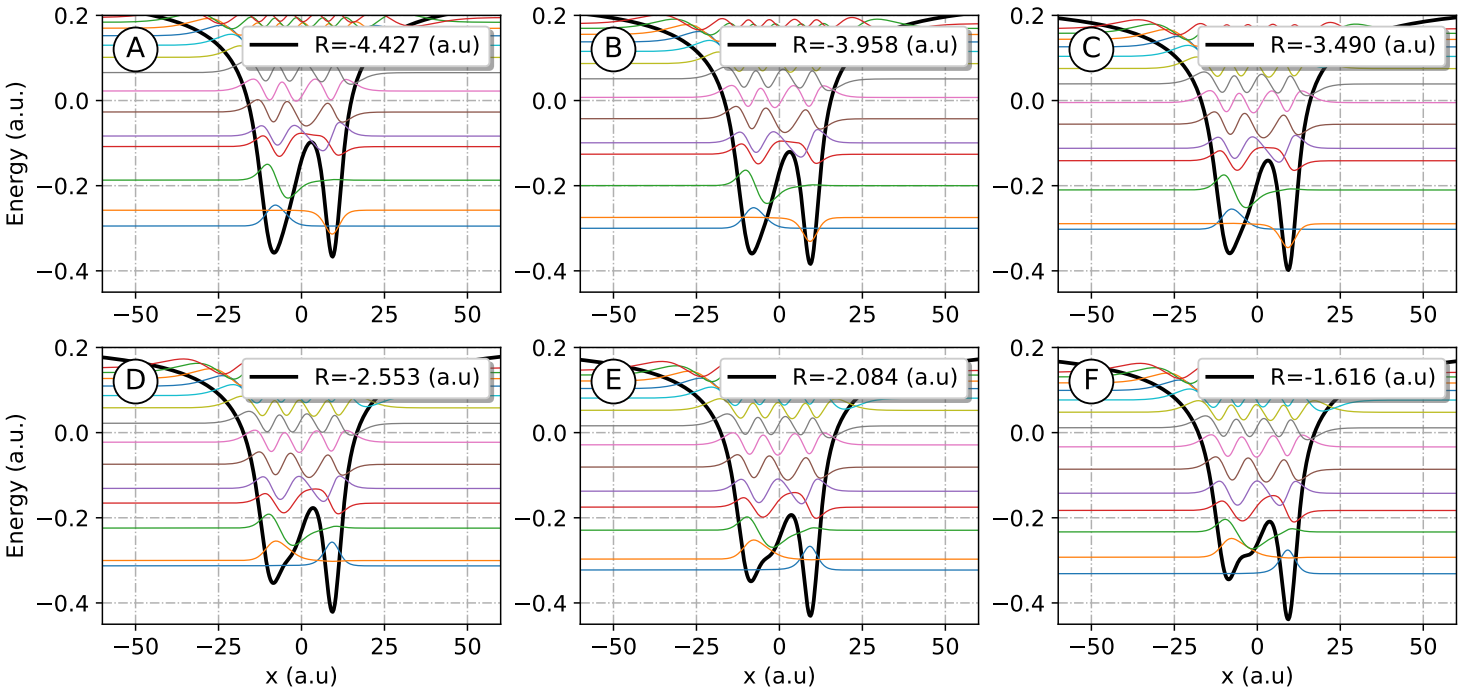

Figure 6.2:
Electronic wave functions for different possible nuclear configurations around the first avoided crossing $R_c = -3.021\ a.u$. Figures A, B and C are for distances such that $R < R_c$. Figures D, E and F are for distances such that $R > R_c$.

We also compute the dipole matrix elements (equation 2.39), both for the permanent diagonal dipoles and the transitions one, for the three lowest electronic eigenstates. Note that molecular properties like dipole moments must show the effect of the presence of avoided crossings, where there is a dramatic change in the electronic wave functions for the first avoided crossing and a soft change in the second avoided crossing; consequently in any matrix element.
The transition dipole moments (Figure 6.3B) between the electronic states $\phi_0(x,;R)$ and $\phi_2(x;R)$ converge to $d_{2,0} = -0.004\ a.u.$, $\phi_2(x;R)$ and $\phi_1(x;R)$ converge to converge to

$d_{2,1} = 0.078$ $a.u.$, whereas the transitions between the states $\phi_0(x,;R)$ and $\phi_1(x;R)$ converge to $d_{2,1} = 1.537$ $a.u.$. In the first and second crossing avoided this transitions might not have abrupt changes in the adiabatic curves.
The permanent dipole moments (Figure 6.3A) for the electronic states $\phi_0(x,;R)$, $\phi_1(x;R)$ and $\phi_2(x;R)$ the presence of the crossings avoided generate abrupt changes, the permanent dipole moments of the electronic states $\phi_0(x,;R)$ and $\phi_1(x;R)$ are inverted abruptly in the first crossings avoided, whereas the permanent dipole moments of the electronic states $\phi_1(x,;R)$ and $\phi_2(x;R)$ are inverted smoothly in the second crossings avoided.

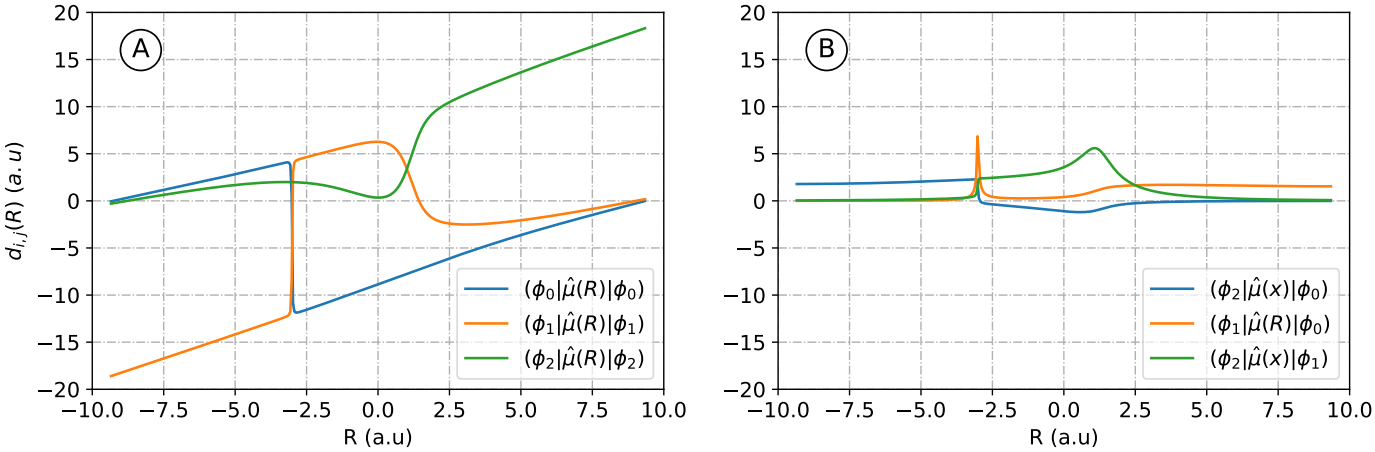

Figure 6.3:
Figure A: Permanent dipole moments for electronic states $\phi_0(x;R)$, $\phi_1(x;R)$ and $\phi_2(x;R)$.
Figure B: Transition dipole moments between the electronic states $\phi_0(x;R)$, $\phi_1(x;R)$ and $\phi_2(x;R)$

Next, solving the nuclear Hamiltonian for the potential energy curves $E_0(R)$, $E_1(R)$ and $E_2(R)$, we obtain a set of BO vibrational eigenfunctions for each potential curve. This wave functions, shifted to their energy eigenvalue for the three lowest electronic states are shown in the Figures (6.4A), (6.4B) and (6.4C) respectively.

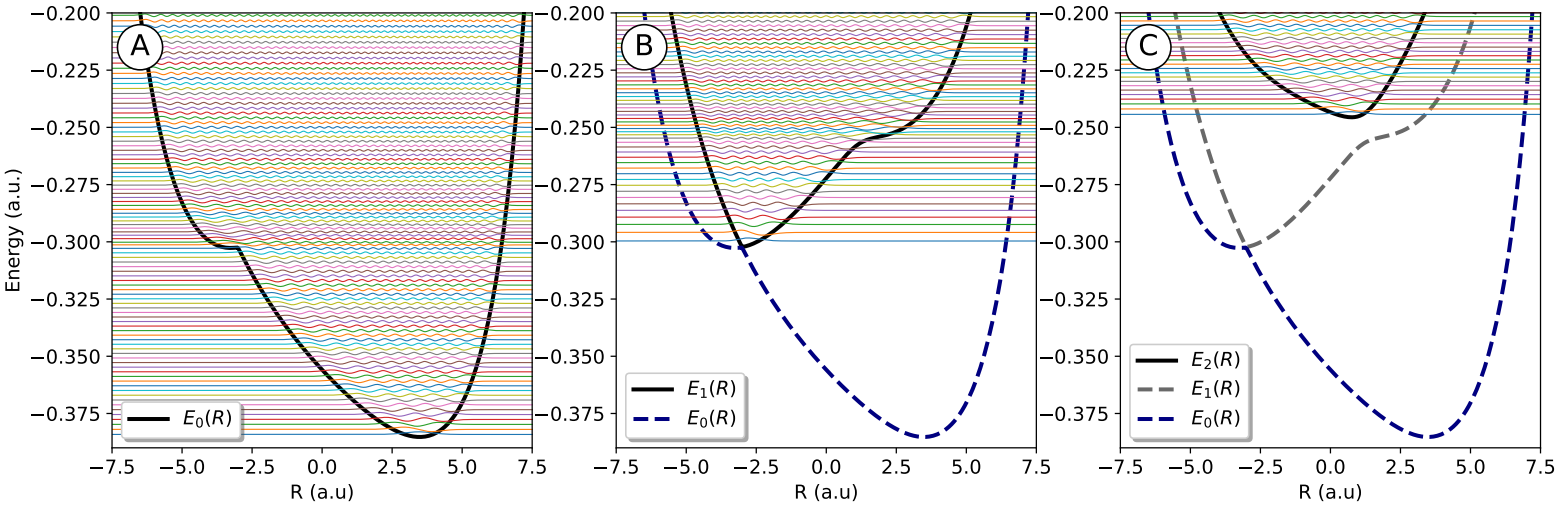

Figure 6.4:
Vibrational wave functions $\chi_{n,m}(R)$ (shifted to their eigenvalues) computed for the three lowest adiabatic potential energy curves $E_n(R)$ for: $n = 0$ (Figure A), $n = 1$ (Figure B) and $n = 3$ (Figure C) of the Shin-Metiu molecular model.

Entropy

We have calculated the entanglement measure with von-Neumann and linear entropies for each eletro-nuclear BO state $\phi_n(x; R)\chi_{n,m}$, with $n = 0, 1, 2$ and we include these results in the Figure (6.6).

1. State $\phi_0(x; R)\chi_{0,m}(R)$. In the Figure (6.6) we can see how both von-Neumann and linear entropies increase monotonically and slowly with the vibrational excitations energy, until it reaches the energy position of the avoided crossing at $R = -3.021\ a.u.$, then it shows and abrupt increasing until a peak for the vibrational state $\chi_{0,41}(R)$ which is the closest lying state to the energy position of the avoided crossing.
   We split the states above the 41-rst vibrational state in two half-spaces, for analyze the oscillation, the first H_1 is for $R < R_c$ and the second H_2 is for $R > R_c$ as is indicated in the Figure (6.5).

   First, we found the trace of the density operator for each subspace, Table 6.1. This

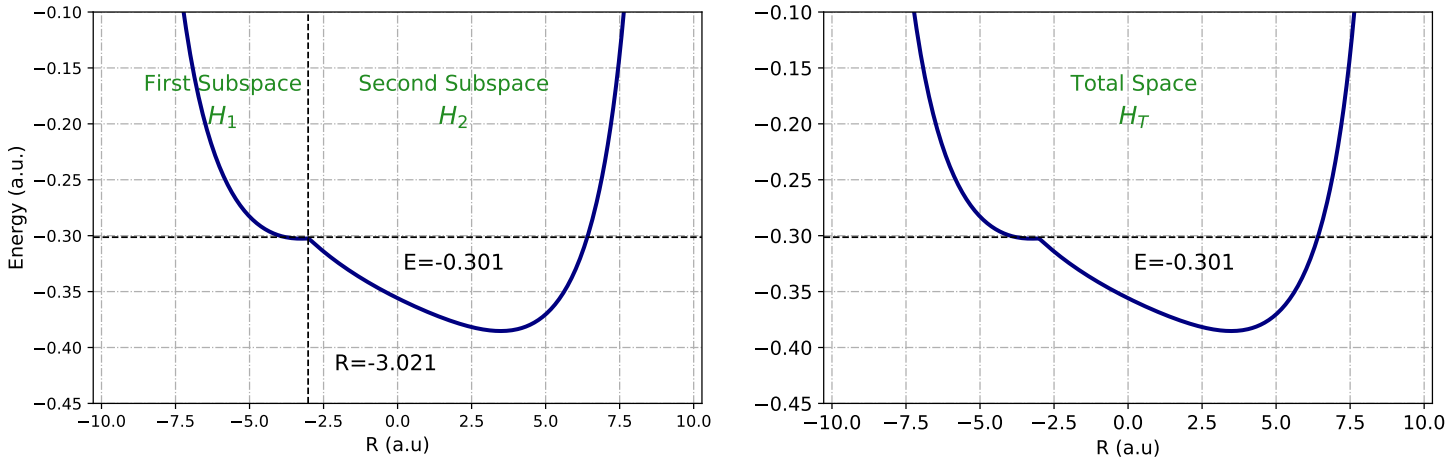

Figure 6.5:
Hilbert configurational space separated at the position of the avoided crossing $R_c = -3.021$ $a.u.$ in two half-spaces H_1 (for $R < R_c$) and H_2 (for $R > R_c$). The energy position of the sharp crossing avoided also divides the energy in two regions, below and above the avoided crossing with energy E_c

values are offset so that the trace in the total space is equal to one, separating the density operator in two sub-spaces, showing the linearity of the trace. There is a relation between the variation of the entropy and the variation of how the first eigenvalue (the principal eigenvalues) of each sub-space is changing.

Thus, we will analyze the relation of the Schmidt eigenvalues of the two Hilbert configurational subspaces with the Schmidt eigenvalues of the whole system. According to the Table 6.2, we see how each principal Schmidt eigenvalue for each Hilbert configurational subspace can be related with a Schmidt eigenvalue of the total space H_T. The first eigenvalues of the Hilbert subspaces H_2 and H_1 are very similar to the first and second Schmidt eigenvalues respectively of the total Hilbert space. An important characteristic is that the larger Schmidt eigenvalue and which has the biggest weight for the entropy is given by the second subspace H_2.

In order to find the origin of the oscillations in the entropy, we know that the diagonal elements in the density operator (matrix representation) give the largest contributions to the Schmidt eigenvalues. The largest contributions in the diagonal elements are

	$\mathbf{Tr}[\hat{\rho}]$		
State	$\mathbf{H_1}$	$\mathbf{H_2}$	$\mathbf{H_T}$
$\phi_0(x;R)\chi_{0,41}(R)$	0.446	0.554	1.0
$\phi_0(x;R)\chi_{0,42}(R)$	0.390	0.610	1.0
$\phi_0(x;R)\chi_{0,43}(R)$	0.266	0.734	1.0
$\phi_0(x;R)\chi_{0,44}(R)$	0.404	0.596	1.0
$\phi_0(x;R)\chi_{0,45}(R)$	0.329	0.671	1.0
$\phi_0(x;R)\chi_{0,46}(R)$	0.309	0.691	1.0
$\phi_0(x;R)\chi_{0,47}(R)$	0.371	0.629	1.0

Table 6.1: Trace of the density operator in the sub-spaces $H_1 \oplus H_2$ and the total Hilbert space for the states $\phi_0(x,R)\chi_{0,m}(R)$, where $\{m = 41,..,47\}$

State	**Space**	**Eigenvalues** η_i				**Entropy**
$\phi_0(x;R)\chi_{0,m}(R)$		$i=1$	$i=2$	$i=3$	$i=4$	S_{vN}
$m = 41$	H_1	0.445	0.001	0.000	0.000	0.366
	H_2	0.535	0.017	0.001	0.000	0.415
	$\mathbf{H_T}$	0.550	0.448	0.002	0.000	0.702
$m = 42$	H_1	0.390	0.000	0.000	0.000	0.369
	H_2	0.608	0.002	0.000	0.000	0.318
	$\mathbf{H_T}$	0.608	0.389	0.002	0.000	0.684
$m = 43$	H_1	0.265	0.000	0.000	0.000	0.356
	H_2	0.719	0.013	0.002	0.000	0.310
	$\mathbf{H_T}$	0.720	0.277	0.002	0.000	0.610
$m = 44$	H_1	0.404	0.001	0.000	0.000	0.373
	H_2	0.584	0.095	0.002	0.000	0.371
	$\mathbf{H_T}$	0.587	0.410	0.002	0.000	0.694
$m = 45$	H_1	0.328	0.000	0.000	0.000	0.369
	H_2	0.668	0.002	0.001	0.000	0.290
	$\mathbf{H_T}$	0.669	0.329	0.002	0.000	0.652
$m = 46$	H_1	0.308	0.001	0.000	0.000	0.368
	H_2	0.677	0.011	0.001	0.000	0.330
	$\mathbf{H_T}$	0.679	0.319	0.002	0.001	0.646
$m = 47$	H_1	0.370	0.001	0.000	0.000	0.375
	H_2	0.621	0.006	0.001	0.000	0.341
	$\mathbf{H_T}$	0.622	0.375	0.002	0.000	0.681

Table 6.2: First five eigen-values of the Schmidt decomposition for the two subspaces S_1 and S_2 and the total space S_T for the states $\Psi = \phi_0(x,R)\chi_{0,i}(R)$, where $\{i = 41,..,47\}$

	Square modulus						
	State						
Maximum	$\chi_{0,41}(R_i)$	$\chi_{0,42}(R_i)$	$\chi_{0,43}(R_i)$	$\chi_{0,44}(R_i)$	$\chi_{0,45}(R_i)$	$\chi_{0,46}(R_i)$	$\chi_{0,47}(R_i)$
1	0.016 (−2.974)	0.014 (−2.740)	0.018 (−2.928)	0.010 (6.300)	0.013 (−2.787)	0.015 (−2.974)	0.011 (6.347)
2	0.009 (−2.459)	0.010 (6.253)	0.011 (6.253)	0.010 (−2.600)	0.011 (6.300)	0.012 (6.347)	0.010 (−2.693)
3	0.009 (6.253)	0.009 (−2.272)	0.010 (−2.459)	0.008 (−2.225)	0.009 (−2.366)	0.010 (−2.553)	0.009 (−2.319)
4	0.007 (−2.084)	0.007 (−1.897)	0.009 (−2.084)	0.007 (−2.974)	0.008 (−2.038)	0.009 (−2.178)	0.008 (−2.038)
5	0.006 (−1.710)	0.007 (−1.616)	0.008 (−1.757)	0.007 (−1.897)	0.008 (−1.757)	0.008 (−1.897)	0.007 (−1.757)
6	0.006 (−1.429)	0.007 (5.926)	0.008 (−1.476)	0.007 (5.972)	0.007 (−1.476)	0.007 (−1.616)	0.007 (−1.476)
7	0.005 (−1.148)	0.006 (−1.335)	0.007 (5.926)	0.006 (−1.335)	0.007 (5.972)	0.007 (6.019)	0.007 (6.019)
8	0.005 (5.926)	0.006 (−1.054)	0.007 (−1.194)	0.006 (−1.101)	0.006 (−1.194)	0.007 (−1.335)	0.006 (−1.241)
9	0.005 (−0.913)	0.006 (−0.820)	0.007 (5.691)	0.006 (−0.820)	0.006 (−0.960)	0.007 (−1.101)	0.006 (−1.007)
10	0.005 (5.644)	0.005 (5.644)	0.006 (−0.960)	0.005 (−1.663)	0.006 (−0.726)	0.006 (−0.867)	0.006 (−0.773)
Sum	$0.639 * 10^{-3}$	$0.657 * 10^{-3}$	$0.937 * 10^{-3}$	$0.544 * 10^{-3}$	$0.705 * 10^{-3}$	$0.846 * 10^{-3}$	$0.621 * 10^{-3}$

Table 6.3: Location of the ten highest maxima of the probability density function $|\chi_{1,m}(R)|^2$, for $m = 41, .., 47$. The positions of the local maxima are indicated and the value of the function at this point is given for each state.

given by the square modulus of each local maximum. We show in the Table 6.3 the square modulus (see the equation 4.13) of the fist ten local maxima of the states $\chi_{0,j}(R)$ where $\{j,\ j = 41, ..., 47\}$ and the sum of the square modulus of these maxima values.

As an approach, considering only the main values (diagonal elements) in the density operator, one can compute the linear entropy (2.38) finding the trace of the square of each element (the last line in the Table 6.3), which follows the behavior in the inset of the Figure 6.6. Thus the oscillations in the linear (and hence in the von-Neumann) entropy are a consequence of the number of the local maxima and their values of each vibrational state in the second configurational subspace.

We tabulate the von-Neumann and linear entropy for the first sixty states and the first four Schmidt eigenvalues in the Appendix C, Table C.1.

2. State $\phi_1(x; R)\chi_{1,m}(R)$. In the Figure (6.6) we include the linear and von-Neumann entropy corresponding to the BO wave functions $\phi_1(x; R)\chi_{1,m}(R)$ with $m = 0, 1, ...$ We understand that the energy regions close to the two avoided crossings for the potential energy curve $E_1(R)$ involve a noticeable increase of the entanglement separating two plateaus with a monotonically smooth increasing. The dramatic enhancement of the entanglement entropy could be understood in terms of the enlargement of the configurational space available for the vibrational wave functions for energies above

a given avoided crossing (this concept is from information theory and entropy). Also, the adiabatic electronic wave function modifies its character across the avoided crossing (character exchange) and this modifies the factor with the overlap of the electronic wave functions at two distances ($\int dx\phi_n(x;R_i)\phi_n(x;R_j)$) in the reduced matrix elements in the equation (4.13).

3. State $\phi_2(x;R)\chi_{2,m}(R)$. In the Figure (6.6) we can see how both, von-Neumann and linear entropies increase monotonically with the vibrational excitations energies. We understand that the energy region close to the second avoided crossings for the potential energy curve $E_2(R)$ involve a noticeable increase of the entanglement, the second crossing avoided match with its minimum value of energy of the curve $E_2(R)$ generating a faster increase in the enhancement in the first region of the entanglement entropy. Also, the enlargement of the configurational space available for the vibrational wave functions for distance energies above a given avoided crossing increasing the entropy slowly.

Schmidt decomposition

1. Electronic ground state $\phi_0(x;R)$. We choose three vibrational states within the potential energy curve $E_0(R)$, with vibrational numbers $m = 15, 30, 41$ in order to analyze their BO entanglement content through the Schmidt decomposition.

   (a) BO state $\phi_0(x,R)\chi_{0,15}(R)$ We see in the Figure (6.7) how this wave functions can be separated approximately as $\Psi(x,R) \sim u_1(x)v_1(R) \sim \phi_0(x;R=3.490)\chi_{0,15}(R)$. The BO electronic wave function depends parametrically of the variable R evaluated only at the minimum value of the potentential energy curve $E_0(R)$ i.e. $R = 3.490$. This wave function may be written approximately as a the direct product of the first element of the electronic and nuclear basis of the Schmidt decomposition $\eta_1 \sim 1$.

   (b) BO state $\phi_0(x,R)\chi_{0,30}(R)$ We see in the Figure (6.8) how this state also allows be separated as a single term in the Schmidt decomposition, since the highest eigenvalue is $\eta_1 = 0.997$; very close to unity. It can be well compared with the BO wave function evaluated at the equilibrium position $R_e = 3.490$ $a.u.$

   (c) BO state $\phi_0(x,R)\chi_{0,41}(R)$. We see in the Figure (6.9) how this wave functions cannot be separated as the product of an electronic and vibrational Schmidt functions. The first two highest eigenvalues at the Schmidt decomposition η_1 and η_2 have comparable weights; $\eta_1 = 0.550$ and $\eta_2 = 0.448$. This state has the

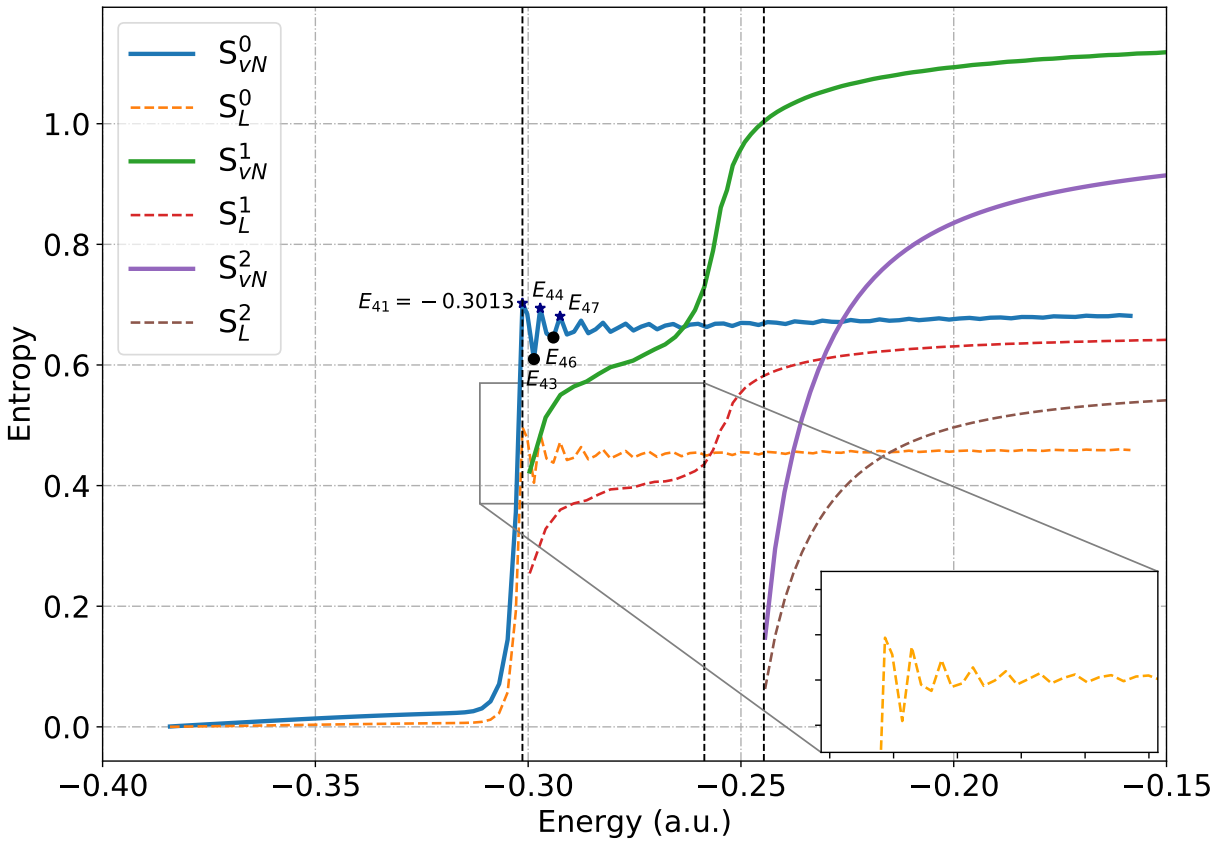

Figure 6.6:
von-Neumann and linear entropies for the total BO wave function $\phi_n(x;R)\chi_{n,m}(R)$ for $n = 0, 1, 2$. The upper index in the entropies correspond to values of the entropy associated to each electronic state n. The vertical lines indicates the energy position of the first sharp avoided crossing at $R_C = -3.023$ $a.u.$ and the energy region of the second avoided crossing at $R = 1.194$ $a.u.$

highest value for entropy of entanglement and it is because this state is located very close to the sharp crossing avoided, the first crossing avoided located at $R_c = -3.021$ $a.u.$

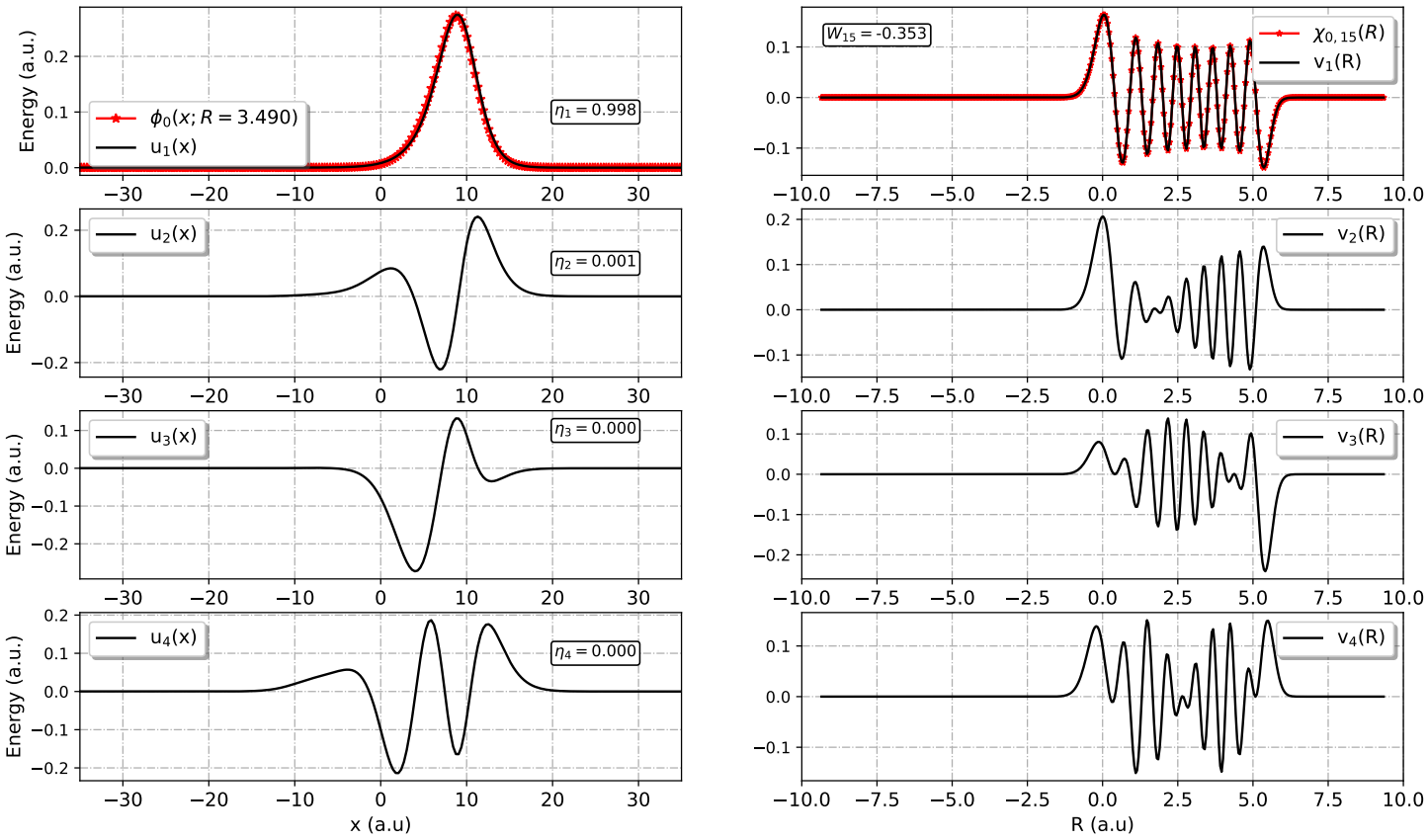

Figure 6.7:
First four lowest eigenfunctions and eigenvalues of the electronic and vibrational reduced density operators (Schmidt bases) for the BO wave function $\Psi(x, R) = \phi_0(x; R)\chi_{0,15}(R)$.

6.1.2 Born-Huang

To the calculates within the BH expansion, we start calculating the non-adiabatic couplings A and B.

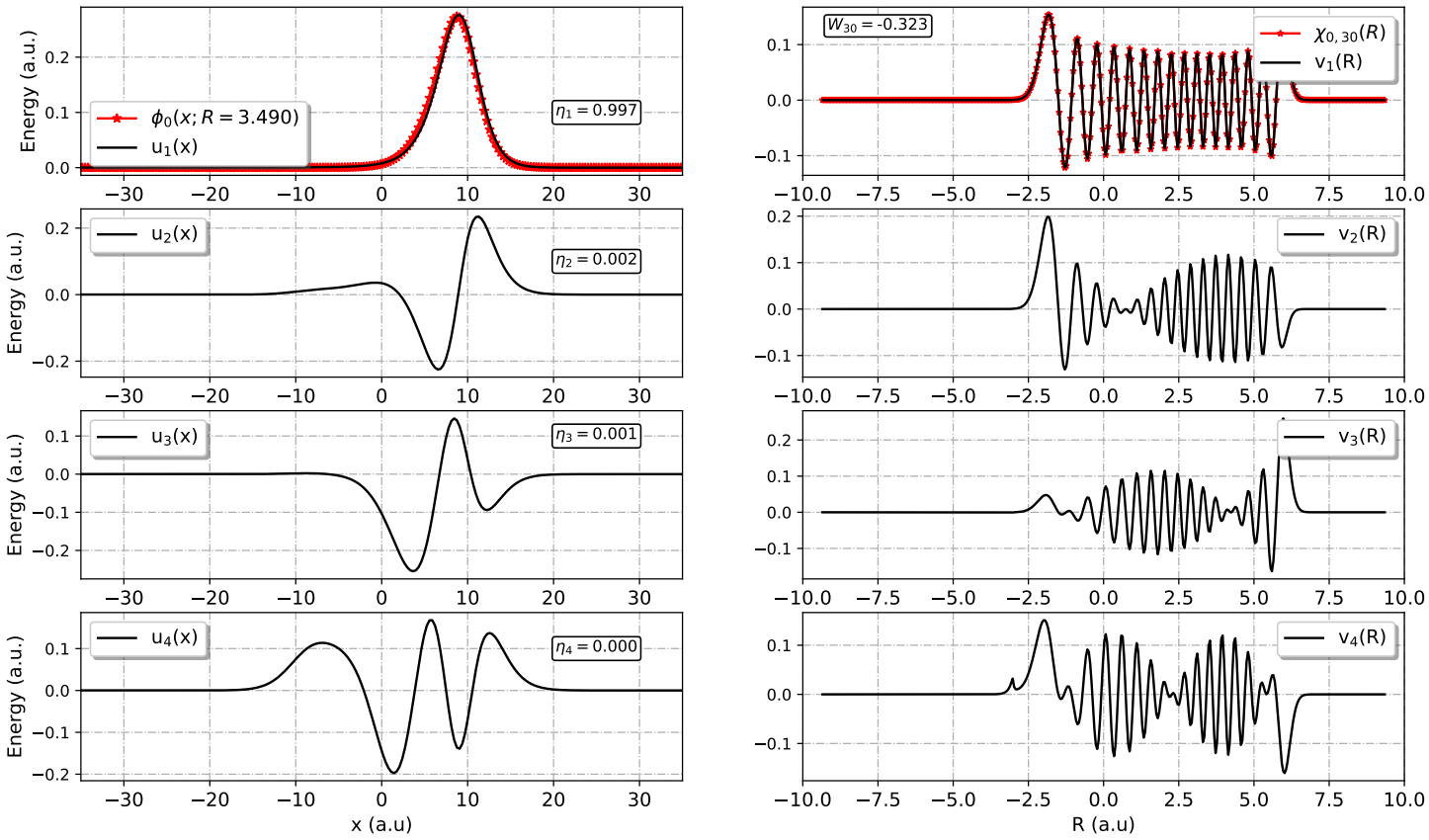

Figure 6.8:
First four lowest eigenfunctions and eigenvalues of the electronic and vibrational reduced density operators (Schmidt bases) for the BO wave function $\Psi(x, R) = \phi_0(x; R)\chi_{0,30}(R)$.

In the Figure (6.10) we show the non-adiabatic couplings A, as we can see that there are couplings between the electronic curves $\phi_0(x, R)$, $\phi_1(x, R)$ and $\phi_2(x, R)$. Also one can see that the non-adiabatic couplings A are anti-hermitian.

In the Figure (6.10) we show the non-adiabatic couplings B, as we can see that there are couplings between the electronic curves $\phi_0(x, R)$, $\phi_1(x, R)$ and $\phi_2(x, R)$. Also one can

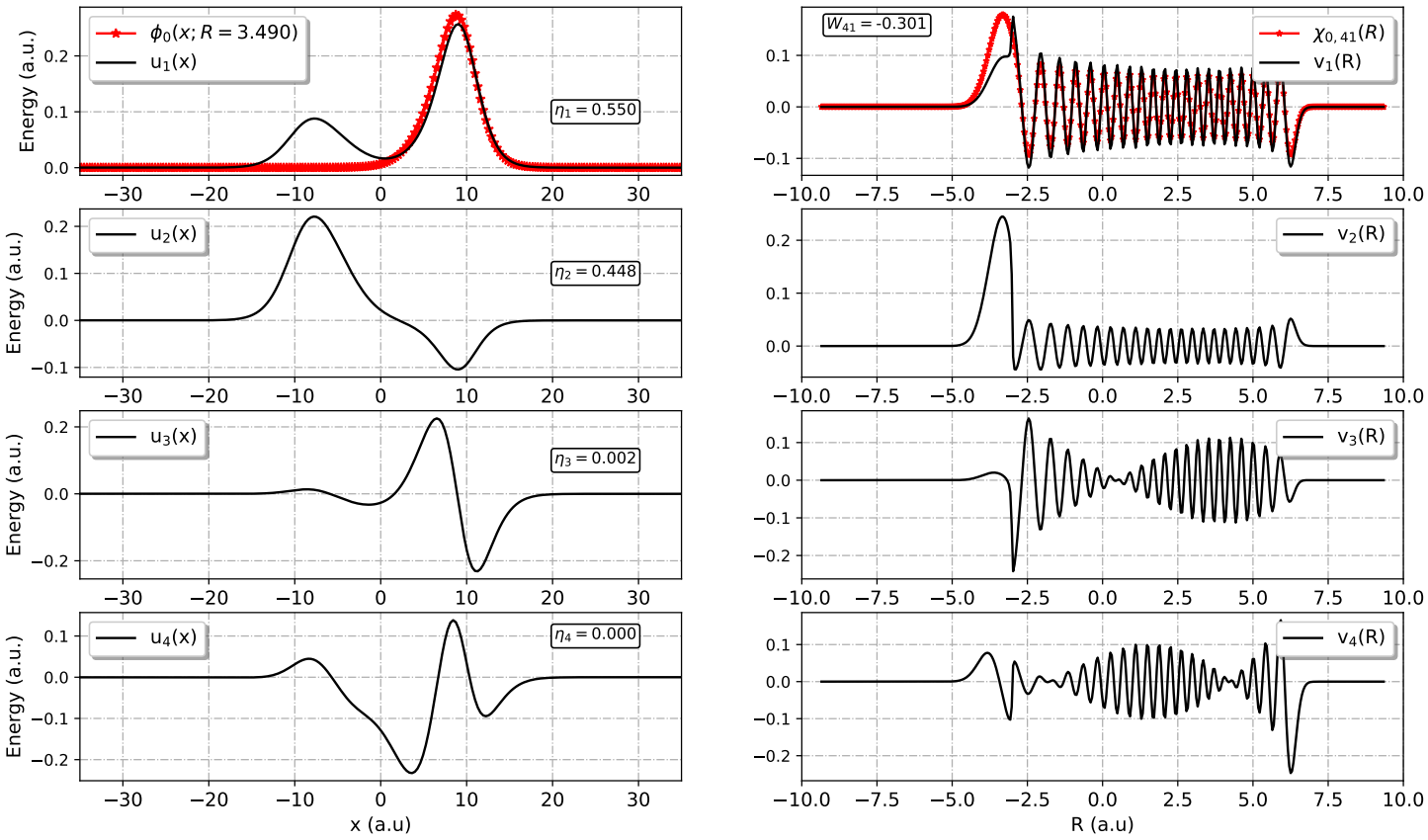

Figure 6.9:
First four lowest eigenfunctions and eigenvalues of the electronic and vibrational reduced density operators (Schmidt bases) for the BO wave function $\Psi(x, R) = \phi_0(x; R)\chi_{0,41}(R)$.

see that the non-adiabatic couplings B are not symmetric or anti-symmetric.

Next, we computed the BH wave functions solving the equation (2.21). With this we found the Schmidt decomposition of the functions $\Psi_0(x, R)$, $\Psi_{25}(x, R)$, $\Psi_{50}(x, R)$ and $\Psi_{75}(x, R)$, which are mixed in the three first electronic wave functions. We note that the BH wave functions $\Psi_0(x, R)$, $\Psi_{25}(x, R)$ have the same behavior compared with the BO

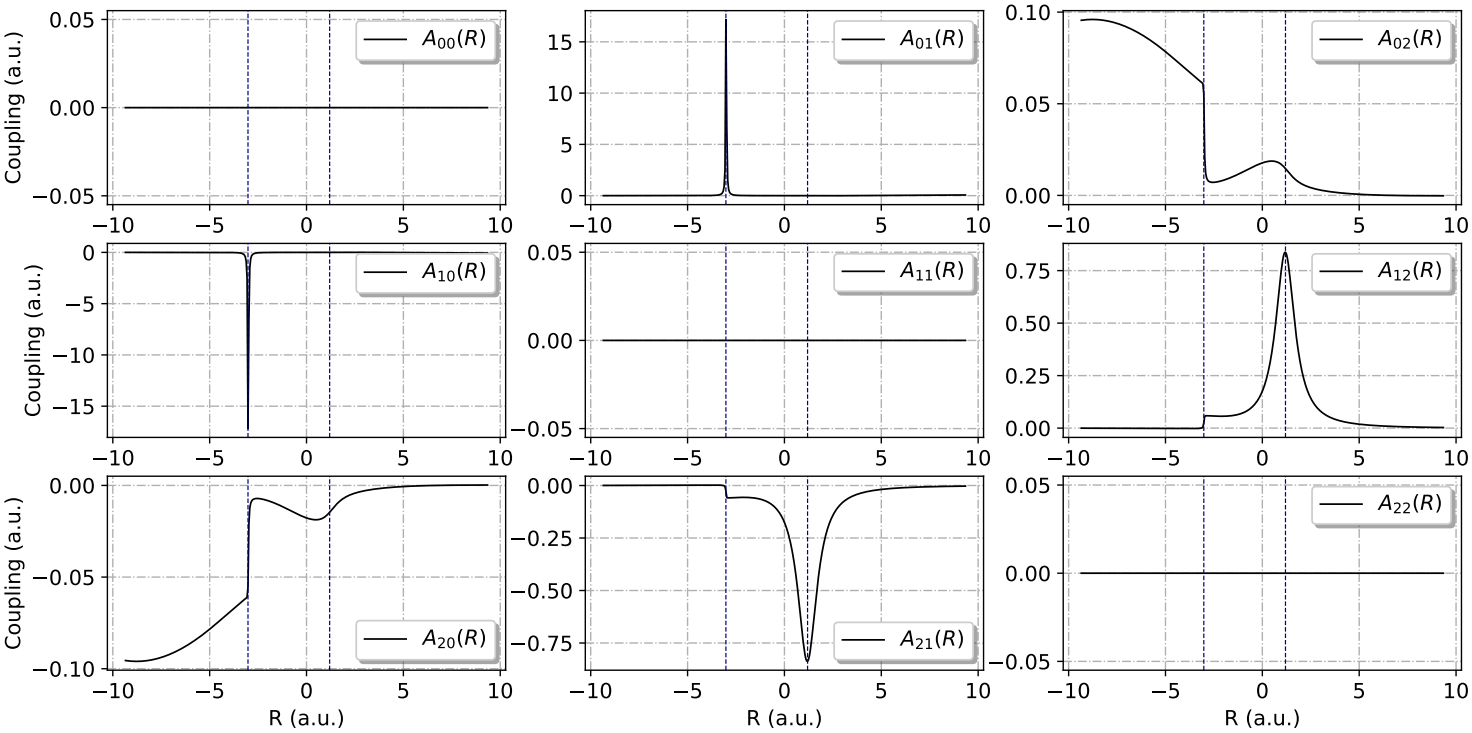

Figure 6.10:
Non-adiabatic couplings A between the electronic functions $\phi_0(x, R)$, $\phi_1(x, R)$ and $\phi_2(x, R)$

wave functions $\phi_0(x; R)\chi_{0,0}(R)$ and $\phi_0(x; R)\chi_{0,25}(R)$, thus the BO and BH states which energies are below the energy of the crossing avoided are very similar.

The von-Neumann entropy for the BH expansion is showed in the Figure 6.15, where is observed how the entropy has a similar behavior in the BO (S^0_{vN}) and BH systems until we reach the region close to the first crossing avoided, where the the second curve of the entropy has an important weigh, thus the entropy oscillates between the different BO entropies.

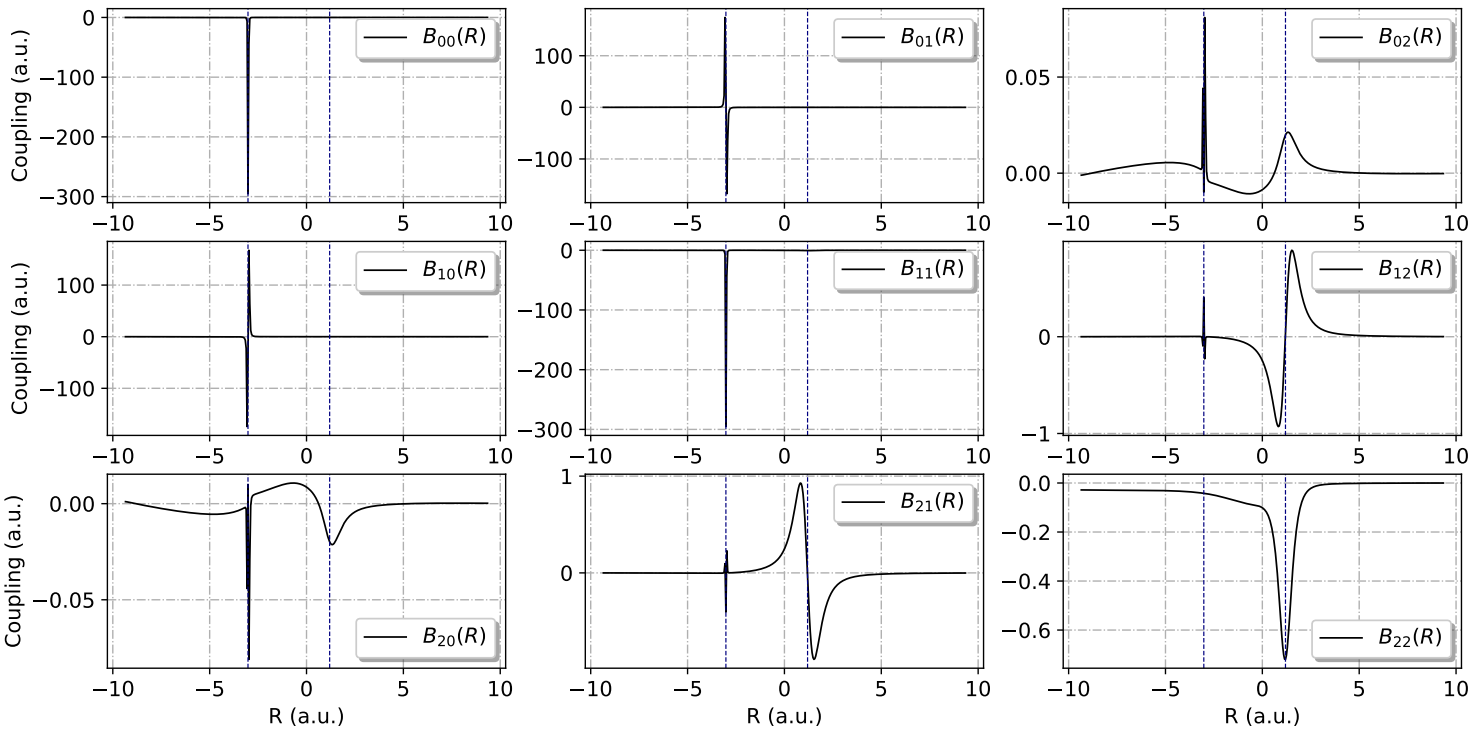

Figure 6.11:
Non-adiabatic couplings A between the electronic functions $\phi_0(x, R)$, $\phi_1(x, R)$ and $\phi_2(x, R)$

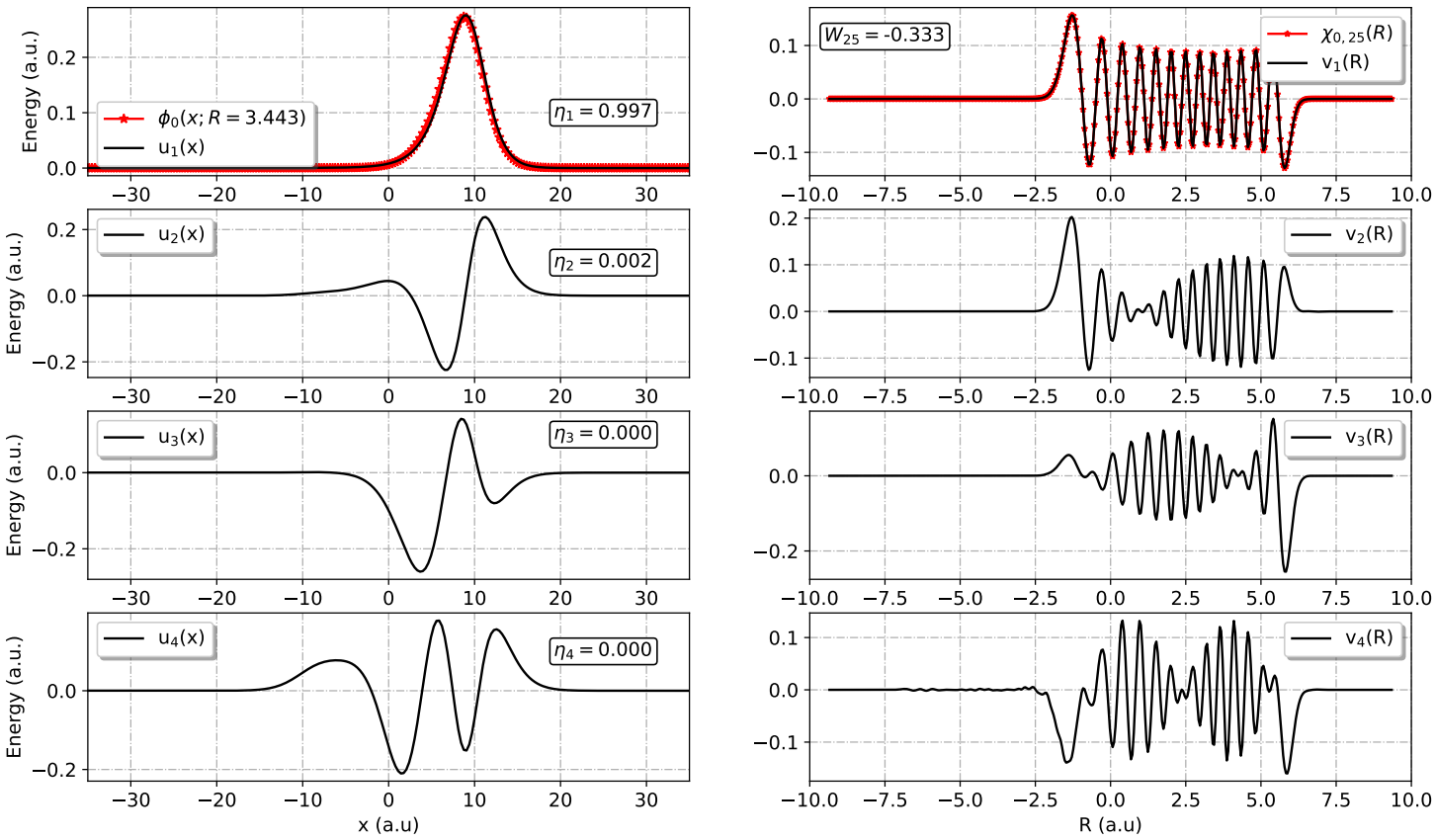

Figure 6.12:
First four lowest eigenfunctions and eigenvalues of the total BH wave function $\Psi_{25}(x, R)$.

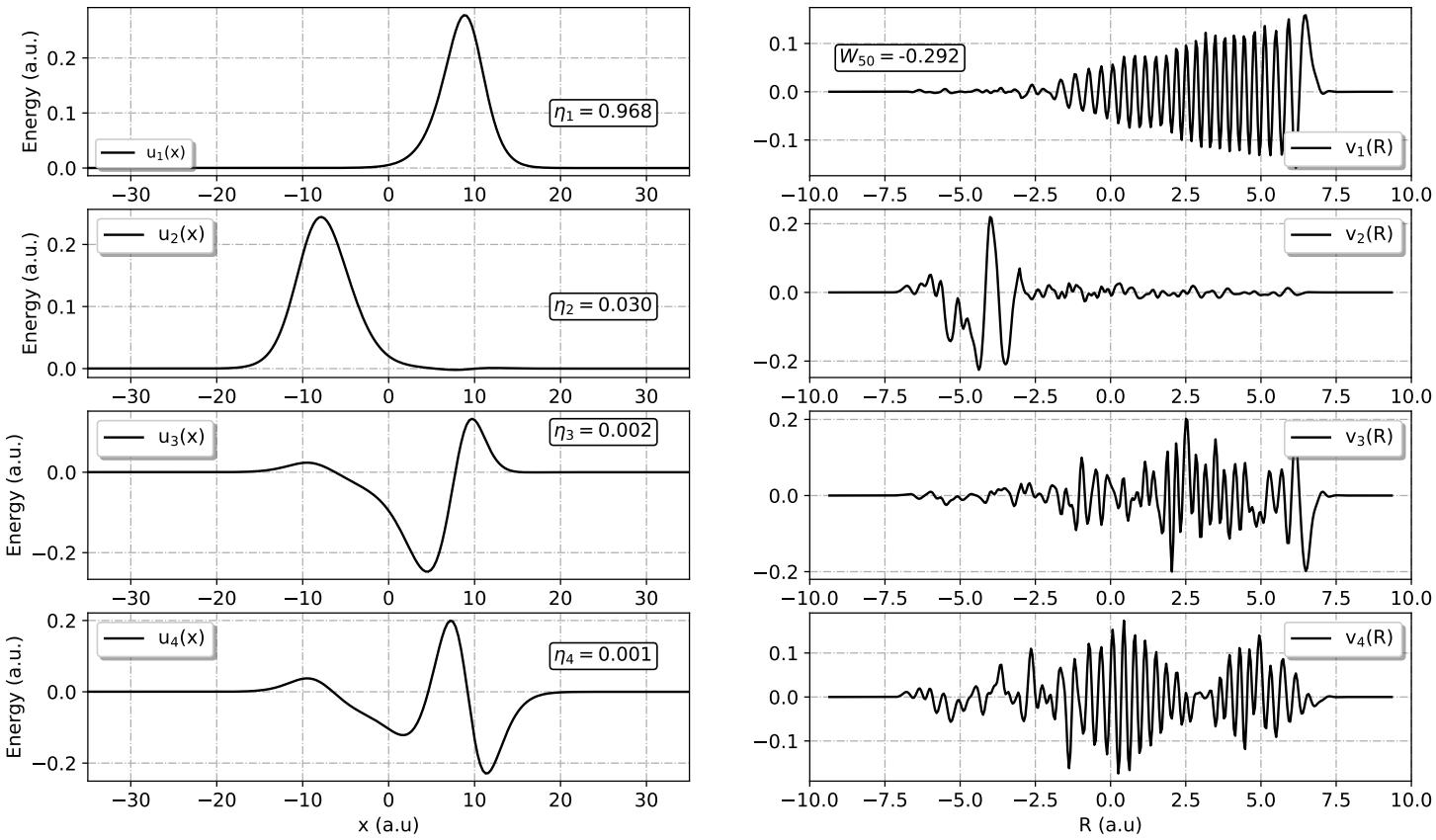

Figure 6.13:
First four lowest eigenfunctions and eigenvalues of the total BH wave function $\Psi_{50}(x, R)$.

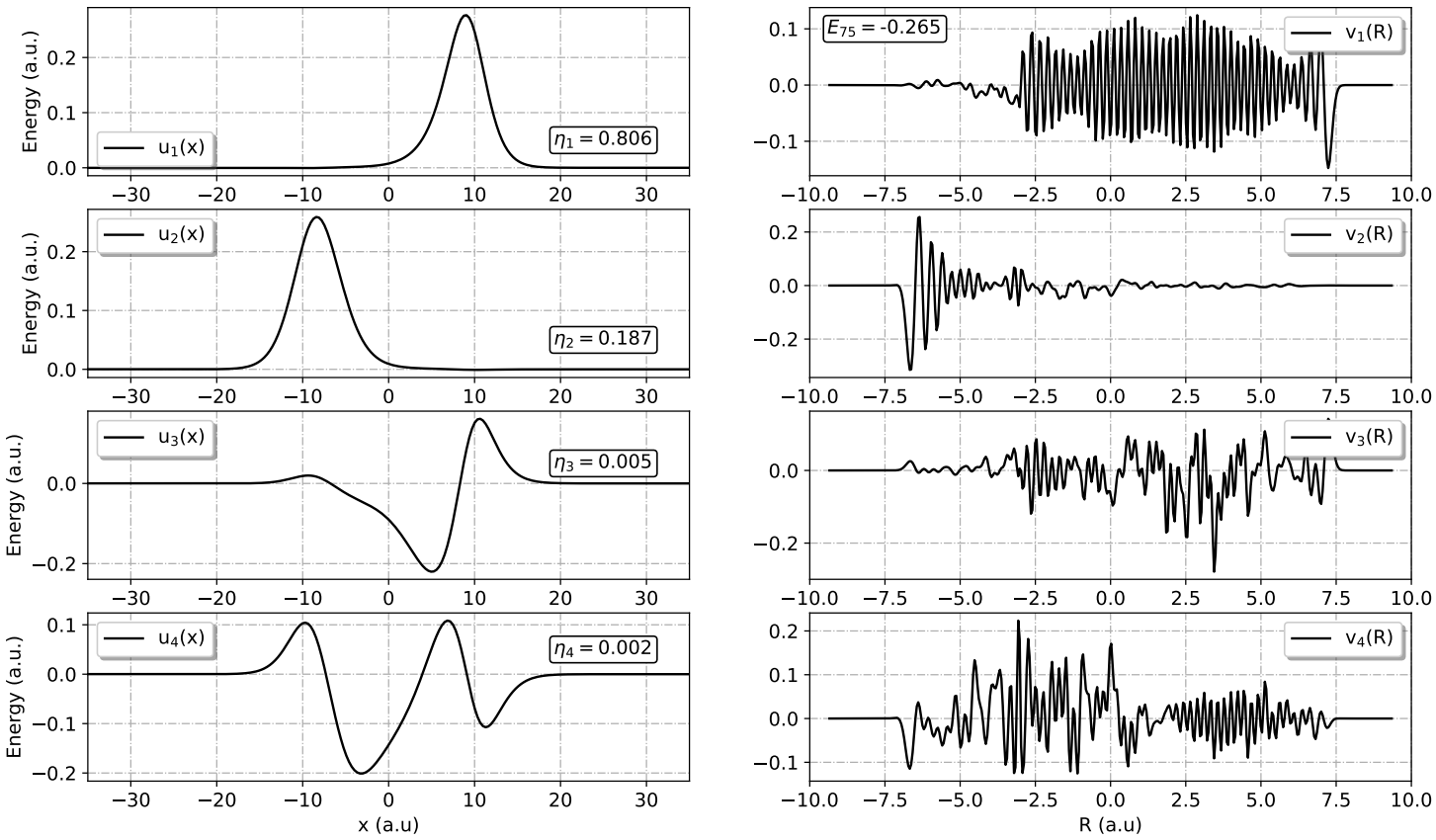

Figure 6.14:
First four lowest eigenfunctions and eigenvalues of the total BH wave function $\Psi_{75}(x, R)$.

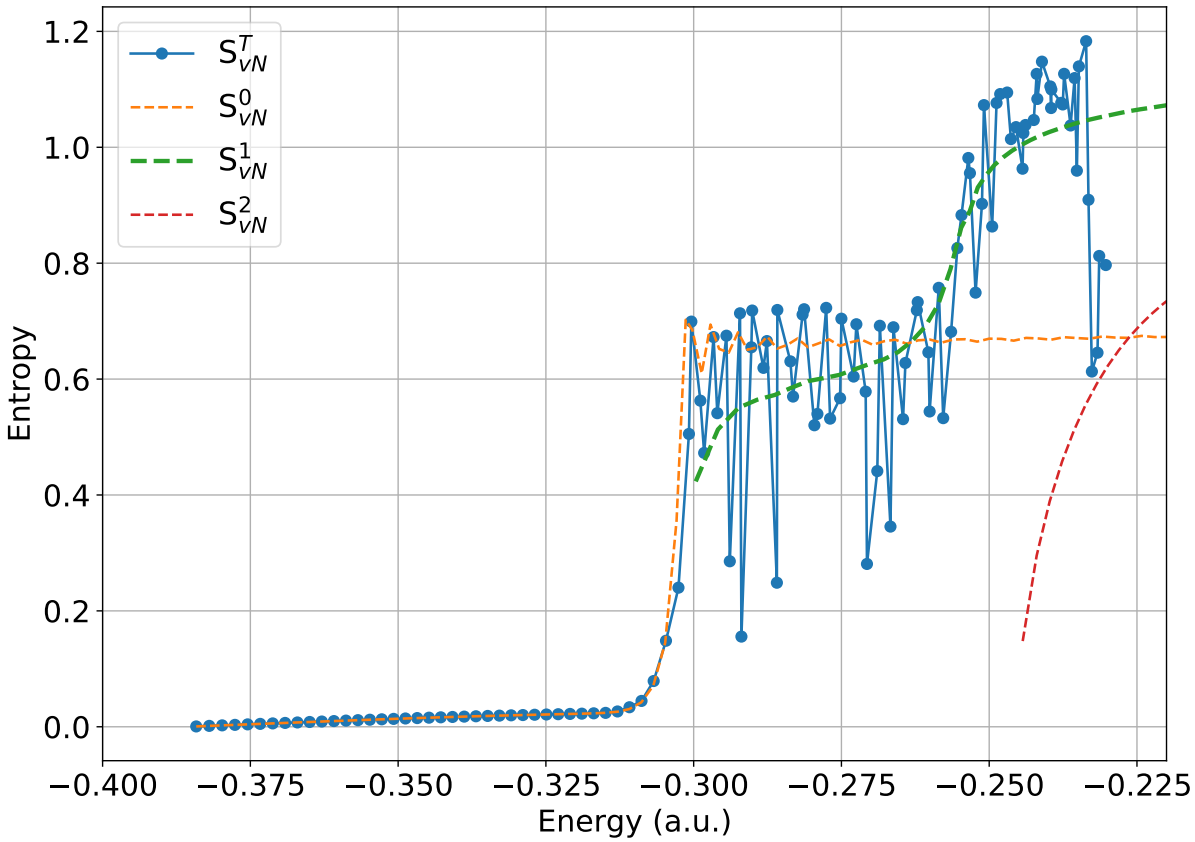

Figure 6.15:
von-Neumann for the total BH wave function compared with the BO von-Neumman entropy for the different electronic states

Chapter 7

Results on Electro-Nuclear Entanglement beyond the BO approximation (Diabatic).

7.1 Diabatic Couplings

7.1.1 Entanglement within the diabatic coupling

We have computed the relation between the diabatic and adiabatic potential energy curves using the relations 2.28 and 2.30 taking into account the adiabatic couplings between the different electronic states for the Shin-Metiu model showed in the Chapter 6 .
In the Figure (7.1) we can see how the first two diabatic energy curves, $D_0(R)$ and $D_1(R)$ (blue and black continuous line), are just generated by an exchange between the potential energy curves $E_0(R)$ and $E_1(R)$ at $R = -3.021$ $a.u.$; orange and gray dotted lines respectively. It is because at this point there is a sharp avoided crossing.

Also due to the soft avoided crossing ($R_c = 1.148$ $a.u.$), we see how are related the diabatic energy curves $D_1(R)$ and $D_2(R)$ and the potential energy curves $E_1(R)$ and $E_2(R)$, where the diabatization is more appreciable in this case, the exchange does not occur in a single point, it occurs around the neighborhood of the soft avoided crossing, the diabatic curves are a mixture of these two adiabatic energy curves (inset Figure (7.1)).

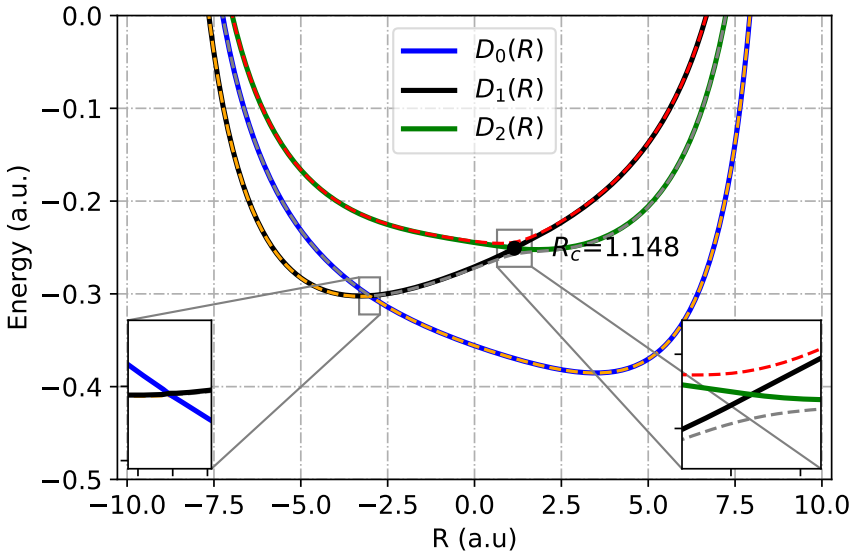

Figure 7.1:
Diabatic potential energy curves $\{D_n(R)\}_{n=0,1,2}$ and their respective adiabatic potential energy curves for the Shin-Metiu molecular model, for the parameters included in the Table 4.2. The diabatization is done around the two avoided crossings which are presented at $R_c = -3.021$ $a.u.$ and $R_c = 1.148$ $a.u.$

Electronic energies and wave functions, which depend parametrically of each nuclear geometry in the adiabatic and consequently in the diabatic case can be compared seeing the Figures (6.2) and (7.2). In Figure (7.2) we have showed the electronic diabatic wave functions (shifted to their diabatic energy eigenvalues) along the corresponding interaction potential, close to the sharp avoided crossing located at $R_c = -3.021$ $a.u.$ $= R_1$, where Figures (7.2A), (7.2B) and (7.2C) are for nuclear configurations below $R = R_1$ and Figures (7.2D), (7.2E) and (7.2F) for distances such that $R > R_1$. One can see how the shape of the diabatic electronic wave function is affected by the diabatization around the avoided crossings.
The total interaction potential $V(x, R)$ has two non-symmetric wells, each one for $x < 0$ and $x > 0$, the former wider than the latter. There is an exchange in the character between the two lowest electronic states across the avoided crossing $R_c = -3.021$ $a.u.$. An almost total exchange of character is a typical feature of sharp avoided crossing.

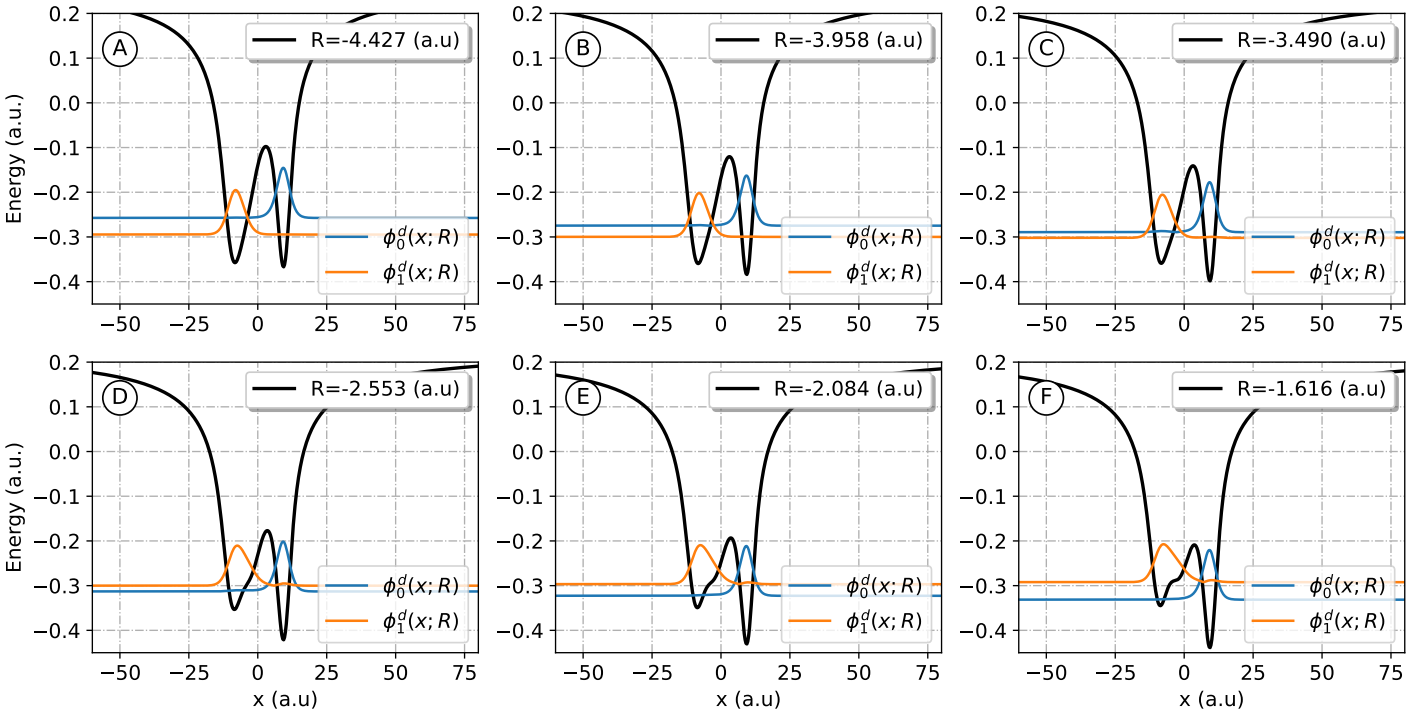

Figure 7.2:
Diabatic electronic wave functions for different possible nuclear configurations around the first avoided crossing at $R_1 = -3.021$. Figures A, B and C are for distances below R_1 and Figures D, E and F are for distances beyond the first avoided crossing.

Next, solving the nuclear Hamiltonian for the diabatic energy curves $D_0(R)$, $D_1(R)$ and $D_2(R)$, we obtain a set of BO vibrational diabatic eigenfunctions for each potential curve. This wave functions, shifted to their energy eigenvalue for the three lowest electronic diabatic states are shown in the Figures (7.3A), (7.3B) and (7.3C) respectively.

Entropy

With the previous data, we have computed the entanglement measure with von-Neummann and linear entropies for each eletro-nuclear BO (diabatic) state $\phi_n^d(x;R)\chi_{n,m}^d$, with $n = 0, 1, 2$ which have been showed in the Figure (7.7).

1. States $\phi_0^d(x;R)\chi_{0,m}^d(R)$. In this case we can see how the entropy for states whose

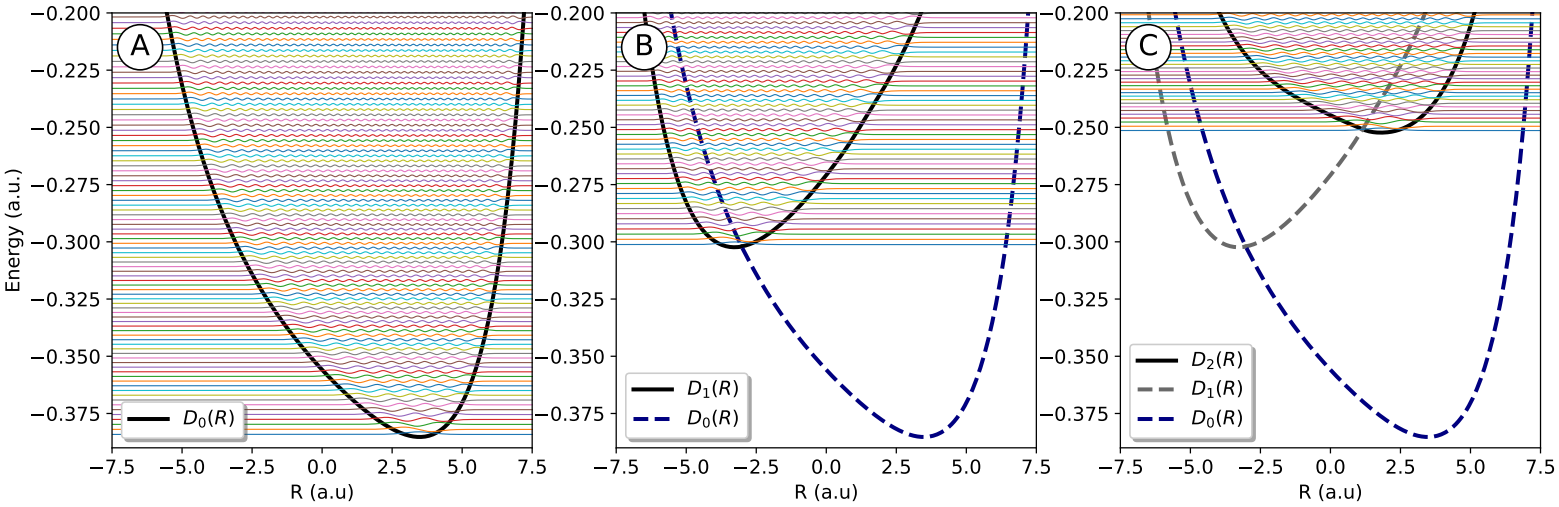

Figure 7.3:
Vibrational diabatic wave functions $\chi^d_{n,m}(R)$ (shifted to their eigenvalues) computed for the three lowest diabatic potential energy curves $D_n(R)$ for: $n = 0$ (Figure A), $n = 1$ (Figure B) and $n = 3$ (Figure C) in the Shin-Metiu molecular model.

energy is below of the sharp avoided crossing and located in the configurational Subspace H_2 (Figure (7.4)) is the same in the both diabatic and adiabatic cases. Specifically, both are the same until the entropy energy reaches the vibrational state E_{37}.

In order to understand the oscillations in the entropy beyond the vibrational state with energy E_{37}, we have splitted the configurational space in four subspaces, how is showed in the Figure (7.4). According to this, the subspace upon the oscillations appear is the Subspace H_2 with $x < 0$.

To show that, in Figure 7.5C, as an approximation, we have compared the von-Neumann and linear entropy with the entropy computed within the subspace H_2 with $x < 0$, and according with this the functional form of the entropy is upon this configurational space.

In Figures 7.5A and 7.5B we plot different electronic have functions for several nuclear configurations; $R \in [-3.021, -2.834]$, for the subspaces located to the left of $x = 0$ $a.u.$ and the subspaces located to the right of $x = 0$ $a.u.$, respectively, where we can see how the electronic wave functions varies abruptly, mostly it occurs close to

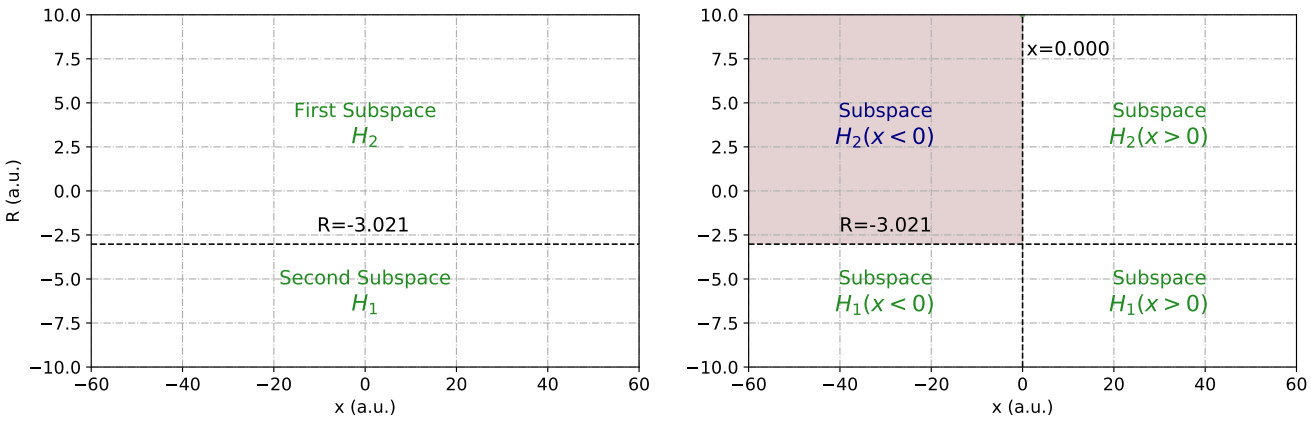

Figure 7.4:
Figure A: Hilbert configurational space separated at the position of the avoided crossing $R_c = -3.021$ $a.u.$ in two half-spaces H_1 (for $R > R_c$) and H_2 (for $R < R_c$).
Figure B: Hilbert configurational spaces separated at the position of the avoided crossing $R_c = -3.021$ $a.u.$ in the nuclear coordinate and also in four half-spaces in the electronic coordinates, for $x < 0$ and $x > 0$.

the avoided crossing, for $x < 0$ (Figure 7.2), opposite case upon happens for nuclear configurations below the first avoided crossing.

In the previous chapter, we see how the sum of the square modulus of each maxima value for each nuclear wave function have a direct relations with the linear entropy and the nature of the oscillations. But in this case, considering only the main values of the density operators (diagonal elements), the nuclear wave functions modulates the result obtained by integrating the product of two electronic wave functions in the equation (4.13).
With this, we see how the local maxima in the entropy coincide with the nuclear wave functions which have a local maxima or minima very close to the first avoided crossing (black lines in Figure 7.6), vibrational states $\chi^d_{0,m}(R)$ with $m \in \{43, 49, 50, 54, ...\}$, in this cases the electronic wave functions for $x < 0$ are modulated with the maxima values in the vibrational state. On other hand, vibrational states $\chi^d_{0,m}(R)$ with $m \in \{47, 52, 56, ...\}$ (blue lines in Figure 7.6) are local minimum in the entropy and have an inflection point close to the first avoided crossing, which modulates the electronic wave function in this subspace to zero. The transitions between a local maxima

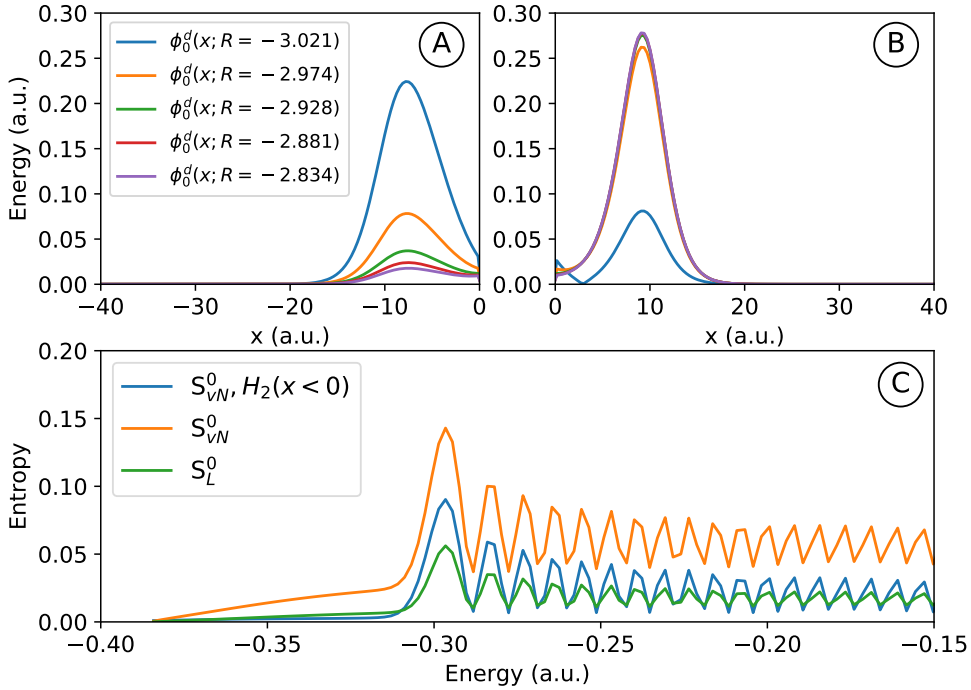

Figure 7.5:
Figure A: Electronic wave functions for $x < 0$ for different nuclear configurations above $R = -3.021$ $a.u.$; first crossing avoided. In this subspace we can see how the electronic wave functions have an abrupt change between different nuclear configurations, specifically for nuclear configurations close to the first crossing avoided. Figure B: Electronic wave functions for $x > 0$ for different nuclear configurations above $R = -3.021$ $a.u.$. In this subspace we can see how the electronic wave functions does not have an abrupt change between different nuclear configurations.
Figure C: Von-Neumann and linear entropies (orange and green lines respectively) for the total BO wave function $\phi_0(x; R)\chi_{0,m}(R)$ compared with the von-Neumann entropy computed in the configurational spaces H_2, with $x < 0$, where this three entropies follow the same functional form.

and minima are because the crossing avoided cross the function in a mid point between a local maxima or minima and and inflection point, which are the green states in the Figure 7.6.

We tabulate the von-Neumann and linear entropy for the first sixty states and the first four Schmidt eigenvalues in the Table 7.1.

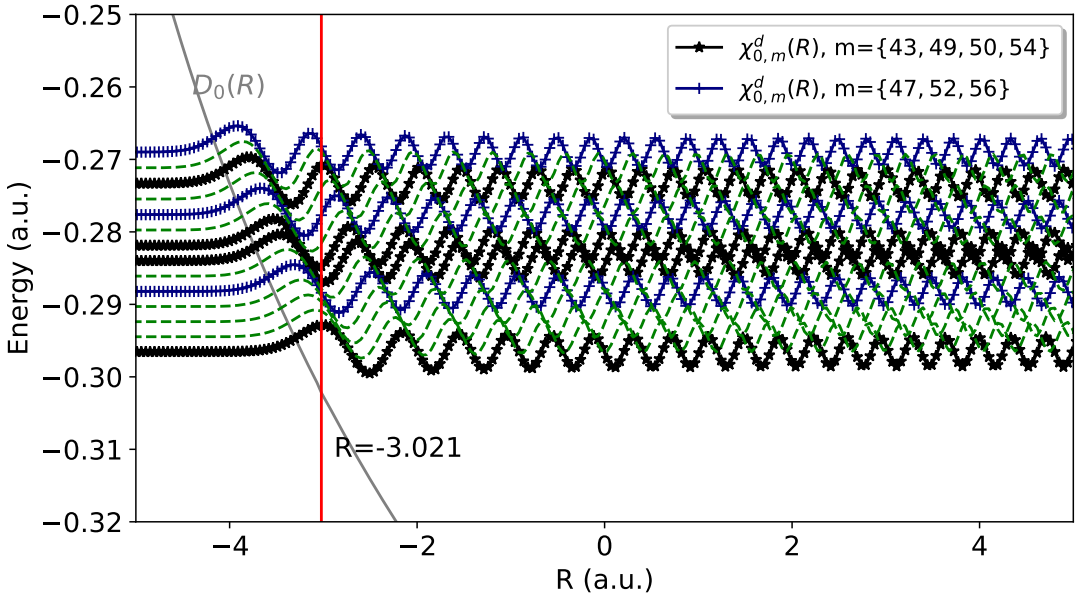

Figure 7.6:
Vibrational wave functions $\chi^d_{0,m}(R)$ with $m \in \{43, ..., 56\}$ computed from $-5 < R < 5$, where the black lines represent the vibrational states which are maximum values in the entropy and blue lines represent the vibrational states which compute minimum values in the entropy. Also the green dotted lines are the vibrational states between a maxima and minima value in the entropy. The black lines intercept with the red line $R = -3.021$ $a.u.$ in a local maxima or minima and the blue lines intercept the red line in a inflection point.

2. States $\phi^d_1(x; R)\chi^d_{1,m}(R)$. In this case we see in the Figure ()

3. States $\phi^d_2(x; R)\chi^d_{2,m}(R)$. In the Figure (6.6) we can see how both von-Neumann and linear entropies increase monotonically with the vibrational excitations energy. We understand that the energy region close to the second avoided crossings for the potential energy curve $D_2(R)$ involve a noticeable increase of the entanglement, the second crossing avoided match with its minimum value of energy of the curve $D_2(R)$ generating a faster increase in the enhancement in the first region of the entanglement entropy. Also, the enlargement of the configurational space available for the vibrational wave functions for distance energies above a given avoided crossing made

State	Eigenvalues η_i				Entropies		
$\phi_0(x;R)\chi_{0,m}(R)$	$i=1$	$i=2$	$i=3$	$i=4$	S_{vN}	S_L	$H_2(x<0)$
$m=0$	1.000	0.000	0.000	0.000	0.001	0.000	0.001
⋮	⋮	⋮	⋮	⋮	⋮	⋮	⋮
$m=37$	0.995	0.003	0.001	0.001	0.033	0.009	0.010
$m=38$	0.994	0.003	0.002	0.001	0.042	0.012	0.018
$m=39$	0.991	0.006	0.003	0.001	0.058	0.017	0.030
$m=40$	0.987	0.010	0.003	0.001	0.080	0.026	0.047
$m=41$	0.980	0.016	0.003	0.001	0.107	0.038	0.066
$m=42$	0.974	0.022	0.003	0.001	0.131	0.050	0.083
$m=43$	0.971	0.025	0.003	0.001	0.143	0.056	0.090
$m=44$	0.974	0.022	0.003	0.001	0.133	0.051	0.082
$m=45$	0.982	0.014	0.003	0.001	0.099	0.035	0.056
$m=46$	0.992	0.005	0.003	0.001	0.056	0.017	0.021
$m=47$	0.995	0.003	0.001	0.001	0.037	0.010	0.008
$m=48$	0.990	0.007	0.003	0.001	0.067	0.021	0.034
$m=49$	0.982	0.014	0.003	0.001	0.100	0.035	0.059
$m=50$	0.982	0.014	0.003	0.001	0.100	0.035	0.057
$m=51$	0.990	0.006	0.003	0.001	0.064	0.020	0.028
$m=52$	0.995	0.003	0.001	0.001	0.037	0.010	0.007
$m=53$	0.990	0.006	0.003	0.001	0.064	0.020	0.031
$m=54$	0.984	0.012	0.003	0.001	0.093	0.032	0.053
$m=55$	0.987	0.009	0.003	0.001	0.080	0.026	0.041
$m=56$	0.994	0.003	0.002	0.001	0.043	0.012	0.010
$m=57$	0.993	0.003	0.003	0.001	0.051	0.015	0.019

Table 7.1: Highest four eigenvalues of the reduced density matrices for the Schmidt decomposition of the total wave function $\phi_0(x;R)\chi_0, m(R)$ with $(m=0,37,...,57)$. The von Neumann S_{vN} and linear S_L entropies for each state are included in the last two columns and the von-Neumann entropy computed within the configurational subspace $H_2(x<0)$ is the last column. The rows in gray belong to the states which are local maximum in the entropy and the rows in yellow belong to the states which are local minimum. The electro-vibrational BO states from $m=0$ to $m=37$ are the same in the diabatic and adiabatic case, they are included in the Table C.1

that the entropy increase slowly.

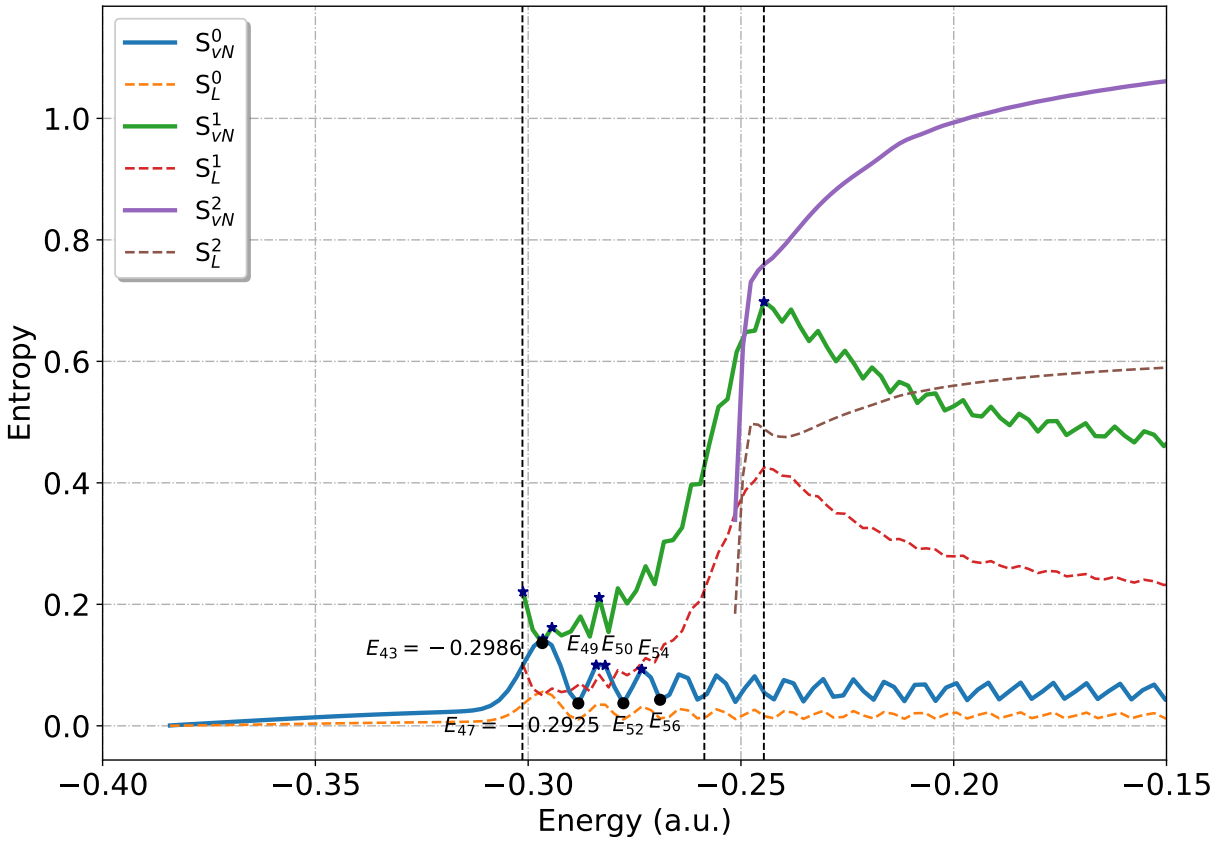

Figure 7.7:
von-Neumann and linear entropies for the total BO wave function $\phi_n(x;R)\chi_{n,m}(R)$ for $n = 0, 1, 2$. The upper index in the entropies correspond to values of the entropy associated to each electronic state n. The vertical lines indicates the energy position of the first sharp avoided crossing at $R_C = -3.023$ $a.u.$ and the energy region of the second avoided crossing at $R = 1.194$ $a.u.$

Chapter 8

Conclusions

We can conclude and remark that we have proposed here a minimal model for charge transfer reactions, which has the virtue that it can be solved numerically exactly and can be used for testing various approximations and physical pictures of the process. The system consists of two fixed ions, a moving ion, and an electron, all confined to a line. It has two degrees of freedom, the position of the ion and that of the electron. This can be viewed as an imitation of a doped zeolite system in which an electron and an ion can migrate from one zeolite cage to another. One can also think of the moving ion as being a simplified representation of a medium, which is polarized (it is displaced) when the electron changes its location. The properties of the system can be varied by changing the length scale of the interaction between the electron and the moving ion. This changes the barrier on the lowest adiabatic state and the energy gap between the ground and the first excited adiabatic state. The distance between the fixed ions is an additional parameter. we have analyzed modifications of ground state chemical reactivity in hybrid cavity-molecule systems, motivated by experimental results showing this effect for vibrational strong coupling.
The BO is good enough for states below of any crossing avoided. As we compute in the Shin-Metiu model, the BO and the BH wave functions are the same. The BO approximation does not have information about the mixture between the different electronic and nuclear states, which are important under the presence of crossings avoided. Thus, the BH treatment in general is correct. The entanglement is presented in the BO solutions too, not only in the BH wave functions. Increasing the electronic or nuclear states generates an increase in the entanglement entropy.
The one-dimensional model for the molecule of H_2^+ is a good approximation to generate the curve $3d\sigma_g$ in the the three dimensional molecule of H_2^+. The p curves cannot be

generated correctly under this model. It would be necessary to adjust more parameters in the interaction potentials.

APPENDICES

Appendix A

Off-diagonal Hellmann-Feynman Theorem

The Hellmann-Feynman theorem that governs the linear changes in the energy with respect to a parameter of the Hamiltoninan is extended to functions of the Hamiltonian. The extension, applicable to a Hamiltonian with both discrete and continuous spectrum is of particular importance for semi-empirical theories of molecular rate processes.
A simple derivation of the off-diagonal formula starts with the Schrodinger equation

$$\hat{H}\left|\phi_n\right\rangle = E_n\left|\phi_n\right\rangle, \tag{A.1}$$

and taking inner product with $(|\phi_n\rangle)^\dagger$ and applying the derivative respect to a parameter ν we have that

$$\frac{\partial}{\partial\nu}\left(E_n\left\langle\phi_m\right|\left.\phi_n\right\rangle\right) = \frac{\partial}{\partial\nu}\left(\left\langle\phi_m\right|\hat{H}\left|\phi_n\right\rangle\right), \tag{A.2}$$

and operating, we find that

$$\begin{aligned} \tfrac{\partial E_n}{\partial\nu} \quad & \left(\left\langle\phi_m\right|\left.\phi_n\right\rangle\right) + E_n\left(\left\langle\phi_m\right|\frac{\partial\phi_n}{\partial\nu}\right\rangle\right) + E_n\left(\left\langle\frac{\partial\phi_m}{\partial\nu}\right|\left.\phi_n\right\rangle\right) \\ = \quad & \left\langle\frac{\partial\phi_m}{\partial\nu}\right|\left(\hat{H}\left|\phi_n\right\rangle\right) + \left(\left\langle\phi_m\right|\hat{H}\right)\left|\frac{\partial\phi_n}{\partial\nu}\right\rangle + \left\langle\phi_m\right|\frac{\partial\hat{H}}{\partial\nu}\left|\phi_n\right\rangle, \end{aligned} \tag{A.3}$$

where we have used the symmetry of the operator. Noting that the first term on the left side is zero by the orthogonality condition of the eigenfunctions and that the last term on the left side is equal to the first term on the right side, thus, simplifying we obtain

$$(E_n - E_m) \left\langle \phi_m \,|\, \frac{\partial \phi_n}{\partial \nu} \right\rangle = \left\langle \phi_m \left| \frac{\partial \hat{H}}{\partial \nu} \right| \phi_n \right\rangle . \tag{A.4}$$

This off-diagonal Hellmann-Feynman theorem [16, 27].

Appendix B

Square matrix and its representation

Consider a operator $\mathbf{A}$ which can be represented in a discrete base (it can be done in the continuous representation, and the procedure is analogous changing the summations by integrals) i, j by a set of coefficients $c_{i,j}$ as

$$\mathbf{A} = \sum_{i,j} c_{i,j} \left|i\right\rangle \left\langle j\right|. \tag{B.1}$$

Thus, the square of the operator $\mathbf{A}$ is

$$\begin{aligned}
\mathbf{A}^2 = \mathbf{A} \cdot \mathbf{A} &= \sum_{i,j} c_{i,j} \left|i\right\rangle \left\langle j\right| \cdot \sum_{l,k} c_{l,k} \left|l\right\rangle \left\langle k\right|, && \text{(B.2)}\\
&= \sum_{i,j} \sum_{l,k} c_{i,j} c_{l,k} \left\langle j|l\right\rangle \left|i\right\rangle \left\langle k\right|, && \text{(B.3)}\\
&= \sum_{i,j,k} c_{i,j} c_{j,k} \left|i\right\rangle \left\langle k\right|, && \text{(B.4)}\\
&= \sum_{i,k} \left(\sum_{j} c_{i,j} c_{j,k} \right) \left|i\right\rangle \left\langle k\right|, && \text{(B.5)}\\
&= \sum_{i,k} S_{i,k} \left|i\right\rangle \left\langle k\right|. && \text{(B.6)}
\end{aligned}$$

The n, m matrix element of the square value of the operator $\mathbf{A}$ is given by

$$\left(\mathbf{A}^2\right)_{n,m} = S_{n,m} = \sum_{j} c_{n,j} c_{j,m}. \tag{B.7}$$

Obtaining thus the matrix element for an operator [22].

Appendix C

Von-Neumann and Linear entropies for the Shin-Metiu model (Adiabatic)

State	Eigenvalues η_i				Entropies	
$\phi_0(x;R)\chi_{0,m}(R)$	$i=1$	$i=2$	$i=3$	$i=4$	S_{vN}	S_L
$m=0$	1.000	0.000	0.000	0.000	0.001	0.000
$m=1$	1.000	0.000	0.000	0.000	0.002	0.000
$m=2$	1.000	0.000	0.000	0.000	0.002	0.001
$m=3$	1.000	0.000	0.000	0.000	0.003	0.001
$m=4$	1.000	0.000	0.000	0.000	0.004	0.001
$m=5$	0.999	0.000	0.000	0.000	0.005	0.001
$m=6$	0.999	0.001	0.000	0.000	0.006	0.001
$m=7$	0.999	0.001	0.000	0.000	0.007	0.002
$m=8$	0.999	0.001	0.000	0.000	0.007	0.002
$m=9$	0.999	0.001	0.000	0.000	0.008	0.002
$m=10$	0.999	0.001	0.000	0.000	0.009	0.002
$m=11$	0.999	0.001	0.000	0.000	0.010	0.002
$m=12$	0.999	0.001	0.000	0.000	0.011	0.003
$m=13$	0.999	0.001	0.000	0.000	0.011	0.003
$m=14$	0.998	0.001	0.000	0.000	0.012	0.003
$m=15$	0.998	0.001	0.000	0.000	0.013	0.003
$m=16$	0.998	0.001	0.000	0.000	0.014	0.003
$m=17$	0.998	0.001	0.000	0.000	0.014	0.004
$m=18$	0.998	0.002	0.000	0.000	0.015	0.004
$m=19$	0.998	0.002	0.000	0.000	0.016	0.004
$m=20$	0.998	0.002	0.000	0.000	0.016	0.004
$m=21$	0.998	0.002	0.000	0.000	0.017	0.004
$m=22$	0.998	0.002	0.000	0.000	0.018	0.005
$m=23$	0.998	0.002	0.000	0.000	0.018	0.005
$m=24$	0.998	0.002	0.000	0.000	0.019	0.005
$m=25$	0.997	0.002	0.000	0.000	0.019	0.005
$m=26$	0.997	0.002	0.000	0.000	0.020	0.005
$m=27$	0.997	0.002	0.000	0.000	0.020	0.005
$m=28$	0.997	0.002	0.000	0.000	0.021	0.006
$m=29$	0.997	0.002	0.001	0.000	0.021	0.006
$m=30$	0.997	0.002	0.001	0.000	0.022	0.006
$m=31$	0.997	0.003	0.001	0.000	0.022	0.006
$m=32$	0.997	0.003	0.001	0.000	0.023	0.006
$m=33$	0.997	0.003	0.001	0.000	0.023	0.006
$m=34$	0.997	0.003	0.001	0.000	0.024	0.007
$\vdots$	$\vdots$	$\vdots$	$\vdots$	$\vdots$	$\vdots$	$\vdots$

State	Eigenvalues η_i				Entropies	
$\phi_0(x;R)\chi_{0,m}(R)$	$i=1$	$i=2$	$i=3$	$i=4$	S_{vN}	S_L
⋮	⋮	⋮	⋮	⋮	⋮	⋮
$m=35$	0.996	0.003	0.001	0.000	0.026	0.007
$m=36$	0.996	0.003	0.001	0.001	0.031	0.008
$m=37$	0.994	0.003	0.002	0.001	0.042	0.012
$m=38$	0.989	0.008	0.003	0.001	0.071	0.023
$m=39$	0.971	0.026	0.003	0.001	0.145	0.057
$m=40$	0.893	0.104	0.003	0.001	0.356	0.192
$m=41$	0.550	0.448	0.002	0.000	0.702	0.497
$m=42$	0.608	0.389	0.002	0.000	0.684	0.478
$m=43$	0.720	0.277	0.002	0.000	0.610	0.405
$m=44$	0.587	0.410	0.002	0.000	0.694	0.487
$m=45$	0.669	0.329	0.002	0.000	0.652	0.445
$m=46$	0.679	0.319	0.002	0.001	0.646	0.438
$m=47$	0.622	0.375	0.002	0.001	0.681	0.472
$m=48$	0.672	0.325	0.002	0.001	0.651	0.442
$m=49$	0.667	0.331	0.002	0.001	0.655	0.446
$m=50$	0.638	0.359	0.002	0.001	0.674	0.464
$m=51$	0.671	0.326	0.002	0.001	0.653	0.444
$m=52$	0.662	0.335	0.002	0.001	0.659	0.449
$m=53$	0.645	0.352	0.002	0.001	0.670	0.460
$m=54$	0.669	0.328	0.002	0.001	0.655	0.445
$m=55$	0.660	0.337	0.002	0.001	0.662	0.451
$m=56$	0.650	0.347	0.002	0.001	0.669	0.457
$m=57$	0.667	0.330	0.002	0.001	0.657	0.446
$m=58$	0.658	0.339	0.002	0.001	0.664	0.452
$m=59$	0.652	0.345	0.002	0.001	0.668	0.456

Table C.1: Highest four eigenvalues of the reduced density matrices for the Schmidt decomposition of the total wave function $\phi_0(x;R)\chi_{0,m}(R)$ with $(m=0,...,59)$ i.e., the BO wave functions. The von Neumann S_{vN} and linear S_L entropies for each state are included in the last two columns. The closer state for the Sharp avoided crossing located at $R=-3.021$ *a.u.* and with energy $E=0.301$ *a.u.* is the state $\phi_0(x;R)\chi_{0,41}(R)$, which has the highest entropy value.

Appendix D

BO wave functions: one-dimensional model of H_2^+

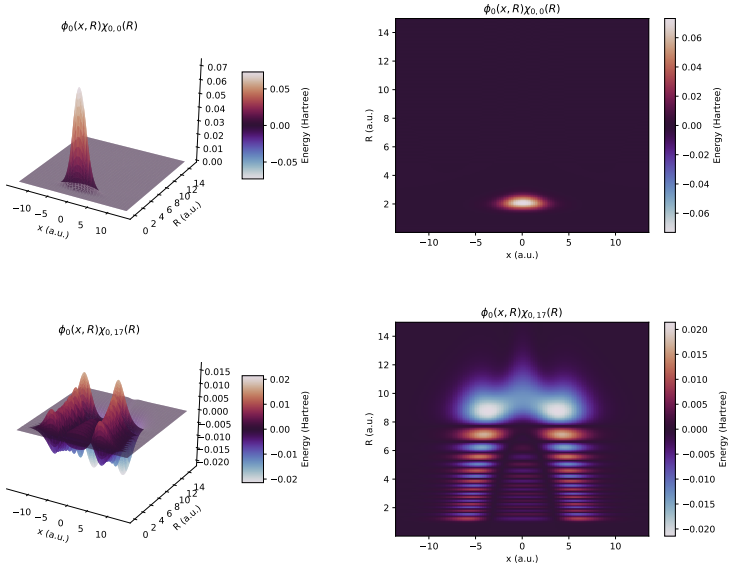

Figure D.1:
Total BO wave functions $\Psi(x, R)$ for the states $\phi_0(x, R)\chi_{0,0}(R)$ and $\phi_0(x, R)\chi_{0,17}(R)$ for the one-dimensional model of H_2^+.

Appendix E

BO wave functions: Shin-Metiu molecular model

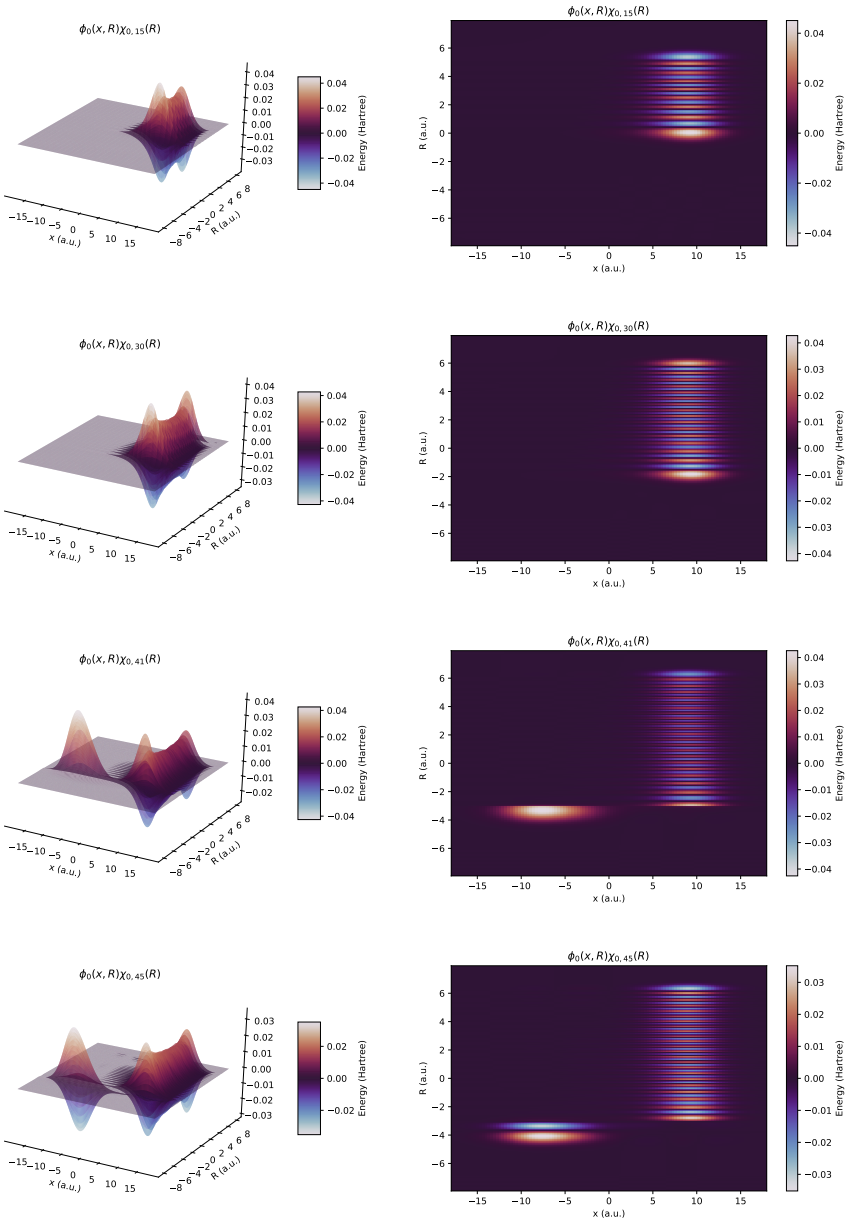

Figure E.1:
Total BO wave functions $\Psi(x,R)$ for the states $\phi_0(x,R)\chi_{0,0}(R)$, $\phi_0(x,R)\chi_{0,15}(R)$, $\phi_0(x,R)\chi_{0,30}(R)$, $\phi_0(x,R)\chi_{0,41}(R)$ and $\phi_0(x,R)\chi_{0,45}(R)$ for the Shin-Metiu model.

Appendix F

Born-Huang wave functions for the Shin-Metiu molecular model

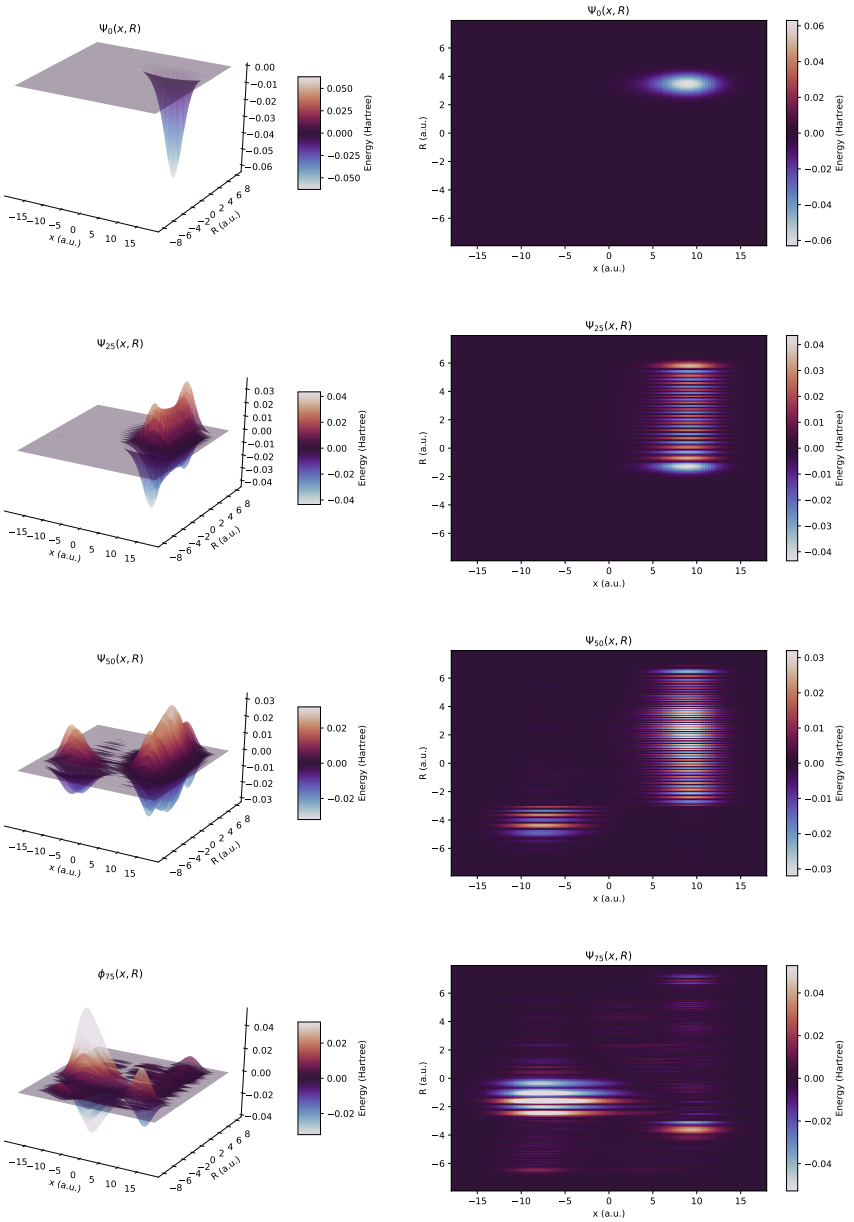

Figure F.1:
Total BH wave functions $\Psi(x,R)$ for the states $\Psi_0(x,R)$, $\Psi_{25}(x,R)$, $\Psi_{50}(x,R)$ and $\Psi_{75}(x,R)$ for the Shin-Metiu model.

References

[1] Jose Luis Sanz-Vicario Andres Felipe Ordoñez-Lasso and Fernando Martín. "Effect of potential screening on the H_2 autoionizing states". In: *Physical Review A* 96 (2017). DOI: https://doi.org/10.1103/PhysRevA.96.052503.

[2] Yehuda B. Band. *Light and Matter: Electromagnetism, Optics, Spectroscopy and Lasers*. Wiley Editorial, 2006, pp. 360–366.

[3] William Barford. *Electronic and Optical Properties of Conjugated Polymers*. 2nd ed. Oxford University Press, 2013, pp. 8–10.

[4] Alisa Bokulich and Gregg Jaesger. *Philosophy of Quantum Information and Entanglement*. Vol. 1. Cambridge University Press, 2010, pp. 134–137.

[5] Max Born and Kun Huang. *Dynamical Theory of Crystal Lattices*. Vol. 1. Oxford University Press, 1954, pp. 406–407.

[6] B. H. Bransden and C. J. Joachain. *Atomic and Molecular Physics*. 2nd ed. Prentice Hall editions, 2003, pp. 101–104.

[7] Frank Grossmann. *Theoretical Femtosecond Physics: Atoms and Molecules in Strong Laser Fields*. Springer, 2008, pp. 43–45.

[8] T. G. Heil and A. Dalgarno. "Diabatic molecular states". In: *Journal of Physics B* 12 (1979). DOI: https://doi.org/10.1088/0022-3700/12/18/005.

[9] Gregg Jaeger. *Entanglement, Information and the Interpretation of Quantum Mechanics*. Springer, 2009, pp. 12–24.

[10] Daniel Pelaez Johan F. Triana and Jose L. Sanz-Vicario. "Entangled Photonic-Nuclear Molecular Dynamics of LiF in Quantum Optical Cavities". In: *J. Phys. Chem. A* 122 (2018). DOI: https://doi.org/10.1021/acs.jpca.7b11833.

[11] Jorge V. Jose and Eugene J. Saletan. *Classical Dynamics: A Contemporary Approach*. Cambridge University Press, 1998, pp. 77–92.

[12] Jhon Fredy Perez-Torres Jose Luis Sanz-Vicario and Germán Moreno-Polo. "Electronic-nuclear entanglement in H_2^+: Schmidt decomposition of non-Born-Oppenheimer wave functions expanded in non-orthogonal basis sets". In: *Physical Review A* 96 (2017). DOI: https://doi.org/10.1103/PhysRevA.96.022503.

[13] F. H. Mies K. C. Kulander and K. J. Schafer. "Model for studies of laser-induced nonlinear processes in molecules". In: *Physical Review A* 53.4 (1996). DOI: https://doi.org/10.1103/PhysRevA.53.2562.

[14] Jorge Kohanoff. *Electronic Structure Calculations for Solids and Molecules: Therory and Computational Methods*. Cambridge University Press, 2006, pp. 3–14.

[15] Ira N. Levine. *Quantum Chemistry*. 5th ed. Prentiece Hall, 2000, pp. 376–381.

[16] R. D. Levine. "An extended Hellmann-Feynman theorem". In: *Proceedings of The Royal Society A* 294 (1966). DOI: https://doi.org/10.1098/rspa.1966.0219.

[17] J. C. Lorquet M. Desouter-Lecomte C. Galloy and M. Vaz Pires. "Nonadiabatic interactions in unimolecular decay. V. Conical and Jahn–Teller intersections". In: *The Journal of Chemical Physics* 71 (1979). DOI: https://doi.org/10.1063/1.438810.

[18] C. Clay Marston and Gabriel G. Balint-Kurti. "The Fourier grid Hamiltonian method for bound state eigenvalues and eigenfunctions". In: *The Journal of Chemical Physics* 91 (1989). DOI: https://doi.org/10.1063/1.456888.

[19] Richard M. Martin. *Electronic Structure: Basic Theory and Practical Methods*. Cambridge University Press, 2004, pp. 1–2.

[20] C. Alden Mead and Donald G. Truhlar. "Conditions for the definition of a strictly diabatic electronic basis for molecular systems". In: *The Journal of Chemical Physics* 77 (1982). DOI: https://doi.org/10.1063/1.443853.

[21] J. P. Restrepo-Cuartas and J. L. Sanz-Vicario. "Information and entanglement measures applied to the analysis of complexity in doubly excited states of helium". In: *Physical Review A* 91 (2015). DOI: https://doi.org/10.1103/PhysRevA.91.052301.

[22] J. J. Sakurai and Jim Napolitano. *Modern Quantum Mechanics*. 2nd ed. Addison-Wesley print, 2013, pp. 18–22.

[23] Benjamin Schumacher and Michael D. Westmoreland. *Quantum Processes Systems and Information*. Cambridge University Press, 2010, pp. 158–159, 390–400.

[24] Seokmin Shin and Horia Metiu. "Multiple Time Scale Quantum Wavepacket Propagation: Electron-Nuclear Dynamics". In: *J. Phys. Chem.* 100 (1996). DOI: https://doi.org/10.1021/jp952498a.

[25] Seokmin Shin and Horia Metiu. "Nonadiabatic effects on the charge transfer rate constant: A numerical study of a simple model system". In: *The Journal of Chemical Physics* 102 (1995). DOI: https://doi.org/10.1063/1.468795.

[26] Attila Szabo and Neil S. Ostlund. *Modern Quantum Chemistry: Introduction to advanced Electronic Structure Theory*. Dover Publications, 1996, pp. 40–46.

[27] David Wallace. "An Introduction To Hellmann-feynman Theory". PhD thesis. University of Central Florida, 2005, pp. 8–12.

[28] Curt Wittig. "The Landau-Zener Formula". In: *J. Phys. Chem. B* 109 (2005). DOI: https://doi.org/10.1021/jp040627u.

[29] Lun Yue and Lars Bojer Madsen. "Dissociative ionization of H_2^+ using intense femtosecond XUV laser pulses". In: *Physical Review A* 90 (2014). DOI: https://doi.org/10.1103/PhysRevA.90.063408.